

UNIVERSITAT ROVIRA I VIRGILI
SELECTIVE HYDROGENATION CATALYSTS FOR ENVIRONMENTAL PROCESSES:
NITRATE AND CHLOROCOMPOUNDS REMOVAL
Noelia Barrabés Rabanal
DL: T-1539-2009/ISBN:978-84-692-4557-6

*Front page and back page
illustrated by
Manuel Mesa Serrato*

UNIVERSITAT ROVIRA I VIRGILI
SELECTIVE HYDROGENATION CATALYSTS FOR ENVIRONMENTAL PROCESSES:
NITRATE AND CHLOROCOMPOUNDS REMOVAL
Noelia Barrabés Rabanal
DL: T-1539-2009/ISBN:978-84-692-4557-6



Department of Chemical Engineering
Rovira i Virgili University
Spain

Selective hydrogenation catalysts for environmental processes: nitrate and chlorocompounds removal

Thesis submitted by
NOELIA BARRABÉS RABANAL
to obtain the European degree of
Doctor from the Universitat Rovira I Virgili
Tarragona, 13th March 2009

UNIVERSITAT ROVIRA I VIRGILI
SELECTIVE HYDROGENATION CATALYSTS FOR ENVIRONMENTAL PROCESSES:
NITRATE AND CHLOROCOMPOUNDS REMOVAL
Noelia Barrabés Rabanal
DL: T-1539-2009/ISBN:978-84-692-4557-6

Dr. Francesc Medina Cabello and Dr. Anton Dafinov, professor and researcher of the Department of Chemical Engineering at the Universitat Rovira i Virgili

Certify: *That the doctoral thesis entitled “ Selective hydrogenation catalysts for environmental processes: nitrate and chlorocompounds removal” by NOELIA BARRABÉS RABANAL to obtain the European degree of doctor from the Universitat Rovira i Virgili has been carried out under our supervision in the Department of Chemical Engineering of the Universitat Rovira i Virgili.*

Tarragona, March 2009

Dr. Francesc Medina Cabello

Dr. Antón Dafinov

UNIVERSITAT ROVIRA I VIRGILI
SELECTIVE HYDROGENATION CATALYSTS FOR ENVIRONMENTAL PROCESSES:
NITRATE AND CHLOROCOMPOUNDS REMOVAL
Noelia Barrabés Rabanal
DL: T-1539-2009/ISBN:978-84-692-4557-6

THESIS TRIBUNAL

Prof. Chris Hardacre
CentACat, School of Chemistry and Chemical Engineering,
Queen's University Belfast, UK

Dra. Karin Föttinger
Institute of Materials Chemistry, Vienna University of Technology
Austria

Dr. Jordi Llorca
Institut de Tècniques Energètiques, Universitat Politècnica de Catalunya,
Spain

Dr. Eduardo Palomares
Instituto de Tecnología Química, UPV-CSIC, Universidad Politécnica de
Valencia, Spain

Dra. Yolanda Cesteros
Departamento de Química Inorgánica, Facultad de Química, Universidad
Rovira i Virgili, Spain

RESERVE

Prof. Jesús E. Sueiras
Departament Enginyeria Química, Universidad Rovira i Virgili, Spain

Dr. Jacinto Sá
CentACat, School of Chemistry and Chemical Engineering,
Queen's University Belfast, UK

EXTERNAL REFEREES

Prof. Günther Rupprechter
Vienna University of Technology, Austria

Prof. Bernard Coq
Ecole Nationale Supérieure de Chimie de Montpellier

UNIVERSITAT ROVIRA I VIRGILI
SELECTIVE HYDROGENATION CATALYSTS FOR ENVIRONMENTAL PROCESSES:
NITRATE AND CHLOROCOMPOUNDS REMOVAL
Noelia Barrabés Rabanal
DL: T-1539-2009/ISBN:978-84-692-4557-6

Table of Contents

Acknowledgments

Resumen	pag.i
----------------	--------------

Chapter 1 General Introduction	pag.1
---------------------------------------	--------------

Chapter 2 Objectives	pag.6
-----------------------------	--------------

Chapter 3 Catalytic reduction of nitrates	pag.8
--------------------------------------------------	--------------

1. Introduction	8
1.1. Pollution problem of nitrates	8
1.2. Remediation Technologies	11
1.3. Catalytic hydrogenation of nitrates and nitrites	14
1.4. References	27
2. Experimental	31
2.1. Characterization techniques	31
2.2. Set-up equipment	35
3. Active Carbon catalysts	37
3.1. Catalysts synthesis	38
3.2. Results and Discussion	39
3.2.1. <i>Characterization results</i>	39
3.2.2. <i>Catalytic activity</i>	45
3.3. Conclusions	51
4. Ceria catalysts	52
4.1. Catalysts synthesis	52
4.1.1. <i>Bimetallic Pt-Cu/CeO₂ catalysts</i>	52
4.1.2. <i>Monometallic Pt / CeO₂ catalysts</i>	53
4.1.3. <i>Fluorinated ceria catalysts</i>	54
4.1.4. <i>Pt/CeO₂ monoliths</i>	54
4.2. Results and Discussion	55
4.2.1. <i>Characterization results</i>	55
4.2.1.1. <i>Bimetallic Pt-Cu/CeO₂ catalysts</i>	55
4.2.1.2. <i>Monometallic Pt / CeO₂ catalysts</i>	57

4.2.1.3. Fluorinated ceria catalysts	63
4.2.1.4. Pt/CeO ₂ monoliths	67
4.2.2. Catalytic activity	68
4.2.2.1. Pt-Cu/CeO ₂ catalysts	68
4.2.2.2. Pt/CeO ₂ catalysts	70
4.2.2.3. Pt/FCeO ₂ catalysts	72
4.2.2.4. Pt/CeO ₂ monoliths	74
4.3. Conclusions	76

Chapter 4 Catalytic hydrodechlorination of trichloroethylene pag.78

1. Introduction	78
1.1. Pollution problem of trichloroethylene	78
1.2. Remediation Technologies	81
1.3. Catalytic hydrogenation of TCE in gas phase	83
1.4. References	87
2. Experimental	90
2.1. Characterization techniques	90
2.2. Set-up equipment	91
3. PdCu / Alumina catalysts	93
3.1. Catalysts synthesis	93
3.2. Results and Discussion	94
3.2.1. Characterization results	94
3.2.2. Catalytic activity	99
3.3. Conclusions	102
4. Pt,Pd-Cu hydrotalcites catalysts	103
4.1. Catalysts synthesis	104
4.2. Results and Discussion	105
4.2.1. Characterization results	105
4.2.2. Catalytic activity	115
4.2.2.1. Influence of the Mg:Cu ratio	115
4.2.2.2. Influence of the noble metal	117
4.2.2.3. Influence of preparation procedure	118
4.2.2.4. Suggested reaction mechanism	121
4.3. Conclusions	124
5. Pt/Ceria catalysts	126
5.1. Catalysts synthesis	127
5.2. Results and Discussion	127
5.2.1. Characterization results	127

5.2.2. <i>Catalytic activity</i>	148
5.3. Conclusions	156

Chapter 5 Conclusions **pag.157**

Chapter 6 CV **pag.159**

UNIVERSITAT ROVIRA I VIRGILI
SELECTIVE HYDROGENATION CATALYSTS FOR ENVIRONMENTAL PROCESSES:
NITRATE AND CHLOROCOMPOUNDS REMOVAL
Noelia Barrabés Rabanal
DL: T-1539-2009/ISBN:978-84-692-4557-6

Esta tesis no hubiera sido posible sin la oportunidad que me brindó el Dr. Francisco Medina hace cuatro años. Durante este tiempo me ha supervisado y apoyado en mi trabajo, me ha formado científicamente, aguantado mis cabezonerías y permitido todas mis estancias en el extranjero. Por todo ello y por la gran confianza depositada en mi le doy todo mi agradecimiento.

Mi más profundo agradecimiento al Dr. Anton Dafinov, a parte de ser mi supervisor por ser un gran amigo, quien me ha apoyado en los momentos buenos y malos durante todos estos años. Gracias a él esta tesis ha llegado a ser una "gran recerca".

Vielen Dank an Dr. Hannelore Vinnek und Prof. Günther Rupprechter, dir mir meinen Forschungsaufenthalt im Institut für Material Chemie (Technische Universität) ermöglicht haben. Ein grossen Dankeschön an Dr. K. Föttinger, sie hat mich in den zurückliegenden Jahren immer bestärkt und unterstützt. Sie ist nicht nur eine Arbeitskollegin, sondern auch eine gute Freundin. Ich danke ebenso allen Mitarbeiter und Mitarbeiterinnen (Katy, Christians, Andreas, Michi, Nikkí, Alex, Slavi, Andy, David, Massi, Markus, Oliver, Reinold,...) für die schöne Zeit am Institut. Ich habe mich während meinen Aufenthaltes in Wien mit Waltraud, Sonja, Tove, Max, Bea and Robert aufgefreundet. Ich möchte auch Ihnen meinen innigsten Dank für die angenehme Zeit aussprechen.

Tuve la oportunidad de hacer una estancia en un centro donde se trabaja en un campo completamente diferente a la catálisis y para mi fue una gran experiencia. Esto, además de toda la confianza depositada en mí y el gran apoyo se lo tengo que agradecer al Dr. Jose Luis Toca. Igualmente quiero agradecer a mis compañeras en el laboratorio por haberme ayudado durante todo mi tiempo en Donosti, Aitziber, Verónica, Pavla y Susana. Muy especialmente quiero darle mi agradecimiento a Sara, además de ser mi compañera de piso allí, es una gran amiga quien ha seguido a mi lado en todo momento.

The last stage was in Belfast in the Centacat institute that below to the Queens University. I want to thanks to the Prof. Chris Hardacre for this opportunity and for his supervision. In addition I am grateful to Dr. Youssef Saïh and Dr. Helen Daly who help me all this time there. The two months there were like years, in terms of friends, I could meet really nice people as Meabh, Jacinto, Gaben, Theres, Judith, Inma, Hector and Alberto. I will remember all my nice time there with them and I know that we will have more nice time together in the future. I am thanks too to my colleges in the office, for the funny time there, Matthew, David, Loredana and Cristina.

Quiero agradecer a mis compañeras de piso de estos últimos cuatro años, Eliana, Lorena, Marina, Sabine, Rocío, Dani y Marta. Quienes a parte de tener que aguatarme el día a día, han puesto momentos de risa, alegría y fiesta en mi vida. Y no sólo por ser mis compañeras de piso, sino por ser mis amigas y estar ahí en los momentos felices pero también en los tristes y duros. Os echaré de menos.

Esta tesis tampoco hubiera sido posible sin Sandra, Mayra y Vero, quienes han sido las personas que más fuerzas me han dado para poder seguir adelante en momentos difíciles durante los últimos años, quienes me ha dado todo sin pedir nada a cambio, quienes me han seguido allá

donde fuera, quienes han sido y seguirán siendo mis queridas amigas... (las "Chemicals sisters"... y en algún momento... la loca, la tonta y la vaga...)

Por otro lado, durante estos cuatro años he tenido diferentes compañeros/as y amigos en el laboratorio, a los que quiero agradecerles todo este tiempo: los que aun siguen aquí, como Beteley, Kabe, David, Abel, Isabel y los que ya se fueron como Clara, Sonia, Olga y Chiment. Así como a la gente de la carrera y del departamento: Rafa, Javivi, Sergi, Vanesa, Pepa y Bea. Muchas gracias por toda vuestra ayuda y apoyo.

Dins de la província de Tarragona hi ha un poblet, Valls, on hi ha una gent increïble. Especialment he d'agrair a Ìu per tot el temps junts que m'ha donat força, confiança en mi mateixa i suport. Així com a tota la colla vallenga per tots el bons moments junts.

A lo largo del doctorado he asistido a diferentes congresos donde he tenido la suerte de conocer a gente muy especial como Oihane, Albert, Javi, Silvia, Unai, Manu y Enrique a los que quiero agradecer todas las vivencias compartidas en diversos puntos del mundo. Muy especialmente quiero agradecer a un vasco-navarro quien ha sido mi amigo y compañero de fatigas, apoyándonos mutuamente en esta carrera por la tesis. Quien hizo que mi estancia en Donosti fuera como estar en casa. A tí Asier, por toda tu ayuda y apoyo.

Desde hace muchos años hay dos personitas que siempre han estado a mi lado, creyendo en mí, apoyándome y siendo mis mejores amigas desde casi la infancia. A vosotras, Susana y Ainoa os agradezco de todo corazón haber estado ahí, conociéndome mejor que nadie y dándome ánimos en todo momento. Esta tesis en parte va dedicada a vosotras.

El pilar fundamental de este trabajo ha sido mi familia, a quienes le dedico gran parte de mi agradecimiento. Muy especialmente a mi hermana Laura y a mis padres (y a la Tula), a quienes debo todo. Siempre me habéis apoyado en mis decisiones y ayudado a llegar donde estoy, con amor y comprensión. Habéis sufrido conmigo todas las dificultades y alegrado de mis logros. Y también a mi prima Begoña, quien ha sido como mi hermana mayor, a mi tía Manoli, mi segunda madre en Tarragona y a mis abuelos.

Por último pero no menos importante quiero agradecer a mi enano Frodo, por darme alegría cada día y estar siempre a mi lado.

***Muchas Gracias! Vielen Dank! Thank you very Much!
Eskerrikasko! Moltes Gràcies!***

Resumen

El campo de la catálisis ha sido tradicionalmente asociado a la producción de compuestos químicos y a la refinería del petróleo. La extensión del uso de la catálisis a la protección del medio ambiente, como herramienta fundamental en la prevención y remedio de la contaminación, ha crecido en importancia en las últimas décadas, por lo que la investigación dentro de la catálisis medioambiental representa una oportunidad dinámica y atractiva, tanto en el ámbito académico como en perspectivas industriales. En el fomento de los procesos sostenibles así como de la calidad de vida y del medio ambiente, la reducción de contaminantes en agua y aire es un factor importante.

En el presente trabajo se han diseñado, sintetizado y caracterizado catalizadores heterogéneos. Se ha estudiado la actividad y selectividad, de estos materiales, en el tratamiento de compuestos que comportan problemas medioambientales.

Para la preparación de los catalizadores se han utilizado diferentes técnicas tales como impregnación, proceso redox y combustión. A su vez, se han sintetizado nanopartículas metálicas, depositándolas en diferentes materiales y testado su actividad catalítica. La actividad de estos catalizadores se ha comparado con catalizadores comunes en diferentes procesos. Por otro lado, se han utilizado diferentes materiales, alumina, carbón activo, ceria e hidrotalcitas, con el propósito de estudiar el efecto del soporte.

Estos materiales se han caracterizado utilizando diferentes técnicas avanzadas como fisiorción, quimisorción, microscopia electrónica (SEM-TEM), difracción de rayos X (XRD), reducción a temperatura programada (TPR), espectroscopia fotoelectrónica (XPS), etc... para estudiar la correlación entre las propiedades físico-químicas de los catalizadores y su comportamiento en las reacciones. Para monitorización in-situ de la reacciones, se han empleado las técnicas de espectroscopia FTIR y DRIFT.

La contaminación por nitratos en las aguas subterráneas es un problema importante en determinadas regiones. Esta problemática ha impulsado el estudio de la eliminación catalítica de los nitratos, en la que se enfoca la primera parte de la tesis. Este estudio se realizó en un reactor en continuo de lecho fijo. Se sintetizaron, caracterizaron y ensayaron, varios catalizadores monometálicos, bimetálicos y de nanopartículas soportadas. Una vez determinada la actividad y la estabilidad de los catalizadores se procedió a optimizar los materiales con el fin de mejorar la selectividad de éstos hacia nitrógeno. Los catalizadores bimetálicos soportados en carbón activo mostraron elevada actividad en la reducción de nitratos así como una alta selectividad hacia nitrógeno. Las nanopartículas metálicas soportadas presentan una actividad alrededor de cien veces mayor que los catalizadores comunes, permitiendo la minimización del contenido de metal noble lo que se traduce en una disminución del coste del proceso. Se modificaron las propiedades ácido-base de los catalizadores de ceria con la finalidad de buscar una participación no sólo como fase activa sino también como buffer del medio de reacción. Estas modificaciones minimizaron la formación de amonio, subproducto indeseado, en el proceso de reducción de nitratos.

El presente trabajo ha sido el punto de partida para la puesta en marcha de una planta piloto para el tratamiento de aguas subterráneas reales contaminadas con nitratos. Próximamente será inaugurada una planta de eliminación catalítica de nitratos de aguas subterráneas con capacidad 500m³/día en las proximidades de El Morell (Tarragona).

La segunda parte de la tesis se enfoca en el proceso de hidrodecloración catalítica de compuestos orgánicos clorados como el tricloroetileno. Los experimentos se llevaron a cabo en fase gas utilizando diferentes tipos de catalizadores, los cuales fueron sintetizados y caracterizados. Se emplearon diferentes catalizadores, mono y bimetalicos, para la transformación del tricloroetileno a un producto de valor añadido, como es el etileno. Del mismo modo, se estudió el comportamiento catalítico de hidrotalcitas ternarias de cobre, mostrando alta actividad y selectividad en este proceso. Los resultados evidenciaron la importancia de la presencia de una aleación bimetalica como fase activa para la formación de etileno como producto principal. Estos catalizadores también presentaron una gran estabilidad frente a la desactivación. A partir de los datos obtenidos se ha propuesto un nuevo mecanismo de reacción para la hidrodecloración catalítica del tricloroetileno.

En los catalizadores monometalicos de Pt/ceria se estudió el efecto del método de preparación sobre la actividad y selectividad. El estudio reveló diferencias en el tamaño de partícula, así como diferentes tipos de interacción entre las partículas del platino y la ceria, denotando el fenómeno de epitaxi en ciertos casos. Estas variables mostraron tener una influencia en el comportamiento catalítico de estos materiales. Se aplicaron diferentes pre-tratamientos a los catalizadores conduciendo a cambios en la superficie de éstos. Se encontró, para este caso, una repercusión en la actividad y selectividad en la reacción de hidrodecloración.

El presente trabajo, además de aportar conocimientos fundamentales en la catálisis heterogénea, contribuye a forjar soluciones a problemas medioambientales reales que afectan a la salud humana.

UNIVERSITAT ROVIRA I VIRGILI
SELECTIVE HYDROGENATION CATALYSTS FOR ENVIRONMENTAL PROCESSES:
NITRATE AND CHLOROCOMPOUNDS REMOVAL
Noelia Barrabés Rabanal
DL: T-1539-2009/ISBN:978-84-692-4557-6

Chapter 1

General Introduction

1.1. ENVIRONMENTAL CATALYSIS

Catalysis has been traditionally associated with chemical and refinery production. The extension of the catalysis use outside these fields to environmental protection, as a fundamental tool in pollution prevention, has continuously grown in importance over the last two decades. “Environmental Catalysis” concept is linked the notion of sustainable development: “a process of change in which the exploitation of resources, the direction of investments, the orientation of technological development and institutional change are all in harmony and enhance both current and future potential to meet human needs and aspiration” Janssen and van Santen [1]. Research in environmental catalysis is, therefore a highly timely, dynamic and attractive field both from an academic and from an industrial perspective. The increasingly tighter legislative regulations on emission control as well as the general public awareness for “green” and sustainable chemical production processes are further drivers for this highly interdisciplinary and efficient field of research. Without doubt, environmental catalysis will continue to be not only an interesting and promising area of current and future research, but also an enabling technology on the way to a sustainable economy [2]

Historically, the interest of researchers working in the area of environmental catalysis was initially focused mainly on NO_x control (mobile and stationary sources), and sulfur and VOC abatement, as indicated by the prevailing contributions in this area [3, 4]. Scientific interest progressively then moved from the cleanup approach to the other cited subjects. However, recently new problems and questions have renewed research activity in the area of catalytic cleanup technologies. Three main driving forces may be cited: (i) the need to expand catalytic technologies from gaseous emissions to the treatment of liquid emissions and solid waste, (ii) the need for new post-treatment devices for mobile sources and (iii) the necessity of reconsidering post-treatment technologies in the perspective of process or systems integration [5].

Figure 1.1 illustrates the concept of how environmental catalysis is expanding the range of catalysis use from chemical/energy fields to non-chemical, transport and daily life areas. [6]. The importance of this aspect is not only a broader market for catalysis, but also in terms of new challenges for research in order to overcome the often demanding constraints given by this expanded use of catalysts and in terms of increased social awareness that catalysis is a solution to improve quality of life.

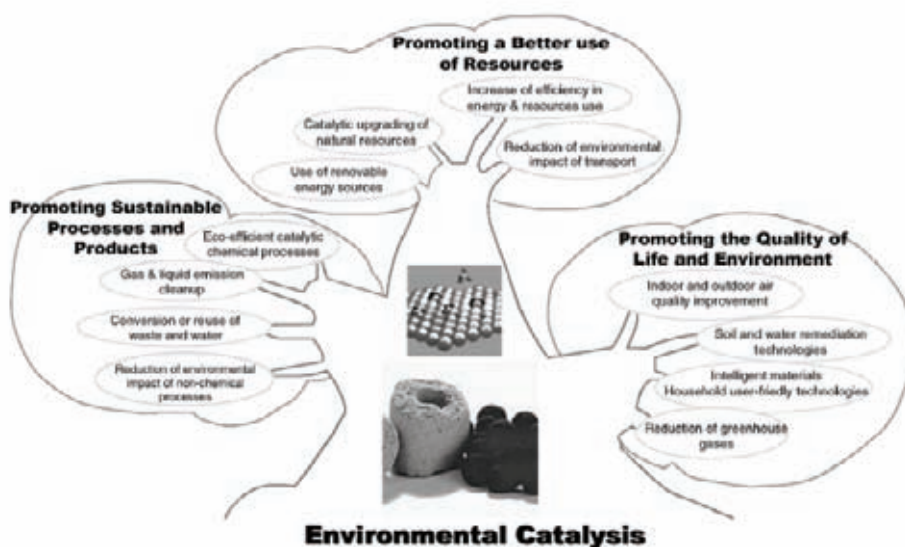


Figure 1.1. The tree of the role of catalysis in promoting environmental protection

In the promoting of sustainable processes and products as well as in the promoting the quality of life and environment, an important point is the reduction of pollutants in water and air streams.

Scientific interest of catalytic water phase processes has awakened within past 10 years. For the time being catalytic water treatment processes are for very limited use only. However, tightening regulations in treatment of aqueous waste have forced to search novel methods in the near future. Groundwater contaminated by agricultural practices (nitrate and pesticides, in particular), leakage of non-biodegradable compounds from underground fuel tanks and pipelines, and accidental spills and leaking of cleaning solvents and degreasers is becoming a major problem worldwide. The recent reports of the European Environment Agency (EEA) “Dobris Assessment” and “Sustainable use of Europe’s water?” highlighted the question that water pollution and deterioration of aquatic habitats are severely hampering the use of water for human consumption and wildlife. Inadequate amounts or poor water quality create a conflict between human demand for water and wider ecological needs.

It is estimated that the market for such technologies will double in the next 5–10 years, but that at the same time current available technologies are often inadequate to meet both economic and ecological demands. Therefore, there are both ecological and economic incentives to develop new technologies for water and air treatment and remediation. Catalysis may play a critical role in the development of these novel technologies, but this issue poses at the same time new challenges for catalysis. In this remediation, the challenge is that the catalysts must be able to efficiently operate on-site, which poses considerable constraints due to the fact that the technology must be compact (to be moved from site to site) and easily manageable

Atmospheric pollution contributes to various important environmental issues, due to emissions to the atmosphere from a variety of mainly anthropogenic activities. Air emissions contribute to the following issues:

- Climate change (emissions of greenhouse gases)
- Acidification and eutrophication (emissions of acidifying and eutrophying pollutants)
- Tropospheric ozone and urban air quality (emissions of ozone precursors, particulate matter and other pollutants)
- Long-range dispersion of hazardous substances (emissions of heavy metals and persistent organic pollutants or POPs)

This environmental problematic nowadays encourage the development of efficient technologies. Treatments that present high yield in contaminant removal and high selectivity to clean products. Catalytic processes appear as an optimal solution for these problems.

Facing the nowadays demand of drinking waters, the catalytic hydrogenation of nitrates is studied in the first part of this thesis. The study is performed in a fixed bed continuous reactor. Several bimetallic, monometallic and supported nanoparticles catalysts have been synthesised characterized and tested in order to improve the activity and the stability and to optimise the selectivity to nitrogen. The present study was further extended and some of the investigated catalysts have been used as a starting point for a Pilot Plant investigation on nitrate elimination in real ground water. At this time a plant with capacity of 500 m³ / day for catalytic reduction of nitrate in ground water is constructed in the vicinity of El Morell, Tarragona and it is in the final start up tests.

The second part of the thesis deals with the catalytic hydrodechlorination of chlorinated organic compounds e.g. TCE. The experiments have been performed in gas phase. Different types of catalysts have been synthesised, characterized and tested. The final objective is to obtain an active and stable catalysts selective toward valuable products e.g. ethylene.

This work tries to contribute in the solutions of real environmental problems that affect the human life, using catalytic technologies.

References

- [1] v.S.R.A. Jassen F.J.J.G., Environmental Catalysis, 2001.
- [2] F. Garin, Catal Today 89 (2004) 255-268.
- [3] J.N. Armor, Appl Catal B-Environ 1 (1992) 221-256.
- [4] G.A. Mills, Abstr Pap Am Chem S (1971) 27-&.
- [5] G. Centi, P. Ciambelli, S. Perathoner, P. Russo, Catal Today 75 (2002) 3-15.
- [6] M. Misono, Toyota Technol. Rev. 44 (1995) 4.

UNIVERSITAT ROVIRA I VIRGILI
SELECTIVE HYDROGENATION CATALYSTS FOR ENVIRONMENTAL PROCESSES:
NITRATE AND CHLOROCOMPOUNDS REMOVAL
Noelia Barrabés Rabanal
DL: T-1539-2009/ISBN:978-84-692-4557-6

Chapter 2

Objectives

The main scope of the present work is to design, synthesized and characterized heterogeneous catalysts as well as to study their activities and selectivity in the treatment of compounds that presents environmental problems.

The specific objectives of the present work are as followed:

- I. Apply different protocols in the catalysis preparation, incipient-wetness impregnation, co-impregnation, redox, and combustion.
- II. Synthesize stable metal nanoparticles with subsequent deposition on different supports.
- III. Compare the activity and the selectivity of the nanoparticle catalysts with the other ones in different processes.
- IV. Study different materials like alumina, active carbon, ceria and hydrotalcites as catalyst supports.
- V. Use different characterization techniques in order to correlate the physical

- and chemical properties of the catalysts with the catalytic behaviour.
- VI. Study different catalysts in a fixed bed reactor for reduction of nitrates improving the selectivity to nitrogen.
- VII. Study the catalytic hydrodechlorination of TCE in gas phase in order to find active and stable catalysts with high selectivity toward ethylene.

Chapter 3

Catalytic reduction of nitrates



UNIVERSITAT ROVIRA I VIRGILI
SELECTIVE HYDROGENATION CATALYSTS FOR ENVIRONMENTAL PROCESSES:
NITRATE AND CHLOROCOMPOUNDS REMOVAL
Noelia Barrabés Rabanal
DL: T-1539-2009/ISBN:978-84-692-4557-6

Introduction

1.1. Pollution problem of nitrates

Wastewater treatment has become a major social, technological, economical and political problem. Diffuse pollution of water resources from agricultural sources is a major environmental issue both in the European Union (EU) and abroad. Nutrients released in surface and ground - waters from cultivated fields and livestock exploitation are the main source of concern, together with pesticides. The main European legislation dealing with protection of water resources from agricultural pollution, nitrogen in particular, is the Nitrate Directive (ND) (EC, 1991). Developed later, the Water Framework Directive (WFD) (EC, 2000) is a broader concept for sustainable management of water resources[1]. In the EU15 countries nitrate contamination is a problem commonly identified. The main sources of nitrate excess are the over usage of fertilisers in agriculture as well as waste effluents from certain industries.

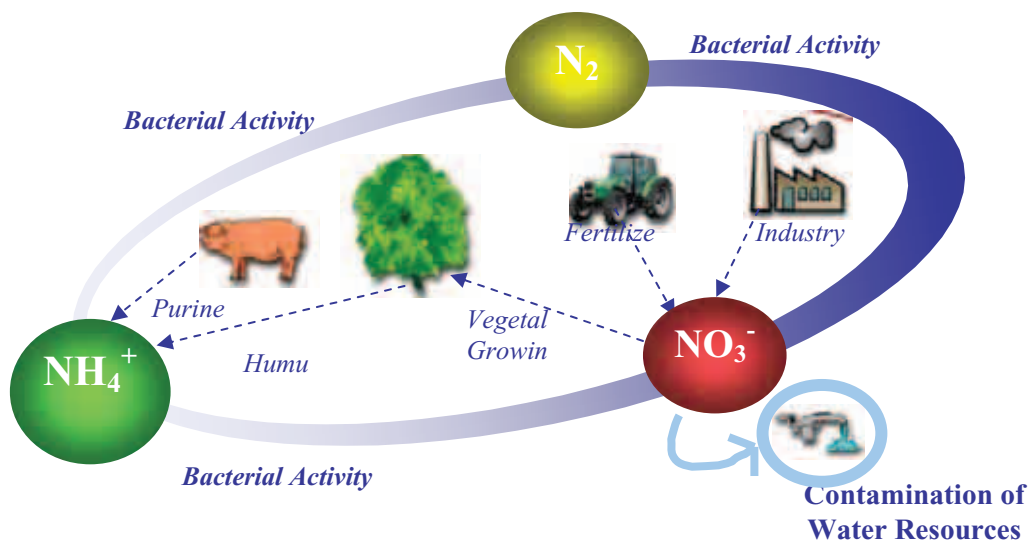


Figure 1.1. Nitrate life cycle

The nitrate anions compounds are proven to be harmful to the mammalian organisms. In the organism the nitrate is transformed to ammonium. An intermediate step is the partial reduction of nitrate to nitrite. The nitrite can cause a blue baby syndrome in the human and it is also a precursor to the carcinogenic nitrous amine[2-4].

The Nitrates Directive (91/676/EEC) aims to control nitrogen pollution and requires Member States to identify groundwaters that contain more than 50 mg/l nitrate or could contain more than 50 mg/l nitrate if preventative measures are not taken [1]. Monitoring data show that a nitrate concentration maximum is exceeded in around one third of the European groundwater bodies for which information is currently available (EEA 2003). The collected data show (Fig.1.2) that nitrate concentrations above 50 ppm are more frequently observed in Belgium, Spain, France, Germany, Denmark, Austria, the Netherlands and the UK[1].

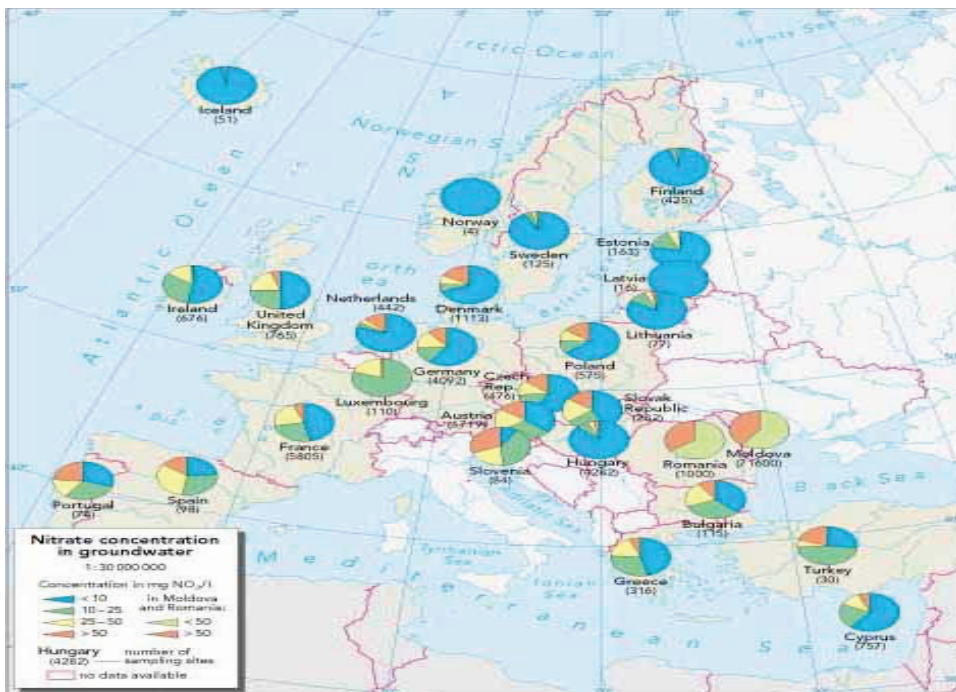


Figure 1.2. Levels of nitrates in groundwater in European countries [1]

These countries have extent zones of agriculture and related activities, which are the main sources of the problem. (see Fig. 1.3)

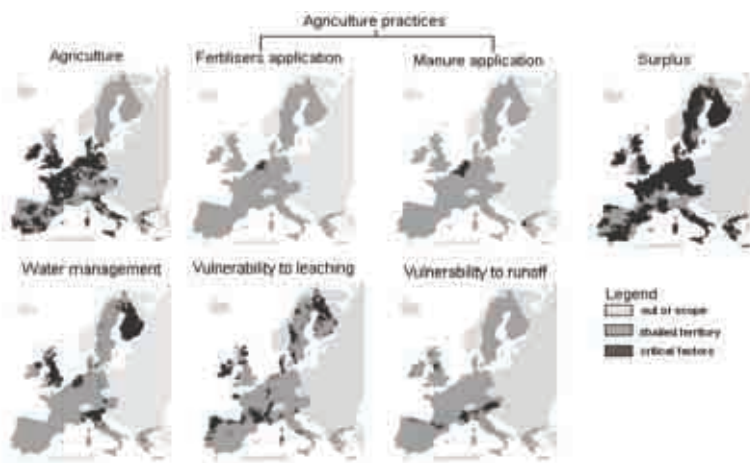


Fig. 6. Spatial distribution of the critical factors.

Figure 1.3. Spatial distribution of critical factors [5]

In front of this situation, one key approach of the Sixth Environment Action Programme of the European Community 2001-2010 is to "integrate environmental concerns into all relevant policy areas". For countries outside the EU the World Health Organisation (WHO) has as one its priorities that "all people, whatever their stage of development and their social and economic conditions, have the right to have access to an adequate supply of safe drinking water". To help achieve this they publish 'Guidelines on Drinking Water Quality' which countries should meet to ensure the health of their population. In this line, WHO recommends a maximum nitrate (NO_3^-) concentration of 10 mg/l, nitrite (NO_2^-) of 0.03 mg/l and ammonium (NH_4^+) of 0.4 mg/l in drinking water. Whereas the legal limits imposed within the EU are 50, 0.1 and 0.5 ppm for NO_3^- , NO_2^- and NH_4^+ , respectively.

1.2. Remediation Technologies

The purification of drinking water from various water sources generally combines a series of physical and chemical steps to eliminate the solid fraction, kill bacteria and reduce the level of chemical pollutants. Most of the processes include a strong oxidation step, based on the use of a strong oxidizing agent such as chlorine, sodium hypochlorite, ozone or hydrogen peroxide. These types of treatments lead to a decrease of the micro - organisms in water to an acceptable level; however the process also affects the chemical composition. Furthermore undesirable ions, such as nitrates, remain unaffected by the oxidative treatments [5].

The urge for the development of robust processes for the abatement of nitrates from water issued by the EEA was based on the observation of a continuous increase of the ion in the water basins. Fig. 1.3 shows the development of organic matter, phosphorus and nitrate in 15 rivers in the EU [1]. The figure 1.4 shows a dramatic decrease of phosphorus and organic matter from 1980 to 1995; however the amount of nitrate has greatly increased.

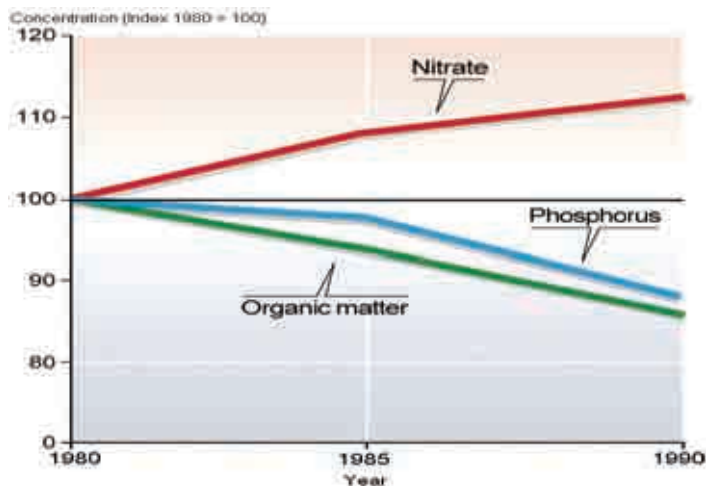


Figure 1.4. Nitrate, phosphorus and organic matter development in EU rivers during the 80's decade [1]

Nitrates are stable and highly soluble ions with a low potential for adsorption or coprecipitation. A number of process have been reported for the abatement of aqueous nitrates that includes physical-chemical, electrochemical, biological and catalytic methods. Physical-chemical processes are based on ion exchange, electrodialysis or reverse osmosis procedures that have the benefit of removing almost completely the pollutant without the introduction of other substances; however the process is not anion selective, which leads to changes in the water quality. Furthermore a secondary step is required for the destruction of the sludge containing the removed species since the process only removes the contaminants from the water. Electrochemical, catalytic reduction and bacterial degradation are more promising processes because convert nitrates to harmless N_2 .

Electrocatalytic removal of nitrates embraces a big part of the nitrogen electrochemistry [6-8]. The main disadvantages of the electrochemical methods are the low rate of the reduction and the production of undesirable side-products such as nitrites, ammonia and N_2O (greenhouse gas).

Biological treatment is highly effective for the removal of most contaminants.

Despite their success and cost effectiveness, biodegradation processes are inherently slow and do not allow for high degrees of removal. The sludge formed during biological treatment has to be disposed of either by landfilling or by burning, and the cost of these disposal methods should be accounted for. In addition, sludge disposal may pose environmental problems. Nitrate removal can also be achieved using chemical reduction by Fe(OH), which generates quantities of iron sludge and by powdered aluminium. Table 1.1 shows a summarized of the main technologies for nitrate removal with the advantages and disadvantages.

Table 1.1. Nitrate removal technologies[4]

	Ion Exchange	Reverse Osmosis	Biological Denitrification	Catalytic Reduction
<i>Fate of nitrate</i>	Absorbed & Concentrated	Concentrated (waste stream)	Transformed to N ₂	Transformed to N ₂
<i>Waste</i>	Waste Brine	Waste Brine	Bacterial Sludge	None
<i>Chemical Additives</i>	NaCl	H ₂ SO ₄ +base	EtOH+H ₂ SO ₄	H ₂
<i>% Efficiency in water purification</i>	95%-98%	75%-80%	98%	98-100%
<i>Flexibility in variable operation</i>	Medium	Medium	Low	High
<i>Energy Use</i>	Low	High	Medium	Low
<i>Type of operation</i>	Periodic regenerations	Continuous	Continuous	Continuous
<i>Odours</i>	No	No	Yes	No
<i>Sensibility to deactivation</i>	Medium	High	High	Medium
<i>Selectivity</i>	Low	Low	High	High
<i>Costs</i>	Medium	High	High	Low
<i>Disadvantages</i>	Generation of waste with anions		Bacterial sludge, complex operation, requirement of large installations	Formation of ammonia

In this sense, catalytic hydrogenation appears as the most promising technology. It offers several advantages as the fact that it can be performed under milder conditions (temperature and pressure). A detailed description of the advances achieved in this area is described below and is the focus of this study.

1.3. Catalytic hydrogenation of nitrates and nitrites

Hydrogenation of nitrate and nitrite over noble metal catalysts was for the first time reported in 1989 by Vorlop et al. [9]. In this study was demonstrated that nitrites are reduced by hydrogen on various hydrogenation catalysts, like palladium or platinum supported on alumina or silica, whereas these catalysts are inactive for nitrate reduction. The next study by Horold and Vorlop [10], “*screening for hydrogenation catalysts and the influence of reaction conditions on activity and selectivity*”, has represented the base for further studies. Several commercial catalysts with Pd, Pt, Ru, Ir and Rh for nitrite hydrogenation were tested. Whereas Ru, Ir and Rh catalyst showed poor activity with ammonia as the main product, Pd and Pt catalysts presented higher activity and selectivity. The best activity was achieved with Pt catalyst; however the formation of ammonia was higher than using Pd catalyst.

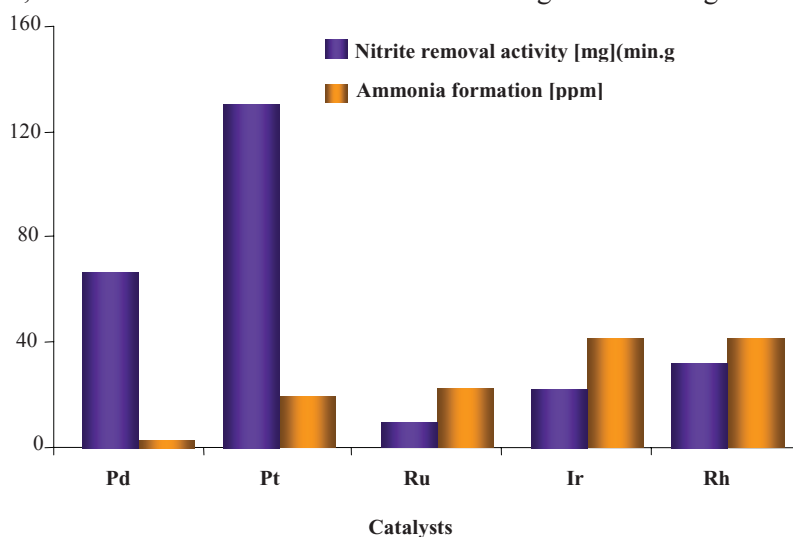


Figure 1.5. Activity and selectivity, in nitrite reduction, using commercial catalysts. Catalysts tested were 5%Pd/Al₂O₃, 5%Pt/Carbon, 5%Ru/Al₂O₃, 2%Ir/Al₂O₃ and 2%Rh/Al₂O₃ [5, 10]

In this way Pd catalyst was chosen for the optimization of other parameters as precursor salt or support. Three different precursors were tested (PdCl_2 , $\text{Pd}(\text{NO}_3)_2$ and $\text{Pd}(\text{NH}_3)_4(\text{OH})_2$) and the best performance was observed with the tetraaminopalladiumhydroxide. This optimum behaviour is presumably related to a better adsorption of the $\text{Pd}(\text{NH}_3)_4^+$ cation. The next point was to test several alumina and silica supports. The supports were chosen because of their different surface areas and pore size distributions, i.e., acid–base properties and/or support functionality were neglected. There are contrasting catalytic performances between the two types of supports. The alumina-based catalysts have a higher activity whereas the silica-based materials are highly selective towards N_2 . The alumina-supported catalysts showed a tendency to decreased ammonia formation as activity fell. On the other hand, Pd supported on silica showed small differences in overall catalytic properties [5]. The authors attribute the outstanding performances of these catalysts to their morphological properties, which limits the effects of diffusion [10].

A final aspect which might influence the performance of Pd catalysts in the removal of nitrites is the noble metal loading. The best value of selectivity was obtained with a Pd loading of 0.8% whereas the best activity was achieved with a 1%wt loading of the noble metal. It is relevant to emphasize the low ammonia formation at all Pd loadings, making them suitable for nitrite hydrogenation.

Despite of these catalysts were promising for the removal of nitrites, their activity in nitrate removal was very poor.

1.3.1. Bimetallic Catalysts

To reduce nitrates, it is necessary to activate the precious metal by addition of a promoter [11], that consists in a metal from the transition group of the periodic table (Cu, Ni, Fe, Sn, In, Ag) [12-15]. It is reported by Hörold et al. [16] that Pd hydrogenation catalysts doped by Cu represent the most active and selective

bimetallic solids for the transformation of nitrates to nitrogen. The main drawback of these solids is formation of the side product, ammonia, which is undesirable in drinking water.

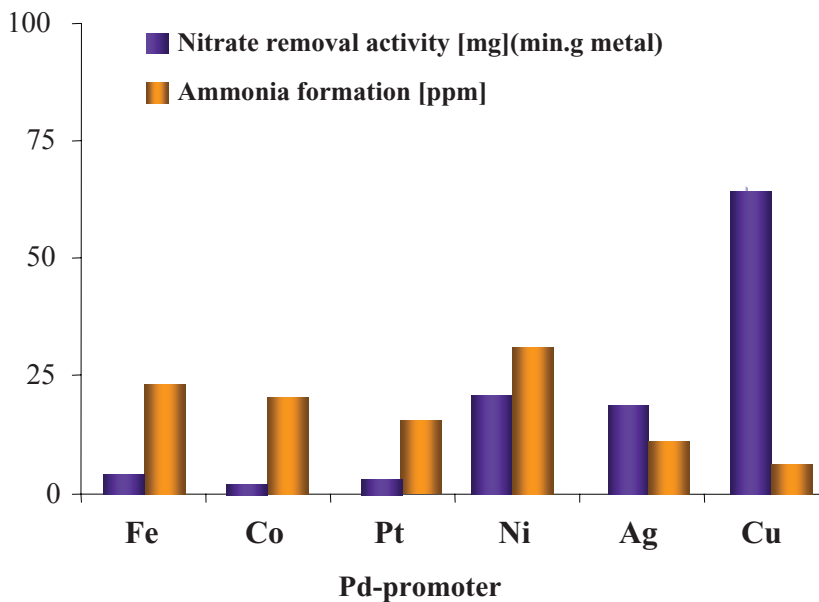


Figure 1.6. Catalytic activity of Pd catalysts with several promoters on alumina [5, 16]

Contrary with the results, Gauthard et al. [12] showed that silver-promoted noble metal catalysts have higher activity than copper-promoter catalysts, depending on the catalysts preparation protocol. The preparation method by catalytic reduction presented the most active catalysts compared to those resulting from classical methods such as co-impregnation or successive impregnation [17]. In terms of selectivity, the best promoter found by Prüsse et al. [18] was tin. Several ratios between noble metal and promoter has been studied, Gauthard et al. [12] found that the activity of palladium-based catalysts for nitrate reduction goes through a maximum for a promoter content about 50%.

Mainly γ -alumina has been used as support of these catalysts [19-22], but other kind of materials as TiO_2 [23-26], SiO_2 [27], ZrO_2 [28], SnO_2 [5, 29], zeolites[30-33], pumice [34], glass fiber[35], resins [36, 37], hydrotalcites [38, 39] and active carbon

[14, 40-43] have also been tested. All the studied catalysts showed minor changes in the overall catalytic performances, only active carbon presented high activity, selectivity and stability. Recently polymers materials have been employed as support in this reaction [44, 45].

The reduction of nitrate leads to the formation of hydroxide ion that causes an unavoidable increase of the pH value up to 10; this pH gradient is unacceptable for drinking water. Furthermore, basic pH induces a polarization of the support and has a repulsive effect on nitrates and nitrites, inducing a decrease of the activity and selectivity to nitrogen [9]. The factors as support, metal composition, preparative method an operation conditions have been discussed to provide insight into the catalytic selectivity. Another parameter studied was the reduction agent. Different solutions have been used to neutralize the hydroxides, like the addition of hydrochloric acid or carbon dioxide during the reaction together with hydrogen [29, 38, 46, 47] or the use of formic acid instead of hydrogen as reducing agent [9, 48]. In this case, the formic acid decomposition can be used as a source of hydrogen and carbon dioxide. Indeed, on a noble metal formic acid can be decomposed to hydrogen and CO₂. A competitive adsorption from coexist ions (SO₄²⁻, CO₃²⁻, HCO₃⁻, etc) on Pd-Cu active sites led to the decrease of catalytic activity and selectivity of nitrate [24, 34]. In this way bimetallic catalysts with satisfying nitrogen selectivity and activity remains challenging.

Another process parameter tested, in order to optimized activity and selectivity, was the configuration of the reactor. The process of catalytic nitrate reduction has been studied so far mostly in batch reactors for kinetics studies [5, 18, 28, 49-51]. Few investigations were published on the reduction of nitrates in continuous-flow reactors [40-42, 52]. In order to decrease or avoid the formation of ammonium ions, other strategies were also tested, e.g., the use of hydrogels of polyvinyl alcohol [53], membranes [28, 54], structured membranes [55] or cloths [56]. Another approach was the use of metal-doped acidic ion exchangers to generate an acidic environment

around the active sites [44]. Most of these efforts were more or less successful; however the selectivity toward nitrogen was still insufficient.

1.3.1.1. Reaction mechanism

The hydrogenation of nitrate on Pd-Cu catalyst has been proposed to have nitrite intermediates [34, 40, 51]. The Cu-Pd ensembles deposited on the supports can provoke the hydrogenation of nitrate to nitrite at the first step; subsequently, hydrogenation of nitrite to nitrogen and ammonia (second step) proceed only on Pd aggregates on the Cu-Pd catalysts. The hydrogenation of nitrite as critical step becomes therefore important in the selectivity to N_2 and NH_4^+ . The first work was from Wörnă *et al.* [51], that suggested this stepwise mechanism involving adsorption of nitrate on to a bimetallic site (Fig. 1.7), reduction to nitrite, desorption in to the aqueous phase and re-adsorption on a monometallic noble metal site where the final reduction to the end products (N_2 and NH_3) occurred.

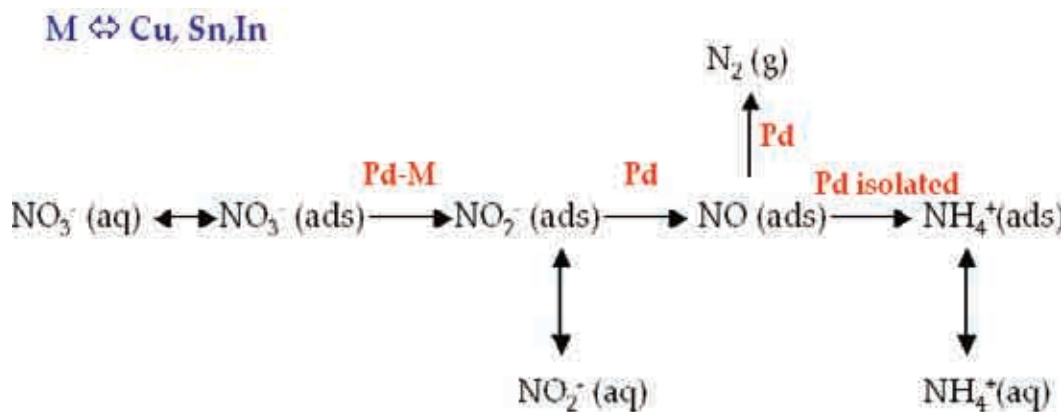


Figure 1.7. Scheme of the stepwise mechanism for the denitrification process involving bimetallic catalysts [51].

They suggested that, in the process of catalytic nitrate reduction, the key intermediate on the noble metal might be NO (ads). Yoshinaga *et al.* [40] went further and suggested the chemical environment of the active sites based on kinetic measurements and hydrogenation power of the species involved. They concluded that the overall selectivity of the nitrate hydrogenation is governed by the nitrite intermediate hydrogenation describing a process structure-sensitive after the first reduction step. Where the low coordinated Pd atoms, essentially Pd in high index planes, and isolated Pd atoms, formed due to terrace dilution by a second metal, are responsible for the formation of ammonium ion. Contrary to this results, Pintar [57] testing several Pd-Cu catalysts, show that nitrate reduction to nitrite is a structure-insensitive and that the overall reaction selectivity is strongly dependent on the amount of nitrites ion that accumulated in the liquid phase. It was also reported that the bimetallic character of clusters has no effect on the activity and selectivity in the liquid-phase nitrate reduction. As far as activity is concerned, Epron *et al.* [17] and Sá *et al.*[58], showed that an active bimetallic site requires only a close proximity between the two metals; an alloy is not a requirement. By close proximity, the authors indicate as a sufficiently short distance that allow the hydrogen activation which is performed on the noble metal sites, to the copper sites by simple surface migration by spill-over [5].

Palomares *et al.*[38] studied the use of copper hydrotalcites as support and active phase. The resulting catalyst was found to be more active and selective than common PdCu/Al₂O₃ catalyst. The results were related to the hydrotalcites capacity in concentrate anions between layers due to ionic forces and the decrease in ammonia formation was assigned to a decrease of the catalyst diffusion limitations. The mechanism proposed follow a similar stepwise proposed by Wärna *et al* [51] (Fig.1.7).

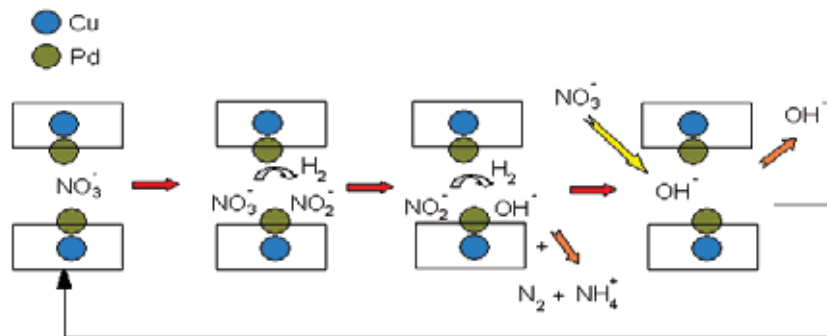


Figure 1.8. Mechanism of nitrates hydrogenation by Pd-Cu/hydrotalcites [38]

This results were confirm by Wang et al. [59]. The synthesis protocol for Pd-Cu/hydrotalcites were studied, the catalyst obtained by coprecipitation method showed higher adsorption and catalytic activity than the prepared by co-impregnation method. In addition by kinetics studies, was showed that the nitrate adsorption is described by the pseudo-second-order adsorption model with the chemisorption as the rate-limiting step. The experimental data of adsorption capacity was adjusted by Langmuir model, based on the assumption that the adsorption occurred on homogeneous surface sites. The reaction mechanism is proposed in Fig.1.8. When calcined catalyst was introduced into the nitrate solution, hydrotalcite structure was reconstructed (memory effect). Taking into account the existence of positive charges on the lamellae and also over external surface of hydrotalcite, nitrate may be intercalated rapidly between the brucite-like layers by electrostatic force and adsorbed on the external surface, which resulted in a high adsorption rate at initial time. Simultaneously, nitrate was reduced by Pd/Cu active sites to nitrite and then it is reduced further to nitrogen. During these reaction steps, the electroneutrality of the system was maintained by the OH^- anions produced.

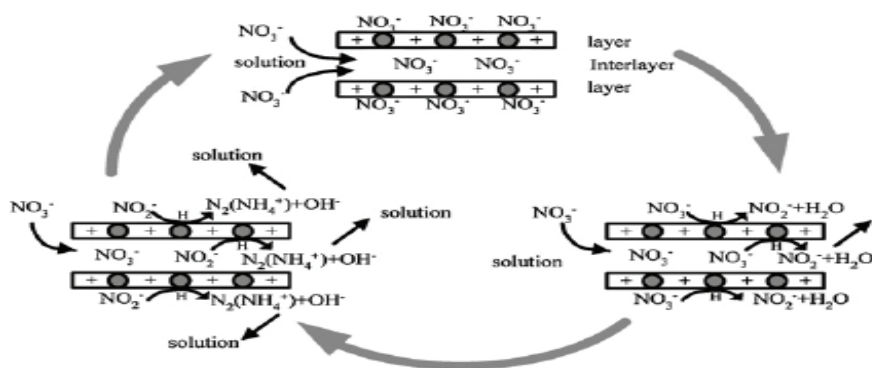


Figure 1.9. The reaction scheme for the catalytic hydrogenation of nitrate on hydrotalcites-supported Pd-Cu catalysts [59]

Recently Zhang et al. [26] reported that the size of the active sites could influence the hydrogenation selectivity. Since the hydrogenation of nitrite can be produced commonly on the monometallic palladium sites, the selectivity of nitrate hydrogenation will be determined by the size of palladium particles as well as the surface coverage of nitrogen species to reductant species. The nitrogen and ammonium formation mechanisms are dissimilar because the formation of nitrogen requires the presence of two nitrogen species adsorbed on close sites. Zhang et al. suggested that on bimetallic ensembles with size below 3.5 nm, the exposed palladium particle becomes too small to adsorb and activate two N species simultaneously for the formation of nitrogen (see Fig. 1.10). Oppositely, the hydrogenation of nitrite produced from nitrate will proceed. Since the formation of ammonium required only one N species, the size effect is not remarkable, and ammonium as byproduct was observed for all the systems. However, the formation of ammonium commonly results from the meeting of N species and hydrogen species on the surface of the active sites by a diffusion effect. Therefore, the selectivity was suggested to depend on the ratio of surface coverage of N species and hydrogen species [48, 50]. The higher the N:hydrogen ratio is, the higher the nitrogen selectivity will be [26].

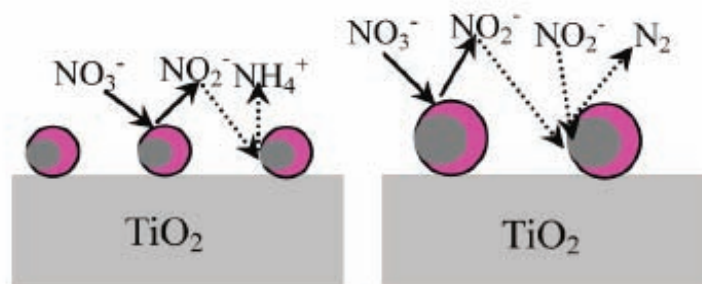


Figure 1.10. Selective hydrogenation mechanism of nitrate on the Pd-Cu/TiO₂ catalysts with different size of active phase: (left) < 3.5 nm; (right) > 3.5 nm. (Opink: Pd-Cu ensembles. Ogray: exposed palladium sites) [26]

Miyazaki et al. [60] studied the effect of the size and the dominant crystallite facets of the Pt particles supported on alumina, in the reduction of nitrites [60]. Different Pt nanoparticles morphologies were synthesized and tested in the catalytic hydrogenation of nitrites. The cubic nanoparticles catalysts were rich in Pt nanocrystals, bounded by low index surfaces relatively free of defects and the common catalysts were composed of polycrystalline Pt particles, rich in high index planes and surface defects. Cubic Pt particle presented lower activity than conventional catalyst but higher selectivity toward nitrogen. This was related with the fact that, the formation of N₂ would be favoured on the terrace sites of the noble metal crystallites because these sites have mild hydrogenation capabilities.

Recently, the in situ monitoring of nitrite reduction was performed by ATR-IR using Pd/Al₂O₃ catalyst [61]. The results showed that the adsorption of NO_{2(aq)}⁻ on H-Pd/Al₂O₃ produce NO_(ads), NH_{2(ads)} and NH₄⁺. These species are originated from the reaction with hydrogen on the palladium surface. Subsequent hydrogenation showed that NO_(ads) is converted into N₂, whereas the hydrogenation of NH_{2(ads)} yields NH₄⁺. The proposed reaction scheme by Ebbesen et al. is showed in Fig 1.11. Where nitrogen and ammonia are formed via two parallel ste-wise hydrogenation processes. This mechanism contradicts reaction schemes for the heterogeneous hydrogenation of nitrite proposed before, where NO has been studied as the intermediate in the

The apparent activation energy of the process was found to be 47 kJ/mol and the heat of nitrate adsorption 22 kJ/mol. The rather low activation energy confirmed the high efficiency and suitability of Pd-Cu catalyst for liquid-phase nitrate hydrogenation [5].

They also proposed that the kinetics of the catalytic removal of nitrates is consistent only with heterogeneously catalysed reaction steps involving ionic intermediates, which require different types of active sites; they discarded the possibility of heterogeneous-homogenous free radical mechanisms. The bimolecular reaction between adsorbed species was considered to be the rate-limiting step which they believed to occur via heterolytic electron transfer. Hence nitrate removal is directly proportional to the fractional coverage of the different sites by the reactants, as it is expected in the Langmuir adsorption model.

1.3.1.3. Influence of other ions in water

Most of the research on this field involved the use of deionised or distilled water with an inorganic salt as source of nitrate ions. It represents a simplified approach but not realistic medium such as conventional tap water. Pintar et al [46] studied the effect of water hardness and dissolved salts in the catalytic removal of nitrates.

The cation in the salt used as source of nitrates had been found to have an influence in the nitrate removal rate. The rate increased in the order: $K^+ < Na^+ < Ca^{2+} < Mg^{2+} < Al^{3+}$. It was concluded that the increase was related to catalyst properties and reaction conditions, taking in account the cations did not influence the nitrate adsorption constant. Hence it was found that the apparent surface reaction rate constant changed proportionally with the ionisation potential of a cation presented in the aqueous solution. Furthermore it was evident that the maximum concentration of accumulated nitrite ions decreased with the order: $K^+ > Na^+ > Ca^{2+} > Mg^{2+} > Al^{3+}$, which further leads to lower formation of ammonium ions. These were ascribed to an increase in the rate of desorption of hydroxide ions from the active sites as the

polarization ability of the cations in solution increased.

The catalysts were tested in waters containing inorganic ions such as Cl^- or SO_4^- and no effect was observed, neither an increase of the nitrate rate disappearance. The authors suggested that these ions, especially Cl^- , caused a possible modification in the concentration and strength of the Brønsted acidic sites, which partially neutralized the hydroxide ions produced. The experimental observations suggested that the permanent water hardness has no inhibitive effect on either the nitrate reduction or reaction selectivity. The only water contaminant which hinders the reaction is HCO_3^- ions. The inhibited effect was explained as a competitive adsorption on the active sites by these ions and nitrate since they are almost isostructural. Hence, catalytic hydrogenation is influenced only by ionic species structurally similar to nitrate ions.

Sa et al. [5] showed an influence of the water matrix on to the overall rate of nitrate disappearance. This is specially depicted for the case where equal concentrations of chloride and nitrate were presented in the test water. The presence of chlorides leads to a drop in activity of ca. 50% without significantly affecting catalyst selectivity. The drop in activity was ascribed to competitive adsorption on the active sites due to the similar net charge of the ions. The ‘poison’ was found reversible, i.e., the original catalytic performances were restored simply by washing the catalysts.

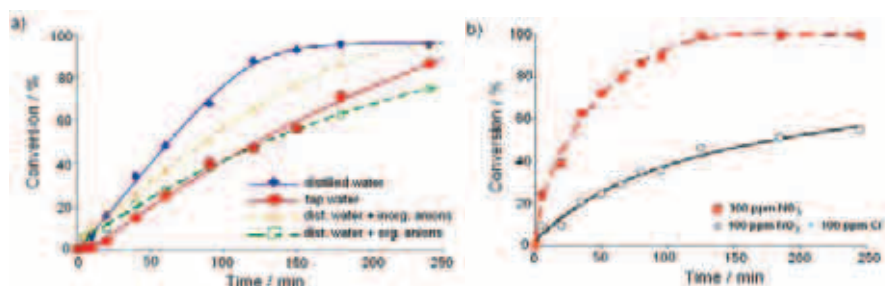


Figure 1.12. Effect of water matrix in the catalytic removal of nitrate at 298 K. a) different water sources and contaminants; b) effect of an isoconcentration of chloride and nitrate [5]

1.3.2. Monometallic Catalysts

Following the idea that, any catalyst containing a noble metal able to chemisorb hydrogen and a component with redox behaviour could catalyze nitrate reduction, the use of metal oxide supports (with redox properties) containing noble metal promoter had been studied.

Gavagnin et al. [29] tested the use of SnO₂. The results were catalysts with comparable activities to the bimetallic catalysts and with higher selectivity. It was related to the low surface area and low support porosity which prevents the occurrence of mass transfer limitations [5].

Epron et al. used CeO₂ as an active support [62]. Pd/CeO₂ catalysts showed high activity in the reduction of nitrates but poor selectivity to nitrogen (80% of the products was ammonia). This work presented how a partially reducible supports for the promotion of noble metal are able to reduce nitrates. The suggested reaction mechanism (Fig. 1.13) involved the oxygen vacancies work as active sites for the reduction of nitrates.

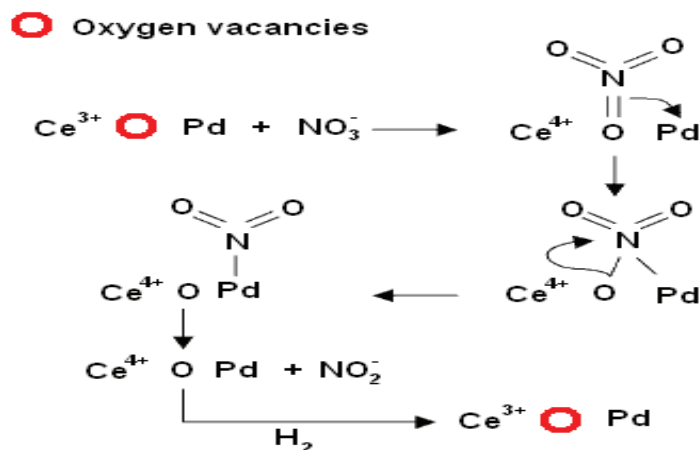


Figure 1.13. Mechanism of nitrates hydrogenation over Pd/CeO₂ [62]

Sá et al. [25] tested the use of TiO₂ in this process. High activity in the degradation of nitrates was observed but insufficient selectivity, in comparison with bimetallic catalysts. This behaviour was also observed with ceria catalysts before. However, TiO₂ catalysts did not show poisoning from CO₂ as the ceria catalysts did. Then, CO₂ can be co-feed to prevent the increase of the pH, which causes an increase on ammonia formation. Nitrate reduction on Pd/TiO₂ catalysts was suggested to be related with the presence of partially reduced TiO₂ deposited on top of Pd (strong support metal interaction (SMSI)) and Ti³⁺ centres [63, 64].

1.4. References

1. <http://reports.eea.eu.int>, <http://reports.eea.eu.int>.
2. Lecloux, A.J., *Catalysis Today*, 1999. **53**(1): p. 23-34.
3. Pintar, A., *Catalysis Today*, 2003. **77**(4): p. 451-465.
4. Centi, G. and S. Perathoner, *Applied Catalysis B-Environmental*, 2003. **41**(1-2): p. 15-29.
5. Sa, J., et al., *Applied Catalysis B-Environmental*, 2007. **73**(1-2): p. 98-105.
6. Polatides C., D.M., Kyriacou G., *Electrochi. Acta* 2005. **50**: p. 5237.
7. Dem D., K.E.E., Tarjan P. P. , Englehardt J. D. , *Chem. Eng. Technol*, 2004. **27**: p. 56.
8. Bockris J. O'M. , K.J., *J. Appl. Electrochem*, 1997. **27**: p. 623.
9. Vorlop, K.D. and T. Tacke, *Chemie Ingenieur Technik*, 1989. **61**(10): p. 836-837.
10. Horold, S., T. Tacke, and K.D. Vorlop, *Environmental Technology*, 1993. **14**(10): p. 931-939.
11. Prusse, U., M. Kroger, and K.D. Vorlop, *Chemie Ingenieur Technik*, 1997. **69**(1-2): p. 87-90.
12. Gauthard, F., F. Epron, and J. Barbier, *Journal of Catalysis*, 2003. **220**(1): p. 182-191.
13. Sa, J., et al., *Catalysis Letters*, 2005. **105**(3-4): p. 209-217.
14. Lemaigen, L., et al., *Catalysis Today*, 2002. **75**(1-4): p. 43-48.
15. Mikami, I., R. Kitayama, and T. Okuhara, *Catalysis Letters*, 2003. **91**(1-2): p. 69-71.
16. Horold, S., et al., *Catalysis Today*, 1993. **17**(1-2): p. 21-30.
17. Epron, F., et al., *Journal of Catalysis*, 2001. **198**(2): p. 309-318.
18. Prusse, U., et al., *Catalysis Today*, 2000. **55**(1-2): p. 79-90.
19. Pintar, A., et al., *Preparation of Catalysts Vii*, 1998. **118**: p. 127-136.
20. Batista, J., et al., *Applied Catalysis a-General*, 2001. **206**(1): p. 113-124.
21. Batista, J., A. Pintar, and M. Ceh, *Catalysis Letters*, 1997. **43**(1-2): p. 79-84.
22. Batista, J., et al., *Applied Catalysis a-General*, 2001. **217**(1-2): p. 55-68.
23. Gao, W.L., et al., *Catalysis Today*, 2004. **93-95**: p. 333-339.

24. Gao, W.L., et al., *Applied Catalysis B-Environmental*, 2003. **46**(2): p. 341-351.
25. Sa, J., et al., *Journal of Catalysis*, 2005. **234**(2): p. 282-291.
26. Zhang, F.X., et al., 2008. **112**(20): p. 7665-7671.
27. Garron, A., K. Lazar, and F. Epron, *Applied Catalysis B-Environmental*, 2005. **59**(1-2): p. 57-69.
28. Strukul, G., et al., *Catalysis Today*, 2000. **55**(1-2): p. 139-149.
29. Gavagnin, R., et al., *Applied Catalysis B-Environmental*, 2002. **38**(2): p. 91-99.
30. Nakamura, K., et al., *Chemistry Letters*, 2005. **34**(5): p. 678-679.
31. Rodriguez, R., et al., *Catalysis Today*, 2005. **107-08**: p. 100-105.
32. Nakamura, K., et al., *Applied Catalysis B-Environmental*, 2006. **65**(1-2): p. 31-36.
33. Pfaff, C., L. Melo, and P. Betancourt, *Reaction Kinetics and Catalysis Letters*, 2002. **77**(2): p. 263-266.
34. Deganello, F., et al., *Applied Catalysis B-Environmental*, 2000. **24**(3-4): p. 265-273.
35. Matatov-Meytal, Y., et al., *Applied Catalysis B-Environmental*, 2000. **27**(2): p. 127-135.
36. Pintar, A., J. Batista, and J. Levec, *Chemical Engineering Science*, 2001. **56**(4): p. 1551-1559.
37. Gasparovicova, D., et al., *Journal of Molecular Catalysis a-Chemical*, 2006. **244**(1-2): p. 258-266.
38. Palomares, A.E., et al., *Journal of Catalysis*, 2004. **221**(1): p. 62-66.
39. Wang, Y., J.H. Qu, and H.J. Liu, *Journal of Molecular Catalysis a-Chemical*, 2007. **272**(1-2): p. 31-37.
40. Yoshinaga, Y., et al., *Journal of Catalysis*, 2002. **207**(1): p. 37-45.
41. Barrabes, N., et al., *Applied Catalysis B-Environmental*, 2006. **62**(1-2): p. 77-85.
42. Matatov-Meytal, U. and M. Sheintuch, *Catalysis Today*, 2005. **102**: p. 121-127.
43. Sakamoto, Y., Y. Kamiya, and T. Okuhara, *Journal of Molecular Catalysis a-Chemical*, 2006. **250**(1-2): p. 80-86.
44. Gasparovicova, D., M. Kralik, and M. Hronec, *Collection of Czechoslovak Chemical Communications*, 1999. **64**(3): p. 502-514.
45. Maia, M.P., M.A. Rodrigues, and F.B. Passos, *Catalysis Today*, 2007. **123**(1-4): p. 171-176.
46. Pintar, A., M. Setinc, and J. Levec, *Journal of Catalysis*, 1998. **174**(1): p. 72-87.
47. Roveda, A., et al., *Inorganica Chimica Acta*, 2003. **349**: p. 203-208.
48. Prusse, U. and K.D. Vorlop, *Journal of Molecular Catalysis a-Chemical*, 2001. **173**(1-2): p. 313-328.
49. Pintar, A., et al., *Applied Catalysis B-Environmental*, 1996. **11**(1): p. 81-98.
50. Tacke, T. and K.D. Vorlop, *Chemie Ingenieur Technik*, 1993. **65**(12): p. 1500-1502.
51. Wa[dieresis]rn<<, J., et al., *Chemical Engineering Science*, 1994. **49**(24),

- Part 2): p. 5763-5773.
52. Pintar, A. and J. Batista, *Catalysis Today*, 1999. **53**(1): p. 35-50.
 53. Prusse, U., S. Horold, and K.D. Vorlop, *Chemie Ingenieur Technik*, 1997. **69**(1-2): p. 93-97.
 54. Ilinitch, O.M., et al., *Catalysis Today*, 2000. **56**(1-3): p. 137-145.
 55. Daub, K., et al., *Chemical Engineering Science*, 1999. **54**(10): p. 1577-1582.
 56. Matatov-Meytal, Y., et al., *Applied Catalysis B-Environmental*, 2001. **31**(4): p. 233-240.
 57. Pintar, A., J. Batista, and J. Levec, *Water Science and Technology*, 1998. **37**(8): p. 177-185.
 58. Sa, J. and H. Vinek, *Applied Catalysis B-Environmental*, 2005. **57**(4): p. 247-256.
 59. Wang, Y., et al., *Catalysis Today*, 2007. **126**(3-4): p. 476-482.
 60. Miyazaki, A., et al., *Chemical Communications*, 2005(29): p. 3730-3732.
 61. Ebbesen, S.D., B.L. Mojet, and L. Lefferts, 2008. **24**(3): p. 869-879.
 62. Epron, F., F. Gauthard, and J. Barbier, *Journal of Catalysis*, 2002. **206**(2): p. 363-367.
 63. Fagherazzi G. , B.A., Polizzi S. , Di Mario A. , Pinna F. , Signoretto M. , Pernicone N. , *Catal. Lett.* , 1995. **32**: p. 293.
 64. Baker R. T. K. , P.E.B., McVicker G. B. , *J. Catal*, 1984. **89**: p. 422.
 65. Liu, Y.Y., et al., *Topics in Catalysis*, 2003. **22**(3-4): p. 205-213.
 66. Achaerandio, I., et al., *Food Science and Technology International*, 2002. **8**(4): p. 239-242.
 67. Navarro, R.M., et al., *Topics in Catalysis*, 2004. **30-31**(1-4): p. 481-486.
 68. Goodby, B.E. and J.E. Pemberton, *Applied Spectroscopy*, 1988. **42**(5): p. 754-760.
 69. Palomares, A.E., et al., *Applied Catalysis B-Environmental*, 2003. **41**(1-2): p. 3-13.
 70. Bera, P., et al., *Chemical Communications*, 2001(10): p. 927-928.
 71. Yao, H.C. and Y.F.Y. Yao, *Journal of Catalysis*, 1984. **86**(2): p. 254-265.
 72. Ricote, S., et al., *Applied Catalysis a-General*, 2006. **303**(1): p. 35-47.
 73. Nagai, Y., et al., *Journal of Catalysis*, 2006. **242**(1): p. 103-109.
 74. Abid, M., V. Paul-Boncour, and R. Touroude, *Applied Catalysis a-General*, 2006. **297**(1): p. 48-59.
 75. Panagiotopoulou, P., et al., *Chemical Engineering Journal*, 2007. **134**(1-3): p. 16-22.
 76. Bae, J.W., et al., *Applied Catalysis A: General*, 2001. **217**(1-2): p. 79-89.
 77. Föttinger, K., R. Schlögl, and G. Rupprechter, *Chem. Commun.*, 2008(3): p. 320 - 322.
 78. Riguetto, B.A., Damyanova, S., Gouliev, G., Marques, C.M.P., Petrov, L., and Bueno, J.M.C., *J. Phys. Chem. B*, 2004. **108**(17): p. 5349 - 5358.
 79. Concepcion, P., et al., *Journal of the American Chemical Society*, 2004. **126**(17): p. 5523-5532.
 80. Binet, C., M. Daturi, and J.C. Lavalley, *Catalysis Today*, 1999. **50**(2): p. 207-225.
 81. Bensalem, A.M., J. C.; Tessier, D.; Bozon-Verduraz, J. *Chem. Soc. Faraday*

- Trans., 1996. **92**: p. 3233.
82. Concepción P., A.C., J. Silvestre-Albero, Topics in Catalysis, 2007. **46**(1-2): p. 31-38.
83. Kepinski, L. and J. Okal, 2000. - **192**(- 1): p. - 53.
84. Bera, P., et al., Chemistry of Materials, 2003. **15**(10): p. 2049-2060.
85. Meunier, F.C., et al., Applied Catalysis a-General, 2005. **289**(1): p. 104-112.
86. Holmgren, A., B. Andersson, and D. Duprez, Applied Catalysis B-Environmental, 1999. **22**(3): p. 215-230.
87. Jacobs, G., S. Ricote, and B.H. Davis, Applied Catalysis a-General, 2006. **302**(1): p. 14-21.
88. Yee, A., S.J. Morrison, and H. Idriss, Journal of Catalysis, 2000. **191**(1): p. 30-45.
89. Choung, S.Y., M. Ferrandon, and T. Krause, Catalysis Today, 2005. **99**(3-4): p. 257-262.
90. Lercher, J.A., C. Grundling, and G. EderMirth, Catalysis Today, 1996. **27**(3-4): p. 353-376.
91. Busca, G., Physical Chemistry Chemical Physics, 1999. **1**(5): p. 723-736.
92. Barbier, J., F. Marsollier, and D. Duprez, Applied Catalysis a-General, 1992. **90**(1): p. 11-23.
93. Bera, P., et al., Journal of Catalysis, 1999. **186**(1): p. 36-44.
94. Sa, J., Anderson, J.A., Applied Catalysis B-Environmental, 2008. **77**: p. 409-417.
95. Kundakovic, L., D.R. Mullins, and S.H. Overbury, Surface Science, 2000. **457**(1-2): p. 51-62.
96. An, W.Z., K.T. Chuang, and A.R. Sanger, Journal of Catalysis, 2002. **211**(2): p. 308-315.
97. D'Arino, M., F. Pinna, and G. Strukul, Applied Catalysis B-Environmental, 2004. **53**(3): p. 161-168.
98. Melendrez, R., et al., Journal of Molecular Catalysis a-Chemical, 2000. **157**(1-2): p. 143-149.

UNIVERSITAT ROVIRA I VIRGILI
SELECTIVE HYDROGENATION CATALYSTS FOR ENVIRONMENTAL PROCESSES:
NITRATE AND CHLOROCOMPOUNDS REMOVAL
Noelia Barrabés Rabanal
DL: T-1539-2009/ISBN:978-84-692-4557-6

Experimental

2.1. Characterization Techniques

i) Crystallographic analysis

X-ray diffraction (XRD) is by far the most important experimental tool in the investigation of crystal structure of solids. A collimated x-ray beam is incident on a specimen and is diffracted by its crystalline phases.



The average crystallite size of a poly-crystalline material can be evaluated from measuring the broadening of the Bragg peaks that the material causes in an X-ray diffractogram. Powder X-ray diffraction patterns of the different samples were obtained with a Siemens D5000 diffractometer using nickel-filtered Cu $K\alpha$ radiation. The patterns were recorded over a range of 2θ angles from 10° to 90° and crystalline phases were identified using the Joint Committee on Powder Diffraction Standards (JCPDS) files.

ii) Specific surface area measurements

The BET analysis was carried out in a Micromeritics ASAP 2010 apparatus. The surface BET area was determined by $N_2(g)$ adsorption at a single- and multi-point partial pressures of $N_2(g)$. Prior to the physisorption



measurements, the samples were outgassed for at least 30 min at 120°C under He. The instrument uses a flowing-gas technique, in which the analysis gas flows into both the sample and blank tubes at the same time. The delivery rate of the gas into the sample tube is controlled by the rate, at which the sample can adsorb the gas onto the surface; the rate of flow into the balance tube is controlled to give the same pressure. As the sample adsorbs gas, the pressure tends to drop in the sample tube. A rapid response pressure balancing system continuously restores the pressure balance between the tubes by admitting more gas into the sample side. The result is that the instrument maintains the pressure constant over the sample, while varying the rate of gas delivery to match the adsorption rate.

iii) Metallic dispersion

The hydrogen chemisorption analysis was carried out in a Micromeritics ASAP 2010 apparatus. Samples were previously reduced in the same conditions in which the catalysts were prepared. After reduction, the hydrogen on the metal surface was removed with 30 ml/min of He for 30 min at 683 K. The sample was subsequently cooled to 303 K under the same He stream. The chemisorbed hydrogen was analysed at 343K using the adsorption-backsorption isotherm method.

iv) Reducibility studies

Temperature programmed reduction (TPR) studies of the samples were performed using a TPD/R/O 1100 (ThermoFinnigan) equipped with a thermal conductivity detector (TCD) and coupled to a mass spectrometer QMS 422 Omnistar.



Before the TPR, the sample (around 100 mg) was dried under flowing helium (20 ml/min) at 120 °C for 24 h. After that, the reduction process was carried out between room temperature and 800 °C at a heating rate of 20 °C/min flowing the reducing gas mixture (5% H₂ in argon with a flow of 20 ml/min).

v) FTIR Spectroscopy

The Fourier transformed infrared (FT-IR) spectra were recorded on a Bruker IFS 28 instrument with a resolution of 4cm⁻¹. The spectrometer cell is connected to a vacuum system working in the 10⁻⁶ mbar range and to a heating system. The cell can be used for in situ



pre-treatments of samples and adsorption of gases. The samples were pressed into self-supporting wafers that were placed inside a ring furnace in the vacuum cell. The catalysts were reduced in situ using 500 mbar of pure H₂. The catalysts were

heated until 300°C in hydrogen atmosphere using a temperature ramp of 10°C/min and kept at that temperature for 30 min. After the reduction, the cell was evacuated for 30 min. The CO adsorption measurements were carried out using 5mbar of pure CO.

vi) XPS Spectroscopy

X-ray photoelectron spectroscopy (XPS) data were acquired in a VG Escalab 200R equipped with a hemispherical electron analyzer operating in a constant pass energy mode. The background pressure in the analysis chamber was kept below 7×10^{-9} mbar during data acquisition. All the spectra were signal-averaged for at least 80 scans and were taken in increments of 0.1 eV with dwell times of 50 ms.

vii) Morphology study

The morphology characterization, along with the elemental distribution and



homogeneity, of the synthesized materials were carried out via scanning electron microscopy (SEM, JEOL JSM-6400) operated at an accelerating voltage in the range of 30-35kV, a work distance between 7-9 mm and a magnification factor till 40.000 to 50.000. Additionally, EDS (Oxford Link GEM) was used for the compositional analysis and for the distribution analysis of the doped



cations. Furthermore, transmission electron microscopy (TEM) observations were acquired on JEOL JEM-2000EX II operated at 80kV.

2.2. Set-up equipment

A simplified diagram of the experimental setting is shown in Figure 2.1. The catalytic reduction of nitrate was performed in a fixed-bed reactor. The liquid feed solution with 60 mg/l of nitrate ions was prepared by dissolving NaNO_3 in Milli Q water and introduced to the reactor by a positive displacement pump (Milton Roy LM1), which is able to work in the range from 20 to 380 ml/h. The gas flow is adjusted by mass flow controller (Mangert Wiltman).

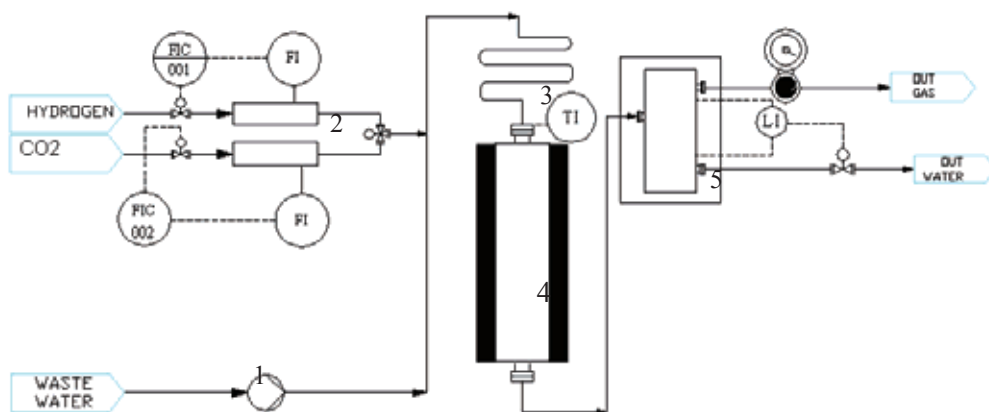


Figure 2.1. Experimental equipment, 1: pump; 2: Mass-Flow Controllers; 3: Pre-Heater; 4: Reactor; 5: Gas-liquid separator.

The tubular reactor, 25 cm long and $\frac{1}{2}$ " OD, is placed in an oven coupled with temperature control system. The reactor was filled with 1g of catalyst. The working pressure is adjusted by a back pressure valve fixed on the end of the gas line. Tubing, fittings and valves of the catalytic system are made of stainless steel 316L. The experimental conditions are listed in the Table 1. In some experiments with CeO_2 catalysts a CO_2 gas was added to the hydrogen flow in order to buffer the pH of the solution.



The reaction products were analyzed by the HPLC coupled with conductivity detector (Shimatzu). Nitrate and nitrite concentration were determined after separation on a Shim-pack IC-A1S column

at 40°C using a conductivity detector. Ammonium ions were quantified using a Shodex IC YK-421 column at 40°C coupled with a conductivity detector.

Table 2.1. Experimental conditions

Experimental conditions during the catalytic denitrification experiments	
Mass of catalytic bed, g	1
Reaction temperature, °C	25
Operating pressure, bar	1
Gas flow rate (H ₂), ml/min	3
Gas flow rate (CO ₂), ml/min	1
Liquid flow rate, ml/h	70
Nitrate feed concentration, mg/l	60
Initial feed pH	5.5

Active carbon catalysts

In the present work different groups of catalyst have been tested. Initially, the activity and the selectivity of two pairs of bimetallic catalysts, Pt-Cu and Pd-Cu, supported on active carbon have been studied. Optimal proportions of Pt-Cu and Pd-Cu in bimetallic catalysts on activated carbon, obtained by wetness impregnation, have been found. Besides, novel catalysts obtained from copper nanoparticles doped with Pd or Pt and supported on activated carbon, have also been studied. For all catalysts the Pt-Cu pair seems to be more selective in the transformation of the nitrates ions to nitrogen compared to Pd-Cu pair. Then bimetallic (Pt-Cu) and monometallic (Pt) catalysts supported on ceria with several proportions of metals have been tested in this process, showing high activity to nitrate reduction but with considerable concentrations of undesired ammonium ions. Considering the noble metal amount, the bimetallic nanosphere catalysts are more active (between 20 and 50) than the impregnated ones. The catalysts have been characterized by hydrogen chemisorption, BET, X-ray diffraction (XRD), scanning electron microscopy (SEM), transmission electron microscopy (TEM) and X-ray photoelectron spectroscopy (XPS) analysis. During the reaction, in active carbon supported catalysts, a considerable amount of the noble metal in its oxidised form has been detected. Based on these results an additional step to the generally accepted reaction mechanism of the nitrate reduction has been proposed. Finally, the Pt-Cu impregnated on active carbon catalysts has been tested in continuous denitrification of groundwater sources contaminated by nitrate ions using a three-

phase reactor. The obtained conversions were above 70% without the generation of the undesired nitrite and ammonium ions. The experiments have been continued for more than a month without any significant decrease of the catalytic activity.

3.1. Catalysis Synthesis

The active metals were supported on active carbon- NoritRox 0.8 with a BET surface area of 790 m²/g and with an average particle diameter of 0.1mm. Two main procedures have been followed for the bimetallic catalyst preparation. Firstly, the dried support, was impregnated by incipient-wetness technique with an aqueous solution of the corresponding noble metal salts (H₂PtCl₆; PdCl₂). After that, the samples were dried at 120 °C for 24 h and then reduced at 350°C in hydrogen flow for 3 h. The amount of the noble metal was maintained constantly at 1% of weight with respect to the support for all the catalysts. Then, at room temperature, the materials were impregnated with an aqueous solution of copper nitrate. The amount of copper was arranged from 0.05 to 5 wt% with respect to the support. After that, the sample was dried at 120 °C for 24 h and reduced again at 350 °C in hydrogen flow for 3 h. The materials obtained from this procedure are called impregnated catalysts (IC).

The second path for catalysts preparation consists of an initial synthesis of copper nanoparticles (nanospheres) following the procedure described by Xia et al. [65]. Once obtained, an ethanol solution of copper nanospheres was mixed with an aqueous solution containing appropriate amount of Pd or Pt salts. The mixture was stirred for 2h at room temperature under inert atmosphere. The corresponding noble metal is reduced by red-ox reaction with the copper nanoparticles, where it is deposited. Then, active carbon was impregnated with the obtained suspensions of Pt-Cu or Pd-Cu nanospheres by incipient- wetness technique. Finally, the materials were dried and then reduced under hydrogen flow at 350 °C for 3 h. The catalysts obtained following this second route were called nanosphere bimetallic catalysts

(NSBC). The amount of bimetallic nanoparticles impregnated on active carbon were 5 wt% with respect to the support. The atomic ratios between noble metal and copper in the nanospheres were 1:2700 and 1:670. These values were roughly estimated to correspond to an atomic ratio of copper:noble metal on the surface of the nanosphere of 1:4 and 1:1, respectively.

Four NSBC catalysts have been prepared and labelled as Cu-Pt 4:1 NSBC, Cu-Pt 1:1 NSBC, Cu-Pd 4:1 NSBC and Cu-Pd 1:1 NSBC. The percentage of weight of noble metal (Pt or Pd) in these catalysts were around 0.0057 wt%, 0.023 wt%, 0.003 wt% and 0.0125 wt%, respectively.

3.2. Results and discussion

3.2.1. Characterization results

In order to study the reducibility of copper nitrate precursor on the support (activated carbon) a TPR analysis was performed. Figure 3.1 shows the TPR profile of a sample containing 5 wt% of copper nitrate precursor, as well as a TPR of support as a blank test. This Figure shows that the reduction of copper nitrate precursor is in the range of 200°C-400°C, under the experimental conditions of TPR equipment. A reduction peak is also observed at higher temperatures (around 650 °C) that can be attributed to the reduction of oxygen species of the support, confirmed by the blank test.

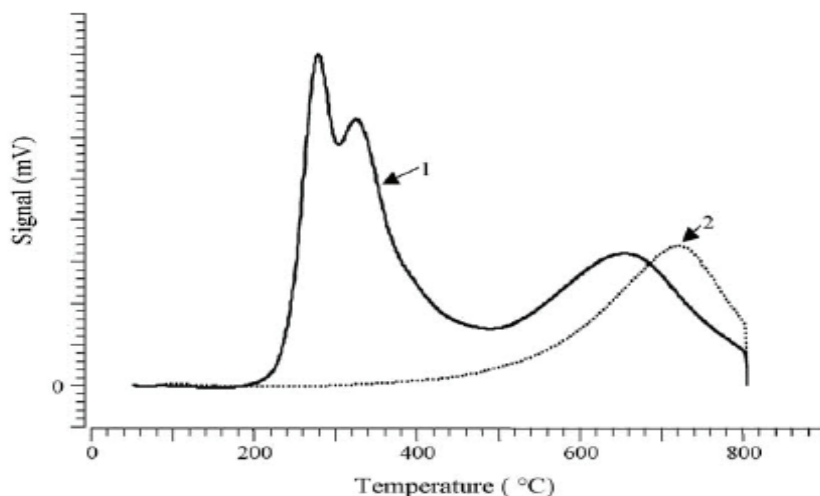


Figure 3.1. TPR profile; 1: 5%wt Cu/AC and 2: AC

The results of the metal areas for Pt-Cu impregnated catalysts (IC) are presented in Table 3.1. With the addition of 0.05 wt% of copper an increase of both metal area and Pt dispersion is observed. However, when the addition of copper increased the metal area and Pt dispersion decreased. A drastic reduction of Pt metal area and dispersion with respect to pure Pt catalyst was observed for 1 wt% of copper. This fact indicates that copper is coating the Pt particles.

Table 3.1. Results of hydrogen chemisorption for Pt-Cu impregnated catalysts.

Catalyst	Pt, wt %	Cu, wt %	Metal area		
			m^2/g sample	m^2/g metal	dispersion, %
IC-1	1	0	0.92	92	37.2
IC-2	1	0.05	1.15	115	50.2
IC-3	1	0.1	0.79	79	31.8
IC-4	1	0.3	0.21	21	8.7
IC-5	1	1	0.08	8	3.2

The metallic areas of Pd-Cu catalysts (1wt% of Pd and a copper amount between 0-1 wt %) have been also measured. No significant differences have been found in metal areas and metal dispersion for these samples. This means that there is no substantial overlaying of copper on the surface of palladium. The metal areas for Pd-Cu impregnated samples are around 74 m² per gram of palladium. This result suggests that the reduction mechanism of copper when deposited on the Pd-AC support is different from the case of Pt-AC.

The results from X-ray photoelectron spectroscopy of some fresh and used catalysts including electron binding energies and atomic percentages (in parenthesis) are summarised in Tables 3.2 and 3.3, respectively. The binding energies (BE) of carbon have values around 284.9 and 286.3 eV. The main part of carbon is in reduced form (284.9 eV), while a minor part (between 22-27%) is in oxidised form (BE around 286.3 eV), that can be attributed to the presence of oxygen species such as lactones, quinones, carboxylic acids, etc. that are common on the surface of activated carbon [66]. This fact has been also confirmed by TPR in Figure 3.1. Tables 3.2 and 3.3 also show the XPS data for Cu 2P_{3/2}. The binding energy value around 934.8 eV is characteristic of Cu²⁺ species in CuO, while the value around 932.8 indicates the presence of Cu⁰ [66-68]. For fresh catalysts, copper is in reduced form. This fact is in agreement with the TPR results which indicate that the reduction process of copper nitrate supported on activated carbon begins at temperatures as low as 200 °C.

Surprisingly, for the used impregnated bimetallic catalysts containing platinum (IC-4 and IC-5 samples) all the copper is in the form of Cu²⁺. Similar results are observed for the used Pd-Cu impregnated catalysts (not shown in Table 3.3). However for used nanospheres catalysts containing platinum or palladium a great part of the copper are in the reduced state which means that the regeneration capability of the noble metals for these catalysts is higher. Besides, when increasing the noble metal content the amount of copper in the reduced state increases. It is important to note the differences between Pd and Pt in NSBC samples.

Table 3.2. Binding energies (eV) of some Cu-Pt(Pd) used catalysts.

<i>Sample</i>	<i>C 1s</i>	<i>Cu 2p_{3/2}</i>	<i>Pd 3d_{5/2}</i>	<i>Pt 4f_{7/2}</i>
IC-4	284.9 (78)			71.8 (67)
	286.3 (22)	934.8 (100)		74.1 (33)
IC-5	284.9 (78)			71.6 (62)
	286.3 (22)	934.8 (100)		74.0 (38)
Cu-Pt 4:1 NSBC	284.9 (73)	932.9 (54)		71.6 (59)
	286.3 (27)	934.8 (46)		74.2 (41)
Cu-Pd 4:1 NSBC	284.9 (73)	932.8 (45)	335.4 (45)	
	286.2 (27)	934.9 (55)	337.3 (55)	
Cu-Pt 1:1 NSBC	284.9 (73)	932.8 (76)		71.5 (54)
	286.3 (27)	934.9 (24)		74.1 (46)
Cu-Pd 1:1 NSBC	284.9 (74)	932.8 (61)	335.3 (45)	
	286.3 (26)	934.8 (39)	337.2 (55)	

When compare the samples with the same proportion of noble metal, the amount of reduced copper is higher for the samples containing Pt than for the samples containing Pd. These results indicate that under same experimental conditions, i.e. the catalytic reduction of nitrate, platinum more easily reduces copper compared with palladium.

Tables 3.2 and 3.3 also show the electron binding energies of Pd 3d_{5/2} for fresh and used NSBC catalysts, respectively. For fresh catalysts all the Pd is in its reduced form (B.E. around 335.4 eV). However, A significant part of noble metal (around 55%) is found in the oxidised state-Pd (II) (binding energy around 337.3 eV) for the used catalysts. The amount of Pd (II) seems to be independent of the palladium

content in the sample. The presence of Pd (II) in Cu-Pd hydrotalcites catalysts during the reduction reaction of nitrates have been reported by Palomares et al. [69].

Table 3.3. Surface atomic ratios determined by XPS for some used catalysts.

Sample	Cu/C x 10 ³	Pt/C x 10 ³	Pd/C x 10 ³	Cu/Pt(Pd)
IC-4	3.45	1.08	-	3.2
IC-5	14.53	1.16	-	12.5
Cu-Pt 4:1 NSBC	14.14	0.16	-	36.9
Cu-Pd 4:1 NSBC	8.85	-	0.27	32.8
Cu-Pt 1:1 NSBC	4.12	0.39	-	25.7
Cu-Pd 1:1 NSBC	7.81	-	0.34	23.0

The last column in Table 3.2 and 3.3 shows the binding energies values of Pt 4f_{7/2} for some fresh and used catalysts, respectively. Two forms of the noble metal are identified, metallic platinum (around 71.6 eV) and Pt (II) (around 74.1 eV). For fresh catalysts all the platinum is in its reduced form, while an important amount of platinum is in the oxidised form for used catalysts.

Table 3.3 shows the surface atomic ratios determined by XPS for IC-4, IC-5 and nanospheres used catalysts. For impregnated catalysts (IC-4 and IC-5), when the copper content increases the atomic ratios of Cu/carbon and Cu/Pt increase, while the Pt/carbon ratio remains practically constant. The Cu/Pt ratio increased from 3.2 for 1wt%Pt-0.3wt%Cu (IC-4 catalyst) up to 12.5 for the 1wt%Pt-1wt%Cu (IC-5 catalyst). Taking into account the amount of Pt and Cu in the samples, the atomic weight ratio between Pt and Cu (around 3), and the important decrease of Pt dispersion detected by hydrogen chemisorption for these samples after copper impregnation (see Table 3.2), we can conclude that copper is well dispersed on the

surface of the support as well as an important part of Cu is deposited on the noble metal.

Figure 3.2 shows a SEM image of isolated nanospheres. The average particle size was around 350 nm. It should be mentioned that no losses of the metal phase and morphological change have been observed during the nitrate reduction process.

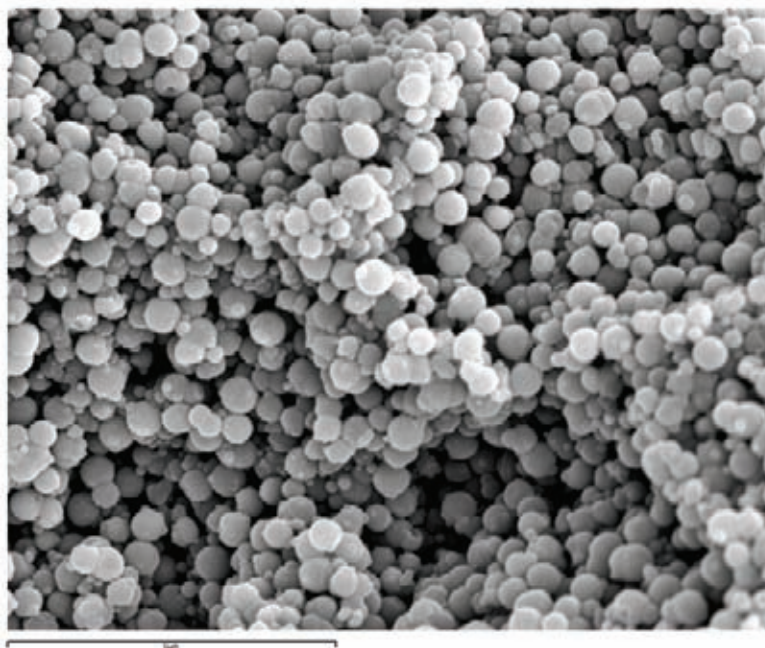


Figure 3.2 SEM image of copper nanospheres.

For nanosphere bimetallic catalysts, as mentioned in the previous section, the atomic ratios between noble metal (Pt or Pd) and copper in the nanospheres were 1:2700 and 1:670. Considering that all the noble metal is deposited on the copper nanosphere surface, we can estimate the atomic ratio between noble metal and copper in the surface of bimetallic nanosphere. This atomic ratios were roughly estimated to represent 1/4 and 1/1 of the surface copper atoms. However the results from XPS for Cu/ Pt and Cu/Pd ratios detected by XPS for Cu-Pt 4:1 NSBC, Cu-Pd 4:1 NSBC, Cu-Pt 1:1NSBC and Cu-Pd 1:1 NSBC catalysts were 36.9, 32.8, 25.7 and 23.0, respectively. This apparent contradiction could be explained taking into

account that XPS detects several atomic layers (about 1 nm in depth). So, the XPS results show that Pt and Pd are very well dispersed on the surface of copper nanospheres.

3.2.2. Catalytic activity

3.2.2.1. Impregnated bimetallic catalysts (IC)

The influence of the copper amount on nitrate conversion for 1wt%Pt-Cu catalysts (wt% of copper between 0.05% up to 5%) at steady state conditions (after 1 day of reaction) is shown in Figure 3.3. There was an increase in the catalytic activity when the copper content increases until 0.3 wt %. Then for higher copper contents a slight decrease of conversion is observed. The maximum activity obtained for 1%Pt-0.3%Cu (IC-4 catalyst) corresponds to an atomic ratio Cu/Pt of around 1 and is in accordance with the results cited by Epron et al. [17] for the same metals deposited on alumina carrier. The low activity of nitrate elimination observed for 1%Pt-0.05%Cu IC (around 10%) is very similar that the obtained by the 1%Pt-0%Cu IC catalyst (free copper). This indicates that the activity is mainly due to the Pt.

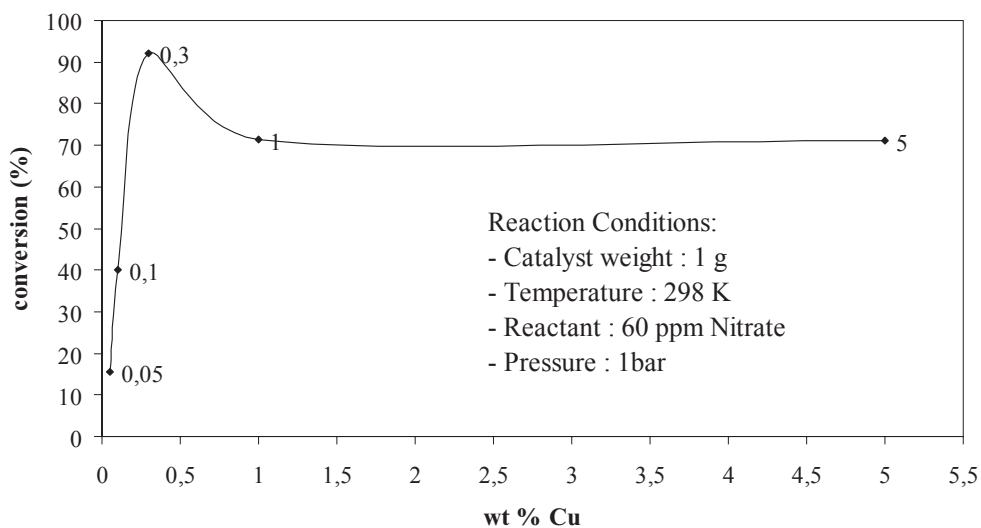


Figure 3.3 Nitrate conversions, at steady state, as a function of the copper load for impregnated catalysts

In order to compare the catalytic behaviour of Pt-Cu with Pd-Cu impregnated catalysts, and considering that the highest performance for platinum catalysts was obtained for a copper amount of 0.3 wt % and 1wt %, two palladium samples (1%Pd-0.3%Cu IC and 1%Pd-1%Cu IC) have been tested in the continuous nitrate reduction process. The results in terms of nitrate conversion as a function of the reaction time are presented in Figure 3.4. The experimental conditions were similar to that of the Pt-Cu bimetallic catalysts. An increasing of activity, from 50% to 65% of nitrate reduction can be noted for the catalyst with higher copper content. This behaviour is a little different from that of the Pt-Cu pair, where maximum activity was obtained, corresponding to the 0.3 wt % of copper. On the other hand the hydrogen chemisorption analysis has shown that there is no significant covering of the palladium by copper in contrast with the results obtained for Pt-Cu catalysts.

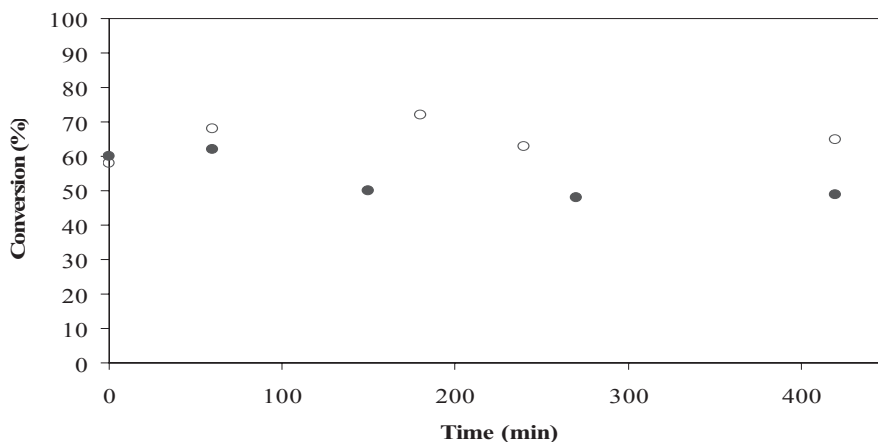


Figure 3.4 Nitrate conversion versus reaction time for Pd-Cu impregnated catalysts (● 1%Pd-0.3%Cu IC, ○ 1%Pd-1%Cu IC)

An important feature is that for all the Pt-Cu catalysts the liquid product is completely free of nitrite and ammonium ions so that the reduced nitrate is completely transformed to nitrogen. In the case of the Pd-Cu bimetallic pair it should be mentioned that nitrogen is not the unique product of the nitrate transformation as in the case of Pt-Cu. Comparative results of both bimetallic catalysts are presented in Figure 3.5. As mentioned above, the Pt-Cu catalysts are

selective for nitrate reduction, leading to nitrogen as a single product. In the case of Pd-Cu bimetallic catalysts a significant amount of nitrite was obtained, for the more active one (1%Pd-1%Cu IC) more than half of the converted nitrate was transformed to nitrite (around 20 mg/l). It should be also mentioned that in the hydrogenation of nitrate using both Pt-Cu and Pd-Cu impregnated catalysts supported on active carbon no ammonium was detected.

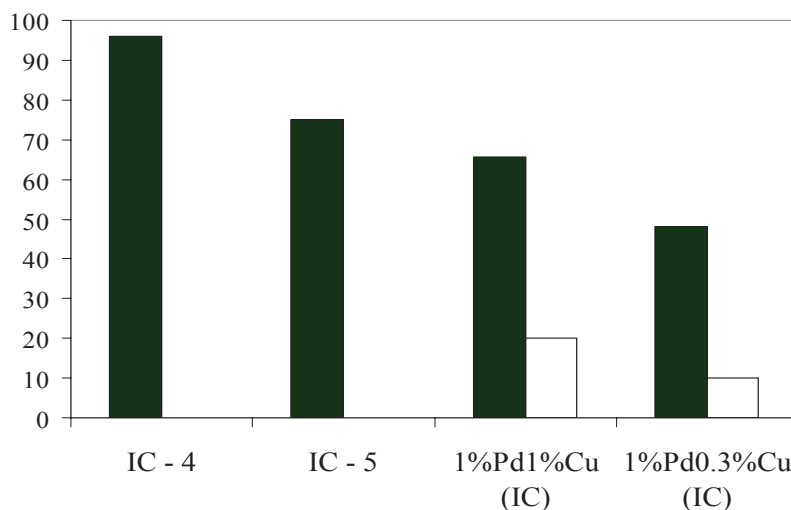


Figure 3.5 Nitrate conversion and selectivity to nitrite for several impregnated catalysts. [■ NO_3^- conversion (%), □ NO_2^- concentration (mg/l)].

3.2.2.2. Nanosphere bimetallic catalysts (NSBC)

One of the objectives with the employment of copper nanospheres as catalysts is that the noble metal is deposited on the external surface of the copper nanoparticles with an exhaustive control, so the amount of noble metal can be minimised. This fact is of great interest from an economical point of view because there is a reduction of the noble metal content between 40 and 350 times with respect to the impregnated catalysts.

Figure 3.6 shows the results for nitrate reduction of Cu-Pd1:1 NSBC catalyst. This Figure shows that the activity of the catalyst slightly increases with the reaction time and complete conversion of nitrate is reached after 7h of run. On the other hand, the

nitrates are mainly transformed to nitrites. These results are in agreement with Pd-Cu impregnated catalysts, indicating that palladium catalysts show a low selectivity to nitrogen.

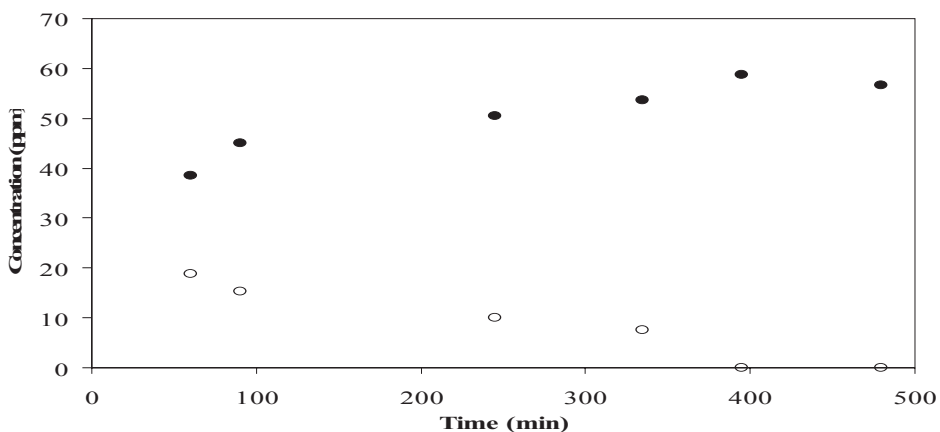


Figure 3.6 Nitrate and nitrite concentrations versus reaction time for Cu-Pd1:1 NSBC catalyst. [● NO₂⁻, ○ NO₃⁻]

Figure 3.7 illustrates the results obtained for Cu-Pt 4:1 NSBC. In this case the catalyst demonstrates a more stable activity in nitrate reduction during testing. An important point to be mentioned is that no nitrites as well as ammonium have been detected as reaction products.

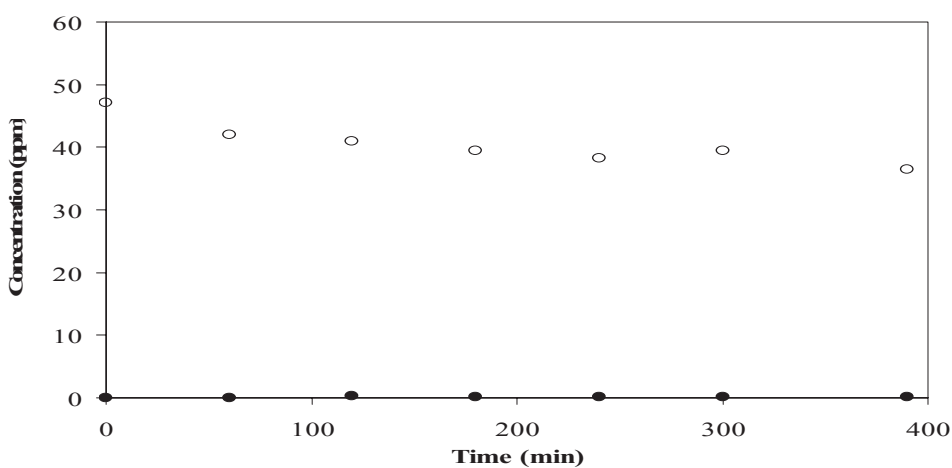


Figure 3.7 Evolution of nitrate and nitrite concentrations versus reaction time for Cu-Pt 4:1 NSBC. [● NO₂⁻, ○ NO₃⁻]

A comparison of activities for nanosphere bimetallic catalysts for nitrate reduction at steady state conditions (after 1 day of reaction), is presented in Figure 3.8. For both series of catalysts it can be noted that when a higher amount of noble metal is used, the activity rises. The catalyst Cu-Pd 1:1NSBC seems to be the most active in the hydrogenation of nitrate. However, practically all reacted nitrate is transformed to nitrite ions, a fact that is not acceptable for the treatment of real effluents. In the case of Cu-Pt nanosphere catalysts, the activity is lower, however no nitrite as by-product is detected. These results are also in agreement with the obtained results from Cu-Pt impregnated catalysts.

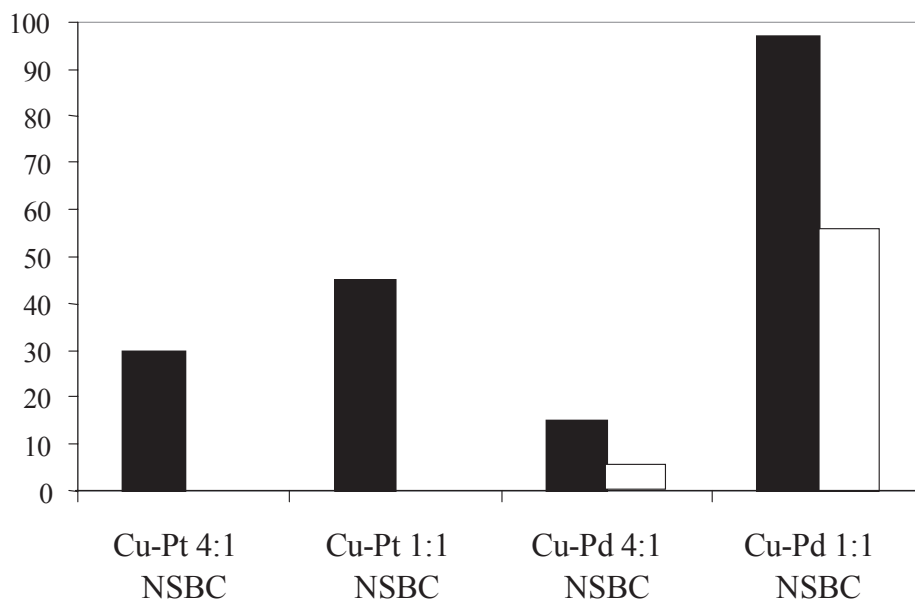


Figure 3.8 Nitrate conversion and selectivity for nanosphere catalysts [■ NO₃⁻ conversion (%), □ NO₂⁻ concentration (mg/l)].

3.2.2.3. Comparison IC and NSBC

If we calculate the activity of the Pt –Cu nanosphere catalysts (Cu-Pt 1:1 NSBC and Cu-Pt 4:1 NSBC, samples) in terms of amount of nitrate converted to nitrogen per

gram of noble metal an per hour and compare it with the corresponding data for the best impregnated catalyst (IC-4), we observe that the nanosphere Pt-Cu catalysts are between 20-50 times more active than the impregnated catalysts (around 7 , 19 and 0.35 grams of NO_3^- converted to nitrogen per hour and per gram of platinum, at steady state conditions, for Cu-Pt 1:1 NSBC, Cu-Pt 4:1 NSBC and IC-4 catalysts, respectively). This fact indicates a more efficiency in the nitrate reduction reaction of Pt in nanosphere catalysts with respect to the impregnated one.

In order to explain the different catalytic behaviour between Pd-Cu and Pt-Cu catalysts related with the presence of nitrites during the nitrate reduction process, we can consider the results obtained by XPS. XPS detected metallic palladium or platinum as well as its oxidised forms Pd (II) or Pt (II) in the used catalysts. Practically, a half of the platinum and palladium are in the oxidised form. This fact could indicate that most of the adopted elemental reaction scheme for the nitrate reduction reaction proposed by Epron et al. [17] and proposed in scheme 1, could be more complex and the function of noble metals is not only the reduction of Cu^{2+} to Cu^0 by means of chemisorbed hydrogen assisted by noble metal. Besides, Epron et al. proposed that noble metal itself is able to reduce the nitrite ions by activated hydrogen. Based on the results ascertained by the XPS technique an additional step, which comprises the red-ox reaction between nitrite ions and noble metal leading the formation of nitrogen and the oxidation of noble metal to M(II), could be proposed. Concurrently the metal is regenerated by hydrogen. The high amount of nitrite obtained using Pd-Cu catalysts in contrast with Pt-Cu (that no shows the formation of nitrites) could be explained taking into account the reduction potentials of Pt(II)/Pt and Pd(II)/Pd (1.2 and 0.83 volts, respectively). However, at this moment it is difficult to discard the nitrite reduction by activated hydrogen, might be, that the two routes are complied.

3.3. Conclusions

The feasibility of two different types of bimetallic catalysts supported on active carbon for the nitrated reduction reaction of water sources in a continuous process has been studied with hydrogen as reducing agent. Two routes have been followed for bimetallic catalysts preparation (Pt-Cu or Pd-Cu), wetness impregnation (IC) and nanosphere preparation followed by deposition on active carbon (NSBC). Independently on the type of catalyst, IC or NSBC, it has been observed that Pt-Cu bimetallic catalysts are more selective for nitrate elimination generating nitrogen as product. The Pd-Cu catalysts showed higher activity, however a large amount of the more harmful nitrite is produced. For the Pt-Cu impregnated bimetallic catalysts it has been observed that the optimal ratio between active metals is 1wt % Pt/ 0.3 wt % Cu. Besides, it has been demonstrated that nanospheres Pt-Cu catalysts are more active (between 20-50 times) than the most active impregnated bimetallic catalyst (IC-4).

The results obtained from the XPS analysis indicate that the molecular reaction mechanism could be more complex than that which is generally accepted. In the used catalysts about the half of the noble metals are in the form of Pd(II) or Pt(II). This fact suggests that the role of noble metal in the nitrate reduction reaction is not simply to regenerate the copper by means of chemisorbed hydrogen. Based on these results a new additional step in the molecular reaction mechanism is proposed.

UNIVERSITAT ROVIRA I VIRGILI
SELECTIVE HYDROGENATION CATALYSTS FOR ENVIRONMENTAL PROCESSES:
NITRATE AND CHLOROCOMPOUNDS REMOVAL
Noelia Barrabés Rabanal
DL: T-1539-2009/ISBN:978-84-692-4557-6

Ceria catalysts

The present work proves that a monometallic Pt catalyst shows a total conversion in the nitrate reduction reaction when ceria was used as support. This fact suggests that the support is directly involved in the reaction. However, in all the catalysts the presence of ammonium was detected. In order to control the ammonium formation the acid-base character of the support was modified introducing several amounts of fluoride species in the CeO₂, using two different methods: impregnation and combustion. A strong decrease in ammonium formation was observed by the introduction of fluoride species. In this way, the acid-base properties of the support play an important role in the control selectivity.. This represents an alternative way to improve the selectivity of nitrate reduction reaction toward nitrogen without the use of additional molecules such as CO₂ to pH control.

4.1. Catalysts Synthesis

4.1.1. Bimetallic Catalysts

Two procedures have been followed in the catalysts preparation. The first one called combustion method, is described as follow: Cerium ammonium nitrate and copper nitrate were used as precursors of ceria and copper. In a Pyrex dish (500ml), a

mixture of ceria ammonium nitrate (7.50g), copper nitrate (0.47g; 5 wt % of copper with respect to the ceria), Pluronic (0.21g) and 4ml of ethanol were introduced and stirred. When the mixture was homogeneous, it was introduced into a muffle furnace preheated to 400°C. The solution boiled with foaming and frothing and ignited to burn with a flame yielding about 2.5g voluminous oxide product within 5 min. The catalysts obtained by this procedure are further named as Cu/CeO₂. In the second route the catalysts precursors were mixed in the same way as described above. To the resulting solution, a solution of ascorbic acid dissolved in ethanol was added drop by drop. The solution became red due to the reduction of the copper ions and the formation of copper nanoparticles. The ascorbic acid was added until no change in the colour was observed. Thereafter the mixture was introduced into the muffle furnace set at 400°C as described in the first procedure. The catalysts obtained by this route are further called Cu*CeO₂.

The Cu/CeO₂ and Cu*/CeO₂ (*reduced), was impregnated by incipient-wetness technique with an ethanol solution of the corresponding noble metal salt (H₂PtCl₆). After that, the samples were dried at 120 °C for 24 h and then reduced at 350°C in hydrogen flow for 3 h. The amount of the noble metal was arranged from 0.1% to 1% with respect to the support for all the catalysts.

4.1.2. Monometallic catalysts

Cerium nitrate was used as precursor of cerium oxide. In a Pyrex dish (500ml), a mixture of cerium ammonium nitrate (7.50 g), Pluronic (0.21g) and 4 ml of ethanol were introduced and stirred. When the mixture was homogeneous, it was introduced into a muffle furnace preheated to 350°C. The solution boiled with foaming and frothing and ignited to burn with a flame yielding about 2.5 g voluminous oxide product within 5 minutes. Ceria were impregnated by incipient-wetness technique with a ethanol solution of the corresponding metal salt (H₂PtCl₆). After that, the samples were dried at 120°C for 24h and then reduced at 350°C in hydrogen flow for 3h.

4.1.3. Fluorinated ceria catalysts

Two procedures have been followed for the preparation of fluorinated ceria. The first is a co-combustion method named (COC). The cerium and the fluoride salts as well as the Pluronic were dissolved in ethanol followed by combustion of the mixture as described before. The second synthesis protocol consists in an impregnation method (IMP) with aqueous solution of ammonium fluoride on ceria already synthesized. The material was dried over night at 120°C and then calcined into a muffle furnace preheated at 400°C. Fluorinated ceria were impregnated by incipient-wetness technique with a ethanol solution of the corresponding metal salt (H_2PtCl_6). After that, the samples were dried at 120°C for 24h and then reduced at 350°C in hydrogen flow for 3h.

4.1.4. Ceria Monoliths

Pt/ceria monoliths were prepared by A. Eleta and O. Sanz from the Basc Country University. The protocol followed was the deposition of colloidal ceria by washcoating on alumina-monoliths. A centrifugation step was done in order to remove the excess in the channels and then it was dried. Finally the monolith was calcined in order to obtain a ceria catalyst.



Then platinum was deposited by ionic exchange. Finally the catalysts were dried and calcined.

4.2. Results and discussions

4.2.1. Characterization results

4.2.1.1. Bimetallic catalysts

Several studies exist on the metal-ceria interactions and its effects on catalytic activity. However, the exact nature of the interaction between the metal ions and the CeO_2 is not yet fully understood. Bera et al [70] have studied the correlation of catalytic properties of Cu/CeO_2 and the electrochemical behaviour of the Cu species. They have shown that the promoting action of CeO_2 is due to the lowering of the redox potentials of Cu^{2+} ions in the CeO_2 matrix.

The SEM analysis of Cu/CeO_2 have shown the typical morphology of CeO_2 in all synthesis used. When the copper nanoparticles synthesis is combined with the co-combustion method different particles groups have been observed by TEM as presented in the Figure 4.1, where the dark particles are the copper and the bulk phase is the CeO_2 .

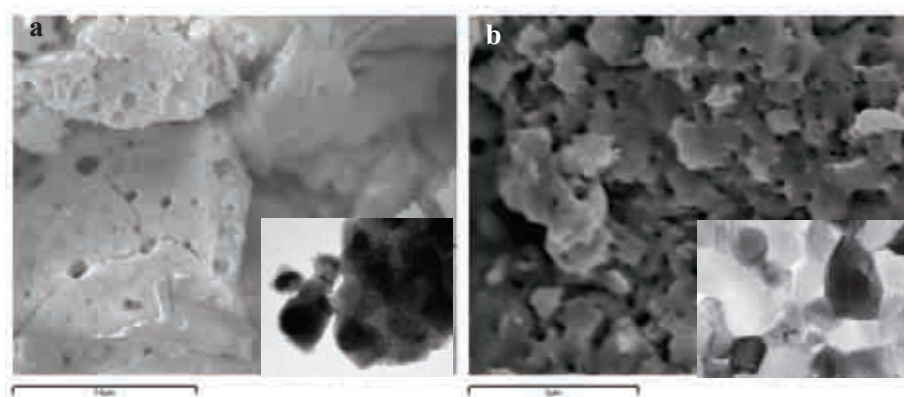


Figure 4.1 SEM (a) Cu/CeO_2 (b) Cu^*/CeO_2 (reduction) with TEM picture detail.

The TPR profiles for the Cu/CeO_2 and Cu^*/CeO_2 samples with the same metal loading are displayed in the Figure 4.2. The main reduction peak in both samples is shifted respect of the common reduction temperature of copper oxide (300°C). The reduction performed between 150°C and 250°C could be attributed to CuO particles formed on the surface and with some Cu^{2+} introduced in the CeO_2 lattice by the combustion preparation [65]. This fact showed how the use of CeO_2 as support enhanced the reducibility of the Cu^{2+} . For the case of Cu^*/CeO_2 sample the observed signal is quite lower than for the other sample, probably because the copper is reduced by the ascorbic acid during the synthesis, so only the surface of the copper is in oxide form.

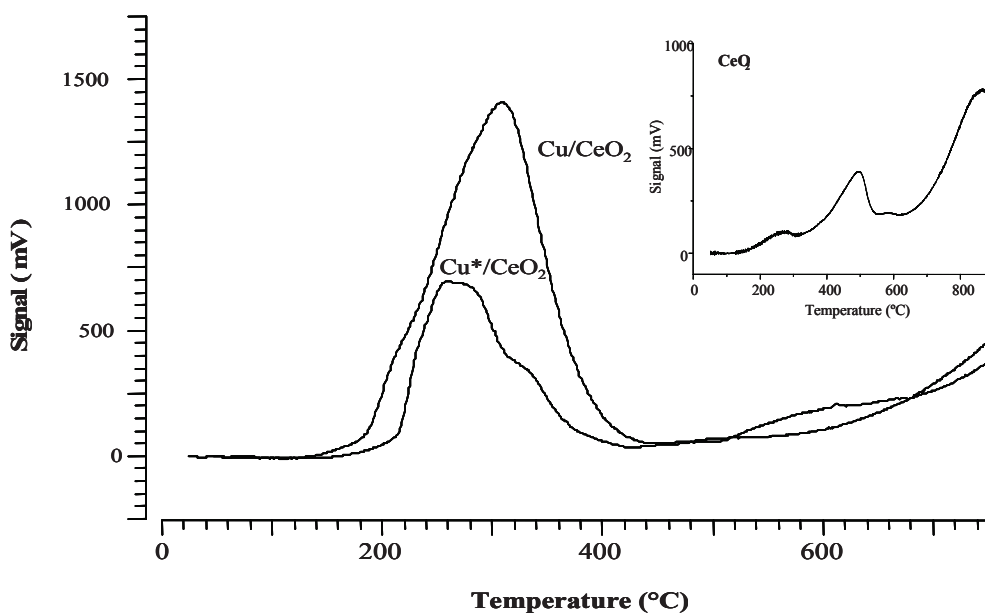


Figure 4.2 Cu^*/CeO_2 and Cu/CeO_2 TPR profiles

The XRD patterns of the sample with and without reduction step are shown in Fig. 4.3. All the samples present fluorite lattice structure patterns and cubic cell, from the CeO_2 . A In the sample without reduction step appeared the CuO phase too. These results indicated that only a part of the smaller size Cu^{2+} (ionic radius: Cu^{2+} 0.79Å

compared to 0.92Å for Ce^{4+}) could enter the CeO_2 lattice to form a solid solution and the rest of Cu^{2+} formed metal oxide particles on the surface of ceria [65].

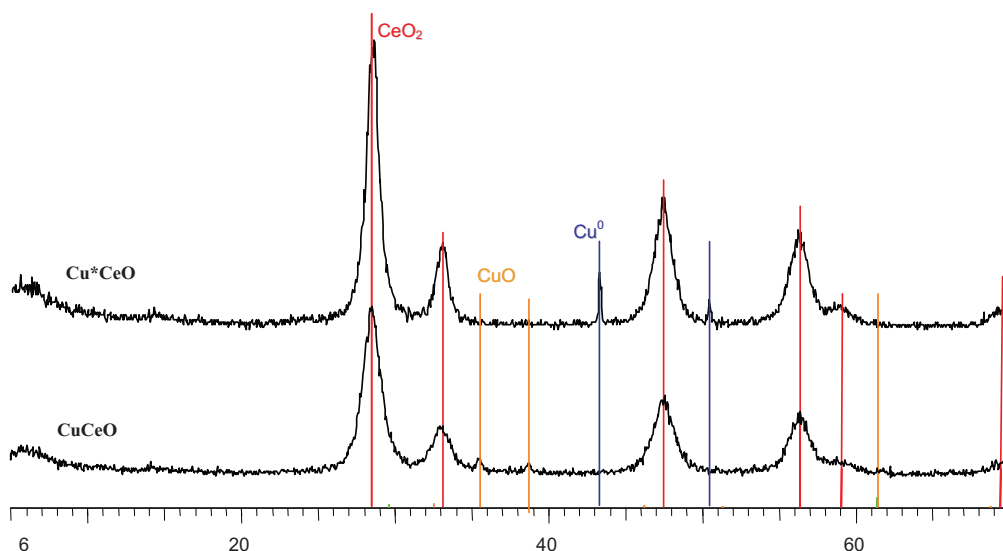


Figure 4.3. XRD profile of Cu^*/CeO_2 and Cu/CeO_2

This results are in agreement with the TPR ones, where is observed how the reduction step decrease the particle size and reduced partially the copper content.

4.2.1.2. Monometallic catalysts

Hydrogen consumption curves (temperature programmed reduction, TPR) of impregnated Pt/CeO_2 catalysts were measured in the temperature range from 25 to 900°C , as shown in Figure 4.4 and table 4.1. H_2 -TPR of the CeO_2 support, which is shown for comparison, is characterized by a two broad reduction peaks: the first between 400 and 550°C and the second reaching temperatures above 700°C .

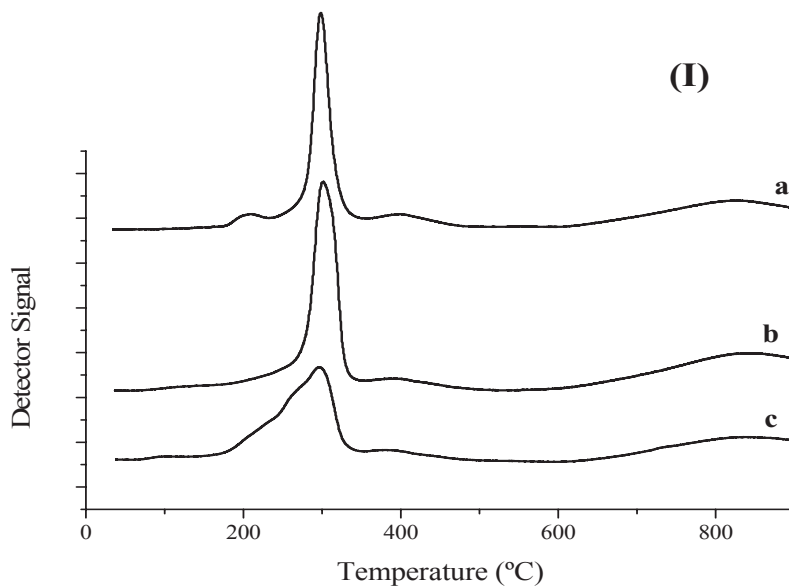


Figure 4.4. TPR profiles of Pt/CeO₂ catalysts prepared by impregnation (I): (a) 0.2%Pt; (b) 0.5%Pt and (c) 1%Pt

It is generally accepted that the CeO₂ reduction occurs via a stepwise mechanism, starting with the reduction of the outermost layer of Ce⁴⁺ (surface reduction) occurring at lower temperature (400-550°C) whereas the reduction of the inner Ce⁴⁺ layers (bulk reduction) occurs at higher temperatures (above 700 °C)[71]. The surface shell reduction may involve several phenomena, like: (1) liberation of surface carbonates, (2) reduction of Ce⁴⁺ surface to Ce³⁺, and (3) formation of bridging OH groups [72]. The TPR results for the CeO₂ support is in agreement with the results obtained for the reduction of CeO₂ of high surface area [73]. The hydrogen consumption for the first peak represents that around a 4% of the Ce⁴⁺ surface is reduced to Ce³⁺. The addition of metals onto the CeO₂ facilitates the surface shell reduction step, likely by reduction of Pt and spillover of hydrogen from the metal to the surface of the oxide, resulting in direct formation of bridging OH groups [74]. This behaviour is indeed observed in Fig. 4.4 for TPR profiles of catalyst with different loadings of Pt incorporated by impregnation. Different peaks between 200°C – 450°C, being related to the reduction of both platinum and CeO₂,

were observed. For the 0.2% Pt/CeO₂ (I) sample, the small peak around 200°C may be attributed to reduction of platinum and ceria in the vicinity of Pt crystallites, as has been suggested by Panagiotopoulou [75]. The main peak detected around 300°C is mainly due to the reduction of the Ce⁴⁺ on the surface of the CeO₂ to Ce³⁺ promoted by the addition of platinum. Around a 14% of CeO₂ is reduced to Ce³⁺. Furthermore, a small peak between 400 and 450°C that could be related to the reduction of surface ceria that represents 1% is also observed. Similar results are obtained when the platinum content in the sample increases. A 18.5% of the surface ceria is reduced at around 300°C for the 0.5% Pt/CeO₂ (I) sample, while a 15.5% is observed for the 1% Pt/CeO₂ (I) sample.

Table 4.1. Pt metal dispersion and reduction degree of surface CeO₂ on Pt-ceria catalysts

Catalyst	Calcination Temperature (°C)	Metal dispersion* (%)	TPR Reduction degree of CeO ₂ (%)
<i>CeO₂</i>	300	--	4
<i>0.2Pt/CeO₂ (I)</i>	300	110	14
	500	53	5
	700	38	4
	900	20	2
	<i>0.5Pt/CeO₂ (I)</i>	300	75
<i>1Pt/CeO₂ (I)</i>	300	70	15.5

In order to study the interaction Pt-ceria and the effect of the particle size, the 0.2%Pt/CeO₂ (I) sample was calcined at different temperatures between 300 and 900°C (see Figure 4.4). By increasing the calcination temperature a decrease of the signals of the reduction peaks and a shift to lower reduction temperatures were observed. The amount of CeO₂ reduced was 14%, 5%, 4% and 2% for the 0.2%Pt/CeO₂ (I) samples calcined at 300, 500, 700 and 900°C, respectively (see Table 4.1). The sintering of the platinum particles as well as the support at higher calcination temperatures could explain this behaviour [76].

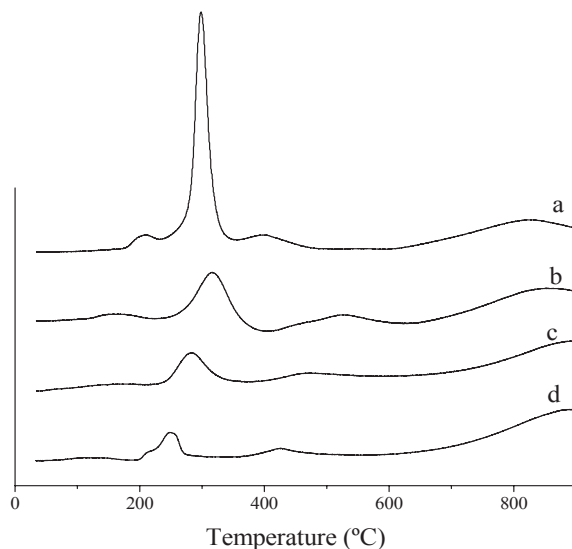


Figure 4.5 TPR profiles of 0.2%Pt/CeO₂ (I) calcined at several temperatures: (a) 300°C; (b) 500°C; (c) 700°C; (d) 900°C

The platinum dispersion of the samples, obtained by hydrogen chemisorption, is shown in Table 4.1. When the amount of platinum increased, a slight decrease of the dispersion was observed. The dispersion of the 0.2%Pt/CeO₂ (I) sample was 110% whereas for the 1%Pt/CeO₂ (I) sample was 70%. By increasing the calcination temperature, a decrease in the metal dispersion was observed. The metal dispersion for the 0.2%Pt/CeO₂ (I) sample calcined at 300°C was of 110% whereas for this sample calcined at 900°C, a metal dispersion of 20% was detected.

The IR spectra obtained after room temperature CO exposure Pt/CeO₂ catalysts (after prior H₂ reduction at 350°C) are shown in Figure 4.6. The results show that the CO is not adsorbed on CeO₂ (except for carbonates species; not shown [77]). For Pt containing catalysts, CO not well resolved bands were observed between 2120-2130 cm⁻¹ and 2080-2070 cm⁻¹. P. Panaglotopoulou et al. [75] proposed that Ce cations influence the adsorption state of CO by enhancing the back-bonding through the metal. The strong bands observed at around 2068 and 2083 cm⁻¹ are attributed to CO linearly bonded to surface-exposed metal Pt atoms [78]. The Pt-

CO IR band at 2083 cm^{-1} is indicative of the presence of metal atoms in less dense close packing arrangements such as 100 faces, while the CO low-frequency band at 2068 cm^{-1} is related to the presence of Pt atoms in defect sites (steps and corners) [78-81]. These results are in agreement with the observations made previously by TEM. Interestingly, no IR bands of Pt-dicarbonyl species (1984 cm^{-1}) and bridge CO species (1908 cm^{-1}) were detected [82]. This fact could be explained by a high dispersion of the Pt in the CeO_2 matrix.

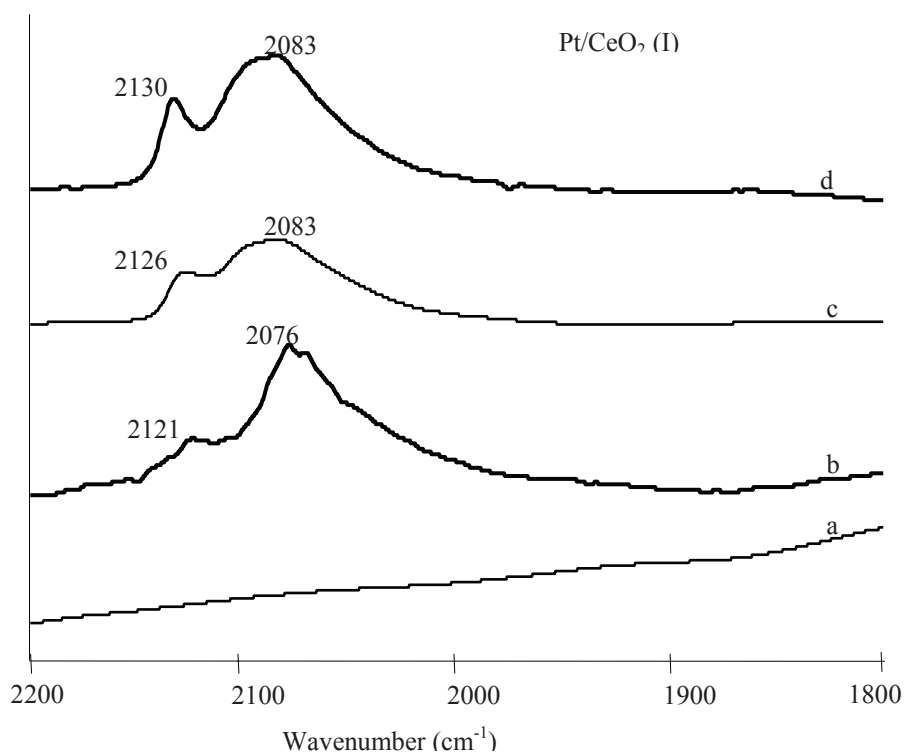


Figure 4.6. FTIR profiles of Pt/CeO₂ catalysts. Profile of CO adsorption followed by short evacuation at room temperature. [a: ceria; b:0.2%Pt; c:0.5%Pt; d:1%Pt]

The bands assignment in the region $2130\text{-}2110\text{ cm}^{-1}$ is a matter of controversy; the general assignment for the Pt-CeO₂ system is shown in Table 4.2. The bands between 2120 and 2130 cm^{-1} may have different origins, but it is mainly attributed to the presence of oxidized Pt in Pt/CeO₂. Pt is shown to be bonded to surface lattice oxygen and this kind of bond is not fully reducible even at high reduction

temperature. Since the vibrational frequency of adsorbed CO is higher when the state of metal is more positive, the bands between 2120 and 2130 cm^{-1} may be due to CO linearly adsorbed on Pt atoms interacting with oxygen; i.e., Pt atoms are in a more unsaturated coordination state (Pt^\square), probably created by a strong metal-support interaction (SMSI) [78]. On the other hand, these bands may also be attributed to the adsorption of CO on Ce^{3+} , as well as to the presence of species like Cl. The presence of Ce^{3+} on the surface is related to a reduction of the CeO_2 promoted by the noble metal as has been detected by TPR. The presence of Cl species could arise from the precursor salt of platinum (H_2PtCl_6) [83]. In addition, using XRD Bera et al. [84] reported the formation of $\text{Ce}_{1-x}\text{Pt}_x\text{O}_{2-\delta}$ and the absence of platinum oxide phases in Pt/ CeO_2 prepared by combustion. However, due to the low amount of Pt in the sample, surface PtO_x phase is difficult to detect by XRD. As a conclusion the IR results indicates a strong interaction between platinum and the support for the Pt- CeO_2 samples.

Table 4.2. IR bands assignment on ceria and Pt/Ceria

<i>Wavenumber (cm^{-1})</i>	<i>Surface Species*</i>
2085-2068	CO linearly adsorbed on reduced Pt^0 platinum sites. OC- Pt^0 without Ce^{3+} interaction
2030 – 2062	OC- Pt^0 with Ce^{3+} interaction
2120-2127	CO linearly adsorbed on Ce^{3+} or on partially oxidized Pt
1820 – 1840	Bridge bonded CO on Pt^0 sites
1765	Pt^0 -CO- Ce^{3+}
1700-1690	Pt_2^0 -CO- Ce^{2+}
1641-1045	Surface formate and/or carbonate species (associated support)

*References : [75, 85-88]

Furthermore, when the calcination temperature was increased for the 0.2%Pt/ CeO_2 (I) sample, some changes in the IR spectra were observed (see Figure 4.7). Increasing the calcination temperature from 300 to 500°C, and after reduction, the IR band located at 2121 cm^{-1} disappears. This could be explained considering that at this calcination temperature the chloride species are removed from the surface

as has been detected by EDS analysis. When the calcination temperature increased up to 700 and 900°C, a new band at around 2110 cm^{-1} was detected. The intensity of this band increases with the increase of the calcination temperature. These facts indicate different CO-Pt interactions by modification of the calcination temperature.

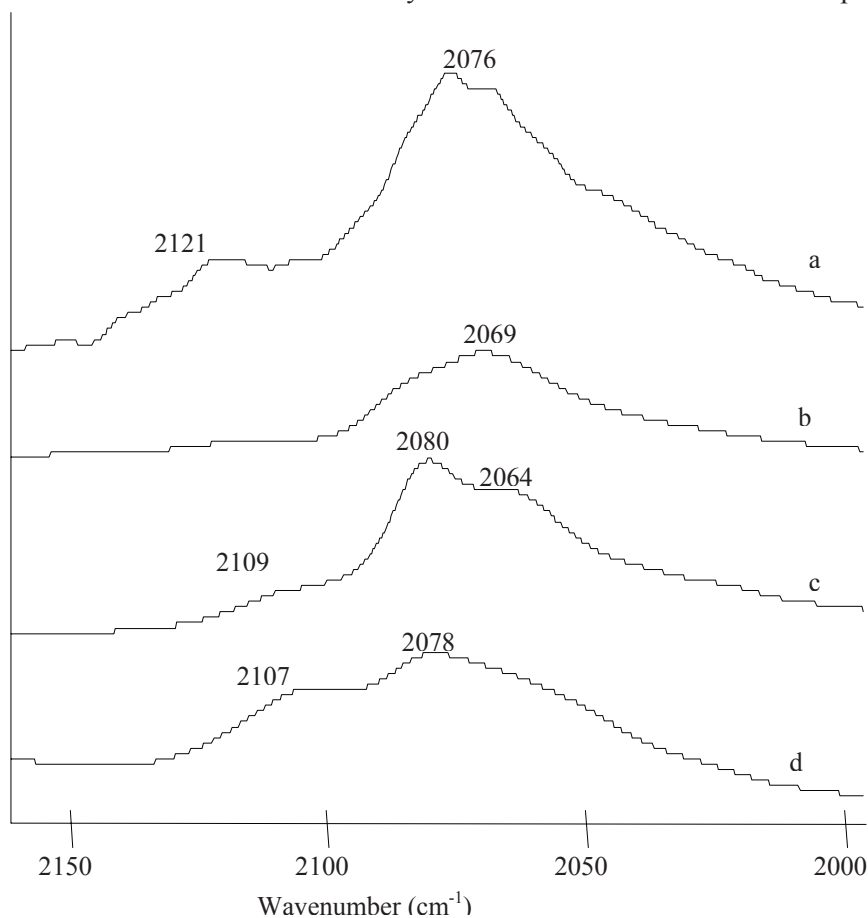


Figure 4.7. CO-FTIR of 0.2%Pt/CeO₂ catalyst calcined at several temperatures: (a) 300°C; (b) 500°C; (c) 700°C; (d) 900°C.

4.2.1.3. Fluorinated catalysts

The BET surface area of the resulting calcined ceria material was 103.07 m^2/g , whereas the Pt/ceria catalysts showed a surface area around 70-80 m^2/g . A slight

increase in the average pore radius after loading the Pt is observed and can be attributed to blocking of the narrowest pore by the metal clusters. Analysis of 1% fluorinated ceria by impregnation method had a surface of $59.50\text{m}^2/\text{g}$ while the obtained by combustion method was $91.40\text{m}^2/\text{g}$. This means that using impregnation technique the fluorine is deposited on the surface whereas if the combustion is employed, F is introduced in the ceria matrix.

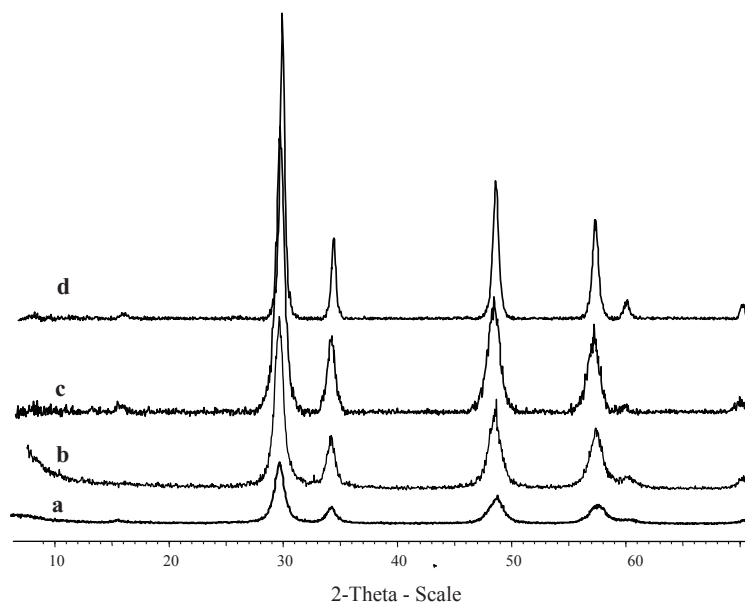


Figure 4.8. XRD profiles of fluorinated ceria catalysts by combustion method [a: CeO₂; b: 0.5%Pt 1%FCeO₂; c: 1%FCeO₂; d: 5%FCeO₂]

XRD patterns of the samples show that CeO₂ obtained by the combustion method has the typical fluorite-type structure (Figure 4.8). Basal reflections at $2\theta = 28.6^\circ$, 33.1° , 47.5° and 56.5° are related, respectively, to the planes (111), (200), (220) and (311) and is in agreement with previous studies [65]. In the fluorinated samples a little shift of the diffraction lines for the F-CeO₂ samples compared to pure CeO₂ was observed. This indicates that F is incorporated into the ceria lattice by the substitution of oxygen [89]. Another fact is an increase in the crystallinity of the sample when the amount of F increased.

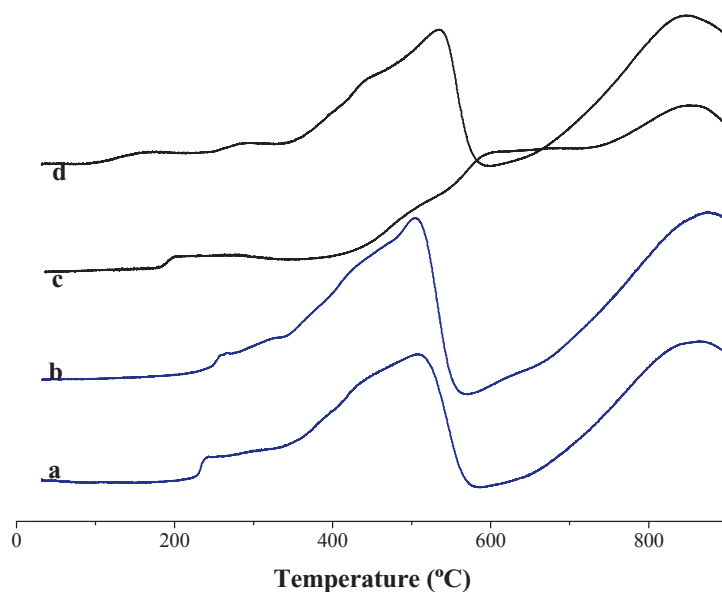


Figure 4.9. TPR F CeO_2 profiles, [a: 5%Fimp ; b:1%Fimp ; c: 5%Fcoc ; d: 1%Fcoc]

Hydrogen consumption curves obtained from the fluorinated CeO_2 samples are shown in Figure 4.9. The TPR profile of the modified CeO_2 sample is characterized by a broad, high-temperature feature, which appears above 600°C and is assigned to reduction of bulk ceria. This peak remains constant independently of the amount of fluorine (between 1-5%w). However the reduction peak at around 500°C that can be attributed to the reduction of surface CeO_2 is modified by the fluorination. Whereas the hydrogen consumption for Fceria COC (peak at 500°C) is less than ceria alone, for the Fceria IMP represent 1.2% more than the surface ceria reduction. This could be related with hydrogen consumption from the Fluor species deposited on the surface by impregnation. Besides, when combustion method is employed Fluor species are incorporated in the ceria lattice as was observed by XRD. TPR profile of 5%Fceria COC presents a broad peak from 500°C that overlaps with the bulk reduction peak. The increase in the Fluor amount in the sample lead to decrease in the surface area, as is observed in the XRD profile, and the requirement of higher temperature reduction.

Ammonia was used as probe molecule for acidity assessment. The ammonium ion shows absorptions at 1450 and 3300 cm^{-1} , and coordinative bound ammonia at 1250, 1630 and 3330 cm^{-1} [90]. Figure 4.10 shows the FTIR NH_3 adsorption for ceria and fluorinated ceria obtained by combustion method. No absorption bands were observed for ceria.

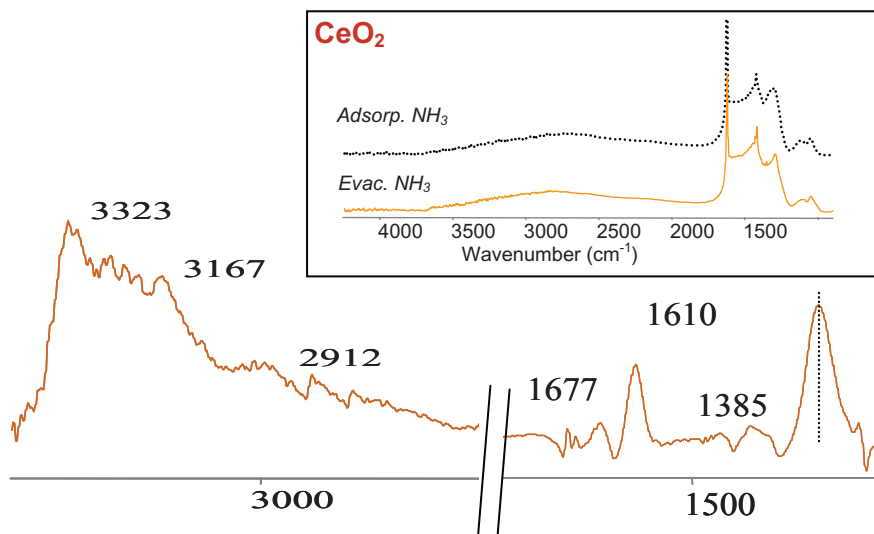


Figure 4.10. FTIR NH_3 adsorption profiles of Ceria and 1%Fceria

Contrarily, for F-ceria several bands at 1250, 1610 and 3232 cm^{-1} of ammonia adsorption were observed. The bands ascribed to Lewis acidity appears in the zone of 1300-1000 while the bands for Bronsted acidity is around 1440 cm^{-1} [91]. These results evidence that, by the fluorination of the ceria matrix, its acid-base properties are strongly modified.

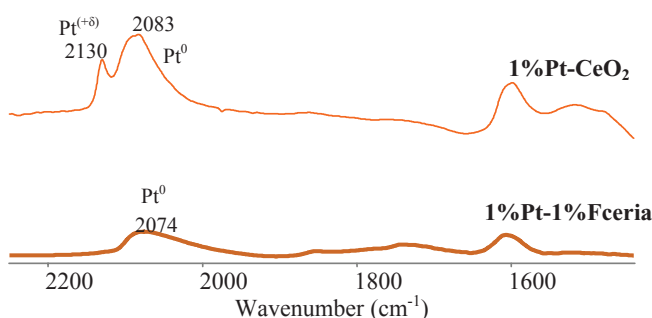


Figure 4.11. FTIR CO adsorption profiles of 1%PtCeria and 1%Fceria

The IR spectra obtained after room temperature CO exposure Pt/CeO₂ and Pt/FCeO₂ catalysts (after prior H₂ reduction at 350°C) are shown in Figure 4.11. The spectra of 1%Pt/CeO₂ has been discussed previously (4.2.1.2). The main difference observed is the disappearance of the band at 2130cm⁻¹ when the Pt is incorporated over fluorinated ceria. The strong band at 2083 cm⁻¹ are attributed to CO linearly bonded to surface-exposed metal Pt atoms [78], is shifted to lower wavenumber 2074cm⁻¹. This could be related with a different interaction of platinum particles on the support due to the presence of fluoride species.

5.2.1.4. Ceria monoliths catalysts

Figure 4.12 shows a view of the surface of the monolith before the deposition of ceria. The phase of Al and Al₂O₃ could be observed.

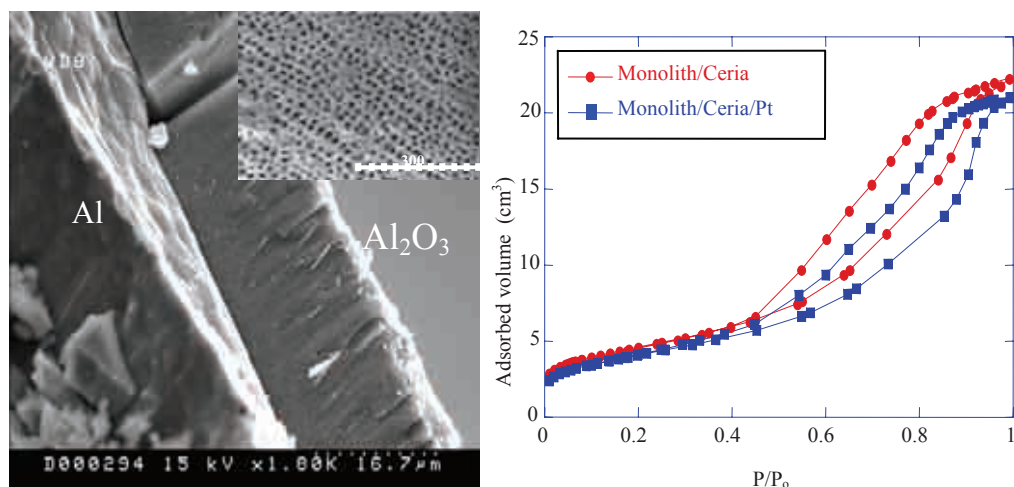


Figure 4.12. SEM from Al-Monolith and N₂ adsorption isotherm

Isotherm adsorption before and after the incorporation of the platinum were performed. No relevant changes are observed, meaning the stability of the ceria deposited on the monolith after the introduction of the platinum.

4.2.2. Catalytic activity

4.2.2.1. Bimetallic catalyst

Figure 4.13 shows that the nitrate is totally reduced on PtCu/CeO₂ catalysts, but with the production of the undesired nitrite and ammonium ions. These results are similar as the presented by Barbier [92] using CeO₂. When the noble metal amount in the catalyst increase, the nitrite concentrate in solution during nitrate reduction decreased. This result could be explained by the high activity of the Pt for the nitrite reduction. However, the reaction is too selective toward ammonia, which is an undesired product.

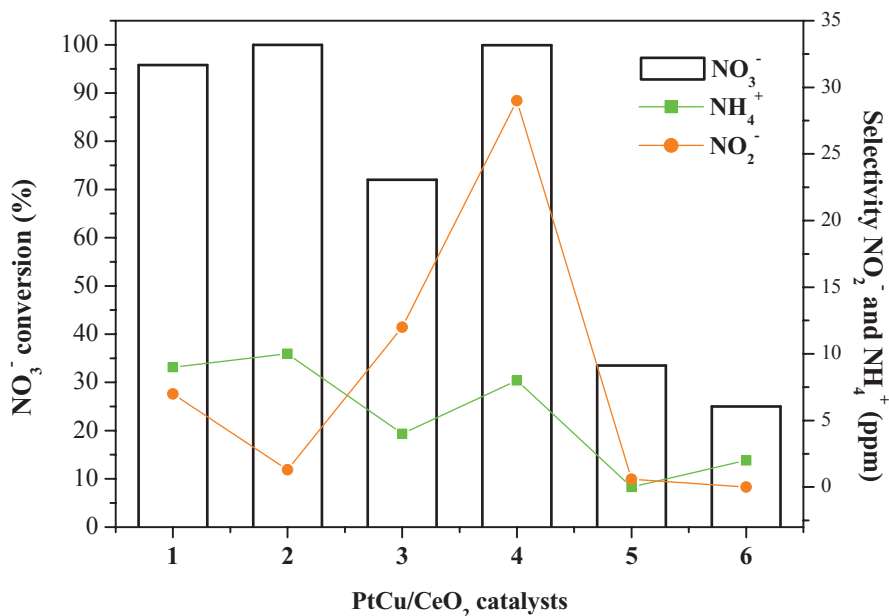


Figure 4.13. CeO₂ Catalysts Activity: (1) 0.1%Pt0.5%Cu; (2) 0.5%Pt0.5%Cu; (3) 0.1%Pt5%Cu; (4) 0.5%Pt5%Cu; (5) 0.1%Pt5%Cu (H₂/CO₂); (6) 0.5%Pt5%Cu (H₂/CO₂)

This high ammonia production could be due to a pH increase of the solution during the reaction. Indeed, the pH is an important parameter that affects the activity and

selectivity of catalysts for catalytic denitrification [10, 62]. To decrease the production of ammonium ions, the pH is buffered saturating the solution with carbon dioxide. Under H₂/CO₂ mixture, only 36% and 25% of nitrate is converted, but the ammonia and nitrite concentrations decrease. As CO₂ is strongly adsorbed on cerium oxides at room temperature, giving rise to carbonates and carboxylates [62], these species may affect the adsorption of N-species on ceria sites and then prevent the nitrate and nitrite reduction on the support. The similar behaviour is observed with the PtCu* catalysts, showing high nitrate reduction but with the undesired products nitrite and ammonium. When the two catalysts are compared, it seems that the PtCu/CeO₂ is better because lower amount of nitrite ions is detected. In this catalyst the nanoparticles (PtCu*/CeO₂ catalyst) does not increase the nitrate reduction.

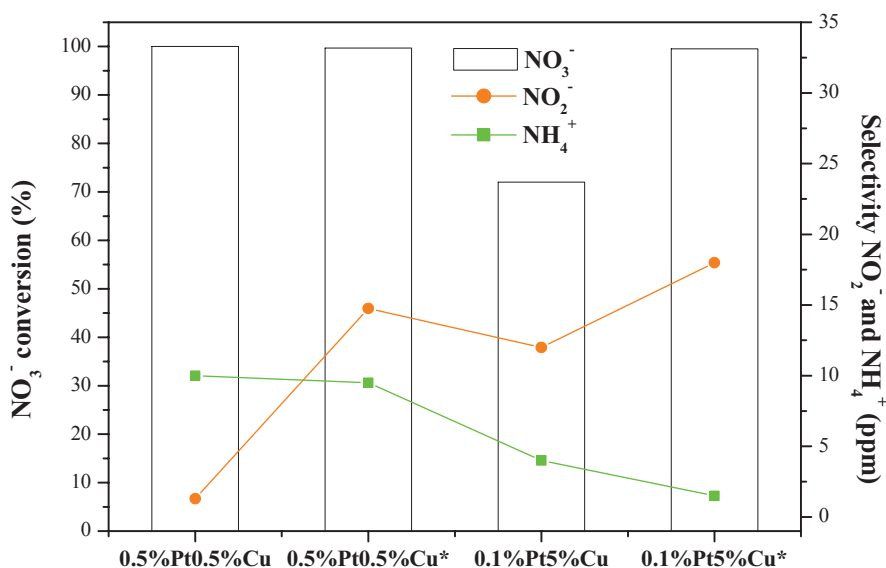


Figure 4.14. Catalytic activity of the bimetallic (PtCu) ceria supported catalysts

The bimetallic catalysts using CeO₂ as support show high reduction of nitrates but with the generation of ammonium ions. The incorporation of CO₂ as buffering agent to the reaction decreases the formation of undesired products but the nitrates removal decline.

4.2.2.2. Monometallic catalyst

The catalytic activity in the hydrogenation reaction of nitrates in water using Pt-CeO₂ catalysts has been studied. The results of the nitrate conversion and the selectivity to nitrite and ammonium are plotted in Fig. 4.15.

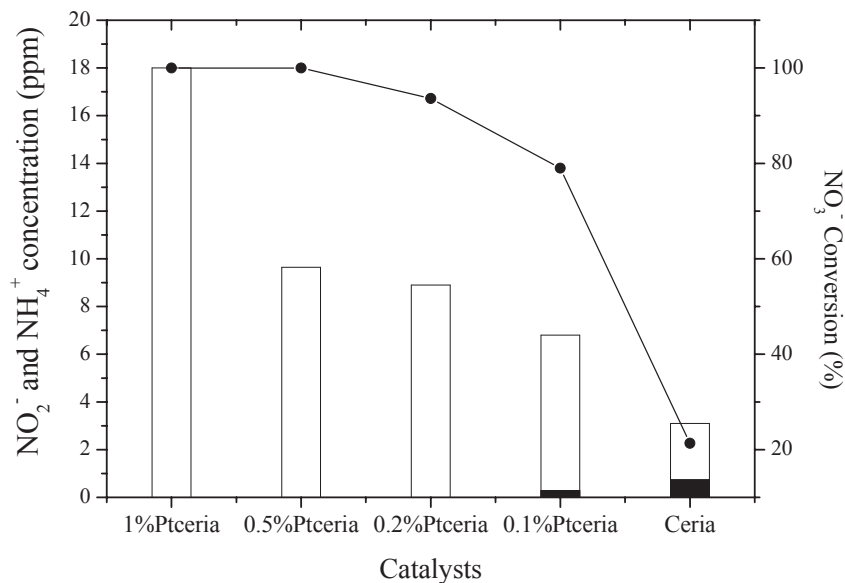


Figure 4.15. Catalytic activity and selectivity of monometallic Pt/CeO₂ catalysts [● nitrate conversion; ■ nitrite concentration; □ ammonia concentration]

The support, CeO₂, displayed also some activity in the hydrogenation of nitrate. A nitrate conversion of around 20%, and selectivity to ammonium, nitrite and nitrogen of around 80%, 18% and 2%, was obtained, respectively. The introduction of platinum increases both the nitrate conversion and the selectivity to nitrogen. Practically a total nitrate conversion was obtained using 1%, 0.5% and 0.2 % Pt-CeO₂ catalysts. The selectivity to ammonium using these catalysts was of around 100%, 53% and 50%, respectively. Consequently the highest selectivity to nitrogen, practically at total nitrate conversion, was obtained for 0.5% and 0.2%Pt-CeO₂ catalyst and was around 50%. No nitrite formation was observed for these catalysts.

A nitrate conversion of around 80% and selectivity to ammonium of around 50% was obtained for the 0.1%Pt-CeO₂ catalyst. For this catalyst some traces of nitrites have been detected (< 0.3 ppm). According to the reaction mechanism proposed by Wärna et al. [51], nitrates are reduced in a stepwise fashion, initially to nitrites over bimetallic sites, before migration to monometallic sites where subsequent nitrite reduction takes place. Generally, this two-step process leads to a release of nitrite into the solution, which may be further reduced at a large stage. In this way a potentially relatively high concentration of nitrites in solution during reaction might exist for the bimetallic catalysts.

However, the nitrite concentration in Pt-CeO₂ catalysts was null or very low. This fact indicates that the active sites for the reduction of nitrates to nitrites are the same as for subsequent steps and that in general, the releases of nitrites into solution followed by subsequent reduction is not the predominant pathway. The general accepted mechanism for the reduction of nitrates to nitrites requires the promotion of the noble metal by addition of a second metal [50]. However, the present results prove that a monometallic catalyst can be active for nitrate reduction by using ceria as support. This fact suggests that the support may be directly involved in the reaction. The nitrate reduction presumably happens through the interaction of oxygen atoms of nitrate with the oxygen vacancies created, after the reduction process, at the ceria surface. In addition, it is considered as a probably reason the promoting effect of ceria, mainly related to the Ce⁴⁺/Ce³⁺ redox couple [62, 70, 93]. Recently Sa et al. [94] show by FTIR studies how nitrates are adsorbed at the oxygen vacancies of the support by electrostatic interaction, in agreement with the hypothesis with CeO₂. In our case, it has been observed the higher reduction degree of CeO₂ by the addition of platinum, creating a large amount of oxygen vacancies. On the other hand, several authors have reported different kinds of interaction between noble metals and ceria and their effects on catalytic activities showing that the nature and the extent of interaction depend on particular noble metal catalyst pre-treatment, preparation technique, size of CeO₂ crystallite, lattice oxygen, and so on [84].

However, Kundakovic et al. [95] found that the adsorption of water on reduced ceria surfaces at low temperature does not lead neither the oxidation of ceria nor the formation of hydroxyls. Like is mention before the nitrate reduction occurs through the interaction of oxygen atoms of nitrate with the oxygen vacancies, assisted by hydrogen in the interphase Pt-CeO₂ or in the metal surface, nitrite is reduced to nitrogen or over reduced to ammonium. Consequently, the high selectivity to ammonium can be related to the electronic properties of the metal. Besides, the chemical environment of Pt as the active component through an electronic interaction between metal and support can significantly change the activity and selectivity of the catalyst [96]. CeO₂ is a basic material; in this way there is an electronic transfer from reduced CeO₂ to platinum that could increase the hydrogenation capacity of platinum.

For the 0.2%Pt-CeO₂ catalyst it has been studied the catalytic activity in function of the calcinations temperature. For all tests the reaction residence time has been adjusted in order to maintain the same conversion level (of around 40%). For the sample calcined at 300°C a selectivity toward ammonia of around 50%, was observed. Besides, it has not been detected the presence of nitrite. It has been observed that increasing the calcinations temperature the amount of ammonium decrease, e.g. for the catalyst calcined at 700°C a 30% of ammonium selectivity was obtained. In all tests it has not been detected nitrite.

4.2.2.3. Fluorinated catalyst

About the mechanism of ammonium formation during the nitrate reduction reaction there are different opinions. The increase of the pH, due to the formation of hydroxide during the reaction, and the existence of different active sites are the causes for the formation of NH₄⁺ decreasing the selectivity to nitrogen. The former has been verified by several authors that report a significant decrease in the ammonium concentration when a buffer, such as CO₂ [16, 18, 97], was co-fed in the reaction. On the other hand, Yoshinaga et al. [40] observed an increase in selectivity

to N_2 with an increase in the Pd crystallite size, suggesting a structure-sensitivity of the process. Furthermore, noble metal with atom of low coordination number (edges and corners positions) has high abilities for deep hydrogenation, leading to ammonia formation, while metal atoms on flat terrace sites yield nitrogen [98]. Sa et al. [94] proposed that ammonia is formed via consecutive hydrogenation of NO, which is absorbed by both support and metal functions but reduced exclusively by the noble metal. Summarizing, it is generally accepted that the ammonium formation is facilitated by the increasing of the pH of the solution, due to the formation of hydroxide ion, as well as the metal particle size and its electronic properties that consequently is related to the interaction between metal particle and the support. The increase of the pH can be avoided using a buffer like CO_2 but with an activity lost. In this work the introduction of acid species like fluoride in the catalyst using two methods (impregnation and combustion methods) have been studied and compared with the effect of the introduction of CO_2 .

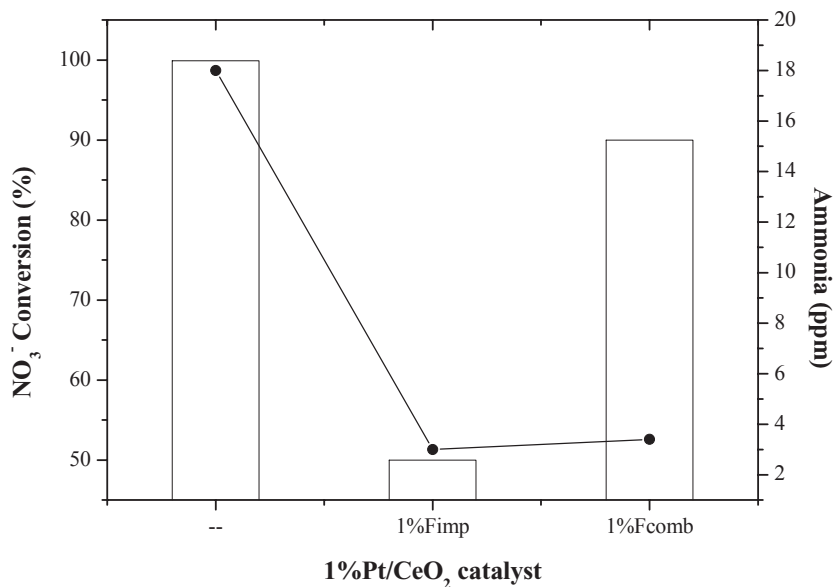


Figure 4.16. Catalytic activity and selectivity of monometallic 1%Pt/CeO₂ catalysts without and with fluorination modification [• ammonia concentration; □ nitrate conversion]

The introduction of CO₂, produces a control in the selectivity to ammonium but at expenses of an important decrease in the activity as is shown in Table 4.3. The results obtained with the modified catalysts are shown in Figure 4.16. When the impregnation method is employed to introduce the Fluor in the ceria catalysts, an important decrease in activity is also observed changing from total conversion to 50% of conversion. However the selectivity to ammonium decreased from 18 to 3 ppm. Whereas when the fluoride was introduced by the combustion method the activity of the catalyst practically remained constant while the amount of ammonium decreased dramatically from 18 to around 3.1 ppm.

Table 4.3. Catalytic activity and selectivity results of 0.5%Pt/ceria catalyst with H₂ and CO₂:H₂ feed.

<i>Catalyst</i>	<i>Feed</i>	<i>Conversion</i> (%)	<i>Selectivity</i>	
			<i>ppm</i> <i>NO₂⁻</i>	<i>ppm NH₄⁺</i>
0.5%Pt/CeO₂	H ₂	99.9%	0.0	9.6
	H ₂ :CO ₂	30.2%	0.0	1.3

4.2.2.4. Monoliths

The application of this technology to industrial scale requires of high flows, low pressure drops and high conversion. Following this idea is studied the used of structured catalysts. With the collaboration from the Vasco Country University, specialist in monoliths, the Pt/ceria monoliths were prepared and then tested in the reduction of nitrate process using a continuous reactor.

Table 4.4. Catalytic activity and selectivity results comparison between powder and monoliths catalysts

	<i>%Pt</i>	<i>CeO₂ mg</i>	<i>mgNO₃⁻/mg catalyst</i>	<i>NH₄⁺ selectivity</i>
Monolith	0.4	77	0.2	60%
Powder	0.5	500	0.1	73%
Monolith	0.2	114	0.3	30%
Powder	0.2	500	0.1	54%

Table 4.4 show the results obtained in the catalytic test in nitrate reduction using monoliths and compared with the ones obtained with powder catalysts. The comparison factor is the amount of nitrate converted respect the amount of catalyst. The used of structured catalyst present higher activity and higher selectivity toward ammonia. This could be related with the decrease in possible diffusion problems and pressure drop using powder catalysts. These are preliminary results, nowadays we are working in the optimization of these monoliths.

4.3. Conclusions

The bimetallic catalysts using CeO_2 as support show high reduction of nitrates but with the generation of ammonium ions. The incorporation of CO_2 as buffering agent to the reaction decreases the formation of undesired products but the nitrates removal decline.

Pt monometallic catalysts supported on ceria are active in the hydrogenation of nitrates reaction, meaning that the support is directly involved in the reaction due to the redox property of the material. 0.2%Pt is the optimal proportion found for this catalysts that correspond the minimum amount of platinum in order to avoid the formation of nitrites.

The addition of fluorine by combustion method in ceria can control the activity of the catalyst and the selectivity to nitrogen. Two possible causes for the ammonia formation are suggested: the increase of the pH of the media due to the OH^- formation and the second, the over hydrogenation by the catalysts. This could be explain by the way that ceria as basic material transfer electronic density to the platinum sites, increasing the hydrogenation capacity, while in the fluorinated ones, fluorine as electronegative compound, removed electronic density from platinum, capping the hydrogenation process.

Further investigation is needed in order to clarify the ammonium formation mechanism during the nitrate reduction process using this type of catalysts, but in this preliminary study we conclude that the use of partially fluorinated ceria as support acts as a buffer and represents a new alternative way to reduce nitrate with high selectivity to nitrogen gas.

From the preliminary results of the use of structure support for Pt/ceria catalysts is observed an increase in the activity and selectivity. This could be related with a decrease in diffusion problems with the powder catalysts and a decrease in the

pressure drop of the system. Complementary studies are required in order to optimize this kind of catalysts.

Chapter 4

Catalytic hydrodechlorination of trichloroethylene



UNIVERSITAT ROVIRA I VIRGILI
SELECTIVE HYDROGENATION CATALYSTS FOR ENVIRONMENTAL PROCESSES:
NITRATE AND CHLOROCOMPOUNDS REMOVAL
Noelia Barrabés Rabanal
DL: T-1539-2009/ISBN:978-84-692-4557-6

Introduction

1.1. Pollution problem of trichloroethylene

Chlorinated organic compounds have been regarded as a source of environmental pollution in air and water. The emissions are related to the problems of ozone layer destruction and contaminated groundwater with high probability of carcinogenic activity and toxicity. One of the most common contaminant is trichloroethylene.

The chlorinated solvent trichloroethylene (also known as TRI, TCE, trichloroethylene, acetylene trichloride, ethylene trichloride¹, 1,1,2-trichloroethylene, ethinyl trichloride and 1,1,2-trichloroethylene²), discovered in 1864, was first commercially produced in Germany at the beginning 1900s. It has been widely used for cleaning of metals and other parts since the introduction of the vapour degreasing process in the early 1930s, and it continues to be the standard to which other cleaning processes are compared. Trichloroethylene is produced as a by-product during vinylidene chloride or ethylene dichloride/vinyl chloride monomer manufacture. Figure 1.1 presents a tree diagram summarizing the production and the use of TCE. The major end use of TCE is as an organic solvent for industrial degreasing; about 85 percent of the TCE supply is applied in vapor degreasing and another 5 percent is used in cold cleaning. These procedures are used in many industrial processes such as the manufacture of automobiles, electronics, furniture, appliances, jewellery, and plumbing fixtures. Approximately 5 percent of

the TCE supply is applied as a chain length modifier in the production of polyvinyl chloride (PVC). The remaining TCE (5 percent) is consumed in other solvent and miscellaneous applications. These applications include (1) solvent in adhesive formulations; (2) solvent in paints and coatings; and (3) miscellaneous chemical synthesis and solvent applications. Today, it is primarily used as an intermediate in the production of hydrofluorocarbon refrigerants and as a metal degreasing agent in industry.

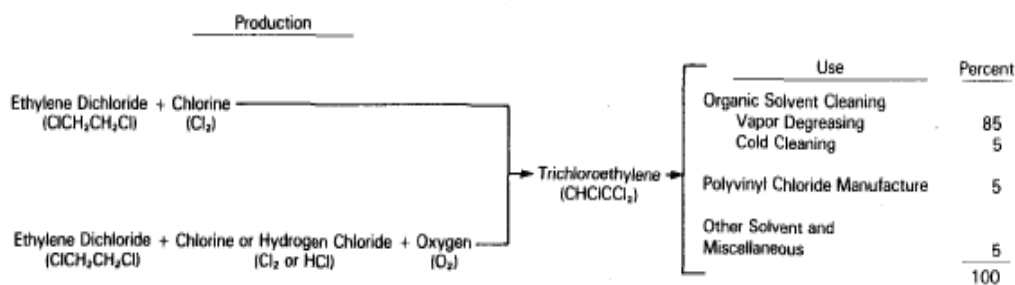


Figure 1.1. Production and uses of TCE

The release of trichloroethylene into the environment can result from the manufacture, use and disposal of the chemical. Trichloroethylene may be emitted by industrial plants in the form of a vapour or liquid effluent. Trace amounts of the chemical may also be found in waste oil and motor vehicle equipment. High contamination levels can arise from accidental spillage (eper web page).

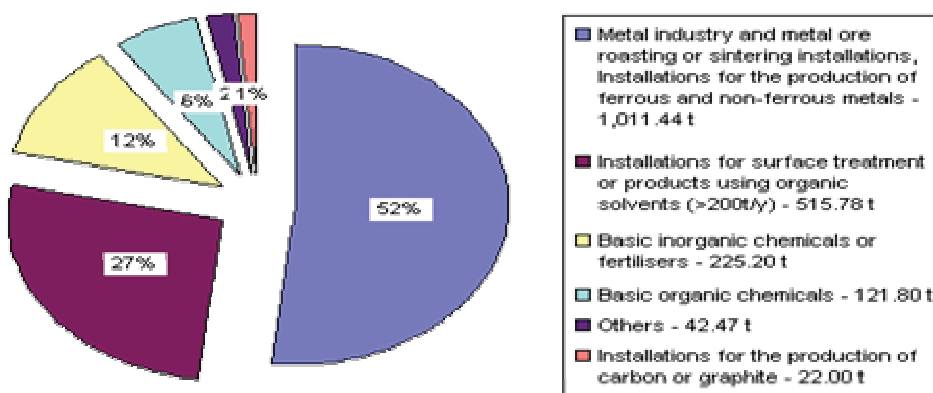


Figure 1.2. Trichloroethylene emissions resources

Trichloroethylene use is regulated under the Solvent Emissions Directive (1999/13/EC). ECSA (European Community Shipowners' Associations) welcomes the implementation of this directive, with its goals of reducing workplace exposures and environmental emissions. Modern equipment allows more efficient use of chlorinated solvents and will continue to contribute to the sustainability of this class of product.

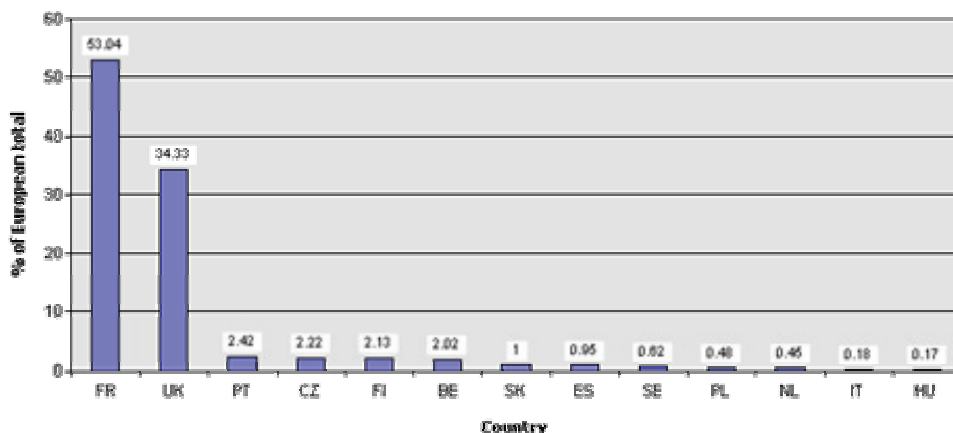


Figure 1.3. Emissions of Trichloroethylene in Europe.

The health effects of trichloroethylene have been studied extensively. The most significant findings to come from many long-term animal studies of this solvent are that it can cause liver and lung tumors in mice. The relevance of these findings to human health is unclear, the research does not apply to humans, This is supported by large epidemiological studies of workers exposed to trichloroethylene that generally indicate no overall increase in cancer risk. Recent studies of small populations of heavily exposed workers in Germany and France appear to show an increase in kidney cancer. Although these studies suffer from major design flaws and are inconsistent with the results of larger, better conducted studies, they were used by the European Union to revise the cancer classification of trichloroethylene. In July 2002, trichloroethylene has been classified in the EU as a category 2 carcinogen

(R45). All products containing this solvent must carry the R45 hazard-warning label: “may cause cancer.”

The three European trichloroethylene producers – Dow Europe, Ineos Chlor and Chimcomplex Borzesti (Romania) – have signed a product stewardship charter aimed at ensuring safe use of this chlorinated solvent in all metal cleaning applications. The charter commits signatories to selling trichloroethylene only to end-users with enclosed equipment, thus minimizing workplace exposure.

1.2. Remediation Technologies

The conventional methods employed for TCE contaminated groundwater treatment are air-stripping and carbon adsorption. Recently alternative processes like bioremediation, reactive remediation, phytoremediation and in situ thermal treatments have been investigated. These methods attempt to convert TCE into a more benign chemical rather than move the contaminant from one phase (water) to another (air/solid), which still requires further treatment.

Due to the small presences of these compounds in groundwater, an interesting treatment approach consists in pre-concentrating and eliminating the contaminant. Water phase technologies involve several disadvantages that could be avoided in gas phase. In this way, the pre-concentration of the pollutant, the transfer to gas phase and the application of the treatment are optimal alternatives.

Incineration which has largely been the favored methodology to handle toxic organic compounds is a difficult task to perform in a technically and environmentally acceptable way when dealing with chlorinated organics. Incineration is unattractive from the standpoint that some products such as dioxins are even more toxic than the halocarbon reactants. In addition, complete combustion of these kind of compounds occurs at such high temperatures ($T > 1700\text{K}$) as to be

economically prohibitive.

Another alternative is the catalytic combustion using catalysis, which does not require as high temperatures as incineration and hence, dioxins are not formed [1]. However, the value of the poly-carbon molecule is lost when burned to carbon dioxide. Thus, an attractive alternative to incineration and combustion is to convert the halocarbons into useful chemicals by replacing either all or selected halogen atoms with hydrogen atoms (hydrodechlorination)[2]. Thermal (non-catalytic) dehalogenation has been successfully applied to a range of halogenated compounds, but elevated temperatures (up to 1173 K) are required to achieve complete (ca 99.95%) dehalogenation. A thermodynamic analysis of gas-phase hydrodechlorination reactions has shown that HCl formation is strongly favored and the presence of a metal catalyst reduces considerably the operating temperature, providing a lower energy pathway for the reaction to occur[3].

Catalytic hydrodehalogenation is established for homogeneous systems where the catalyst and reactants are in the same (liquid) phase and although high turnovers have been achieved. This approach makes it important in organic synthesis. It is not suitable for environmental protection purposes owing to the involvement of additional chemicals (such as solvents/hydrogen donors) and the often difficult product/solvent/catalyst separation steps. It is, nevertheless, worth flagging the reported application of transition metal coenzymes such as vitamin B₁₂ (Co), F₄₃₀ (Ni) and hematin (Fe) to promote homogeneous hydrodehalogenation reactions.

Hydrodechlorination has been successfully promoted using Pd, Pt, Rh and Ni catalysts. It is clear that Pd is the most active dechlorination metal [2-7]. It is accepted that catalytic hydrodechlorination, in common with most hydrogenolysis reactions, exhibits structure sensitivity where the electronic structure of the active metal sites can govern the catalyst performance. One critical issue associated with liquid-phase hydrodechlorination is the appreciable catalyst deactivation caused by

the HCl by-product. For these reasons the hydrodechlorination in gas phase appear as the most promising technology to remove trichloroethylene compounds.

1.3. Catalytic hydrodechlorination of TCE in gas phase

1.3.1. Monometallic Catalysts

Noble metals constitute the main catalytic phase for hydrodechlorination due to their high reactivity for the transformation of chlorinated organic compounds into fully hydrogenated products [8, 9].

The understanding of the carbon-halogen bond dissociation is a key step toward modifying and increasing the activity and selectivity of a catalyst for this reaction. The cleavage of the C-Cl bond has been extensively studied. Metals such as Pt and Pd have been suggested as excellent catalysts for dechlorination reaction [10]. The hydrogenation of TCE on noble metal catalysts was first proposed by Ordóñez et al. [11]. The hydrogenation of double bonds would take place catalytically, while the elimination of HCl would be essentially non-catalytic. The hydrogenation of double bonds is favoured as the number of substituents of the double bonds decreases, especially when the atoms are very electronegative (such as chlorine atoms) because it absorbs electron density from the π bond. Ethylene, formed according to the general mechanism, would be quickly hydrogenated on the surface of a very active hydrogenation catalyst such as Pd[8].

With respect to different supports, alumina-supported Pd catalysts were found to exhibit high activity and stability [12, 13]. The influence of operation conditions (temperature, hydrogen flow, pressure, etc) on both activity and selectivity has also been studied. It was found out that higher reaction temperatures lead to higher initial activity but also to faster deactivation, and the high hydrogen flow rates have

the same effect [14]. Catalyst deactivation in gas-phase hydrodechlorination has been linked to different phenomena. The poisoning of the active phase by the HCl formed in the reaction was proposed by many authors as the main cause of deactivation [5, 11, 12]. Other works claimed that this phenomenon is not so important for several noble metals (including Pd) and suggested that metal particle sintering and coke deposition [14, 15] are the main causes of deactivation. One point is that HCl can react with inorganic supports, such as alumina, causing an increase of surface acidity (Al chlorides are strong Lewis acids), which may favour the formation of carbonaceous deposits on the catalyst surface [16]. Thus, the development of poison-resistant catalysts has gained significant importance in the recent years. The activity of the noble metal is influenced by several factors like method of preparation and metal particle size [17].

Summarizing, monometallic catalysts show high activity in the reduction of trichloroethylene with high selectivity to full hydrogenated hydrocarbons. However, the improvement of this technology in order to increase the selectivity towards valuable compounds is of great interest nowadays. In addition, the main disadvantage of monometallic systems is the high degree of catalyst deactivation.

1.3.2. Bimetallic catalyst

Several authors demonstrated the ability of bimetallic catalysts, composed of metals from Groups VIII and IV, to selectively convert chlorinated alkanes into more valuable alkenes [2, 18]. The best performance of these bimetallic catalysts was observed with Pt-Cu [19, 20] Pt-Sn [21], Pd-Au [22] and Pd-Ag [18] combinations. The catalytic performance, however, depends on the molar ratio between noble and non noble metals. Kovalchuk et al. [2] proposed that the governing factor for the high olefin selectivity of bimetallic catalysts in hydrogen-assisted dechlorination of chlorocarbons is the low adsorption energy for olefins on active sites, which consist of isolated noble metal atoms in a matrix of the modified catalyst's surface. However, the mechanistic details of this phenomenon are still under investigation.

Furthermore, the metal-support interaction also contributes to the change in the nature of the active sites, especially when noble metal is supported on reducible metal oxides such as TiO_2 , CeO_2 , Nb_2O_5 and La_2O_3 [23, 24]. In heterogeneously catalysed processes, structure effects are the most significant parameters governing the catalytic properties of the metal [17]. Ceria-based oxides are widely used for automotive catalysts because of their performance, not only in storing/releasing oxygen, but also in stabilizing precious metal dispersion. Several studies have dealt with Pt sintering and Pt-support interaction in Pt/ceria catalysts. Using laser Raman, Murrell et al. [25] showed that the precious metal interacts strongly with the ceria surface. Nagai et al. [26] showed how the oxygen electron density in the oxide support influences the strength of the Pt-O-M bond, controlling the sintering of supported Pt particles on CeO_2 .

It has been demonstrated that for the crotonaldehyde hydrogenation reaction, the selective hydrogenation of the carbonyl bond occurs when the metal has a strong interaction with the support (CeO_2) [27, 28]. However, the origin of the specific catalytic behaviour of platinum in SMSI (strong metal support interaction) state is still a matter of debate: formation of Pt-Ce alloy [29], electronic effect on platinum particles due to the partial reduction of ceria [27, 30], decoration of platinum particles by patches of partially reduced ceria, etc [31]. This interaction with the noble metals affect the catalytic behaviour, depending on the method of synthesis, pre-treatment etc [27, 32-34]. Recently Shekhtman et al. [33] have shown that Pt/ CeO_2 catalysts exposed at different normal pressure pre-treatment and evacuation regimes have different effects on catalyst surface composition.

Unlike monometallic catalysts, bimetallic ones show a low deactivation during time on stream. This fact, could be related with a possible stabilization of the noble metal by the addition of the second metal. The deactivation is mainly attributed to the poisoning effect of HCl. The surface acidity of inorganic supports, such as alumina, can be increased by forming Al-chlorides, which are strong Lewis acids favoring the

formation of carbonaceous deposits on the catalyst surface [16]. In this way, the use of basic materials as active phase supports could improve the stability of the catalyst.

Layered materials, e.g. hydrotalcite-like compounds, represent an interesting approach for developing catalysts with basic character and tunable properties [35]. Hydrotalcite-type compounds possess two-dimensional layered structures with alternating positively charged mixed metal hydroxide sheets and negatively charged interlayer anions along with water molecules. The general formula for hydrotalcites is given by $\{M(II)_{1-x}M(III)_x\}(\text{OH})_2 \{A_{x/n}^{n-}\} \cdot m\text{H}_2\text{O}$, where M(II) and M(III) are bivalent and trivalent metal ions, respectively, A is an interlayer anion, with x between 0.2 and 0.4.

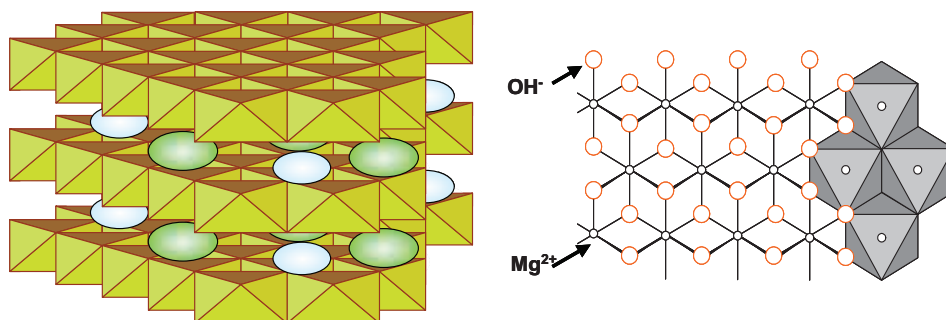


Figure 1.4. Schematic view of the structure of hydrotalcites

Their structure can be deduced from the brucite lattice $\{\text{Mg}(\text{OH})_2\}$ with partial replacement of Mg^{2+} by a trivalent cation like Al^{3+} . The resulting excess positive charge is compensated by anions, usually carbonate, occupying interlayer positions. The hydrotalcite and hydrotalcite-like structure is schematically represented in Fig. 1.4 [36].

Hydrotalcites (HT) containing transition metal, particularly copper-containing hydrotalcites are receiving increasing attention due to their diverse applications in catalysis [37-39]. Alejandre et al. [40] demonstrated that copper ions partially

substitute divalent cations and are incorporated in the layered structure of a HT. In this way, it is possible to synthesize a HT with active metals in the positively charged metal layers of a hydrotalcite precursor, which leads to a high dispersion of the active metal because of electrostatic repulsive forces. These materials exhibit basic properties, high metal dispersion and good stability against sintering. Therefore, they could potentially become interesting new catalysts for hydrodechlorination processes.

1.4. References

1. Coute N., O.J.D., Richardson J.T., Twigg M.V., Applied Catalysis B: Environmental, 1998. **19**: p. 175.
2. Kovalchuk, V.I. and J.L. d'Itri, Applied Catalysis a-General, 2004. **271**(1-2): p. 13-25.
3. Yuan, G. and M.A. Keane, Catalysis Today, 2003. **88**(1-2): p. 27-36.
4. B. Coq, G.F.a.F.F., Reaction Kinetics and Catalysis Letters, 1985. **27**(1): p. 157-161.
5. Coq, B., G. Ferrat, and F. Figueras, Journal of Catalysis, 1986. **101**(2): p. 434-445.
6. Kim, P., et al., Journal of Molecular Catalysis a-Chemical, 2006. **256**(1-2): p. 178-183.
7. Legawiec-Jarzyna, M., et al., Reaction Kinetics and Catalysis Letters, 2006. **87**(2): p. 291-296.
8. Ordonez, S., F.V. Diez, and H. Sastre, Industrial & Engineering Chemistry Research, 2002. **41**(3): p. 505-511.
9. Schreier, C.G. and M. Reinhard, Chemosphere, 1995. **31**(6): p. 3475-3487.
10. Barbosa, L.A.M.M. and P. Sautet, Journal of Catalysis, 2002. **207**(1): p. 127-138.
11. Ordonez, S., H. Sastre, and F.V. Diez, Applied Catalysis B-Environmental, 2000. **25**(1): p. 49-58.
12. Ordonez, S., H. Sastre, and F.V. Diez, Applied Catalysis B-Environmental, 2001. **29**(4): p. 263-273.
13. Finocchio, E., et al., Applied Catalysis B-Environmental, 2004. **51**(3): p. 143-148.
14. Ordonez, S., H. Sastre, and F.V. Diez, Applied Catalysis B: Environmental, 2003. **40**(2): p. 119-130.
15. Ordonez, S., E. Diez, and H. Sastre, Catalysis Letters, 2001. **72**(3-4): p. 177-182.
16. Coq B., et al., Journal of Catalysis, 1993. **141**(1): p. 21-33.
17. Gopinath, R., et al., Journal of Molecular Catalysis A: Chemical, 2004. **223**(1-2): p. 289 - 293.
18. Lambert, S., et al., Catalysis Today, 2005. **100**(3-4): p. 283-289.
19. Borovkov, V.Y., et al., Journal of Physical Chemistry B, 2003. **107**(23): p. 5568-5574.
20. Borovkov, V.Y., et al., Abstracts of Papers of the American Chemical Society, 2003. **225**: p. U140-U140.
21. Rhodes, W.D., et al., Journal of Catalysis, 2002. **211**(1): p. 173-182.

22. Nutt, M.O., J.B. Hughes, and M.S. Wong, *Environmental Science & Technology*, 2005. **39**(5): p. 1346-1353.
23. Srinivas, S.T., et al., *Studies in Surface Science and Catalysis*, 1998. **Volume 113**: p. 835 - 839.
24. Gopinath, R., et al., *Journal of Molecular Catalysis A: Chemical*, 2002. **181**(1-2): p. 215 - 220.
25. Murrell, L.L., et al., *Studies in Surface Science and Catalysis*, 1993. **75**: p. 681-690.
26. Nagai, Y., et al., *Journal of Catalysis*, 2006. **242**(1): p. 103-109.
27. Jacobs, G., S. Ricote, and B.H. Davis, *Applied Catalysis a-General*, 2006. **302**(1): p. 14-21.
28. Abid, M., V. Paul-Boncour, and R. Touroude, *Applied Catalysis a-General*, 2006. **297**(1): p. 48-59.
29. Abid, M., G. Ehret, and R. Touroude, *Applied Catalysis a-General*, 2001. **217**(1-2): p. 219-229.
30. Concepcion, P., et al., *Journal of the American Chemical Society*, 2004. **126**(17): p. 5523-5532.
31. Bernal, S., et al., *Catalysis Today*, 2003. **77**(4): p. 385-406.
32. Bera, P., et al., *Journal of Catalysis*, 2000. **196**(2): p. 293-301.
33. Shekhtman, S.O., et al., 2008. - **253**(- 2): p. - 311.
34. Kepinski, L. and J. Okal, 2000. - **192**(- 1): p. - 53.
35. Centi, G. and S. Perathoner, *Microporous and Mesoporous Materials*, 2008. **107**(1-2): p. 3-15.
36. Alejandre, A., et al., *Journal of Catalysis*, 1999. **188**(2): p. 311-324.
37. Crivello, M., et al., *Catalysis Today*, 2005. **107-08**: p. 215-222.
38. Kannan, S., A. Dubey, and H. Knozinger, *Journal of Catalysis*, 2005. **231**(2): p. 381-392.
39. Kim, Y.H., D.K. Lee, and Y.S. Kang, *Colloids and Surfaces A: Physicochemical and Engineering Aspects*, 2005. **257-258**: p. 273-276.
40. Alejandre, A., et al., *Chemistry of Materials*, 1999. **11**(4): p. 939-948.
41. Batista, J., et al., *Applied Catalysis a-General*, 2001. **206**(1): p. 113-124.
42. Wadayama, T., et al., 2008. **254**(17): p. 5380-5384.
43. Sa, J. and H. Vinek, *Applied Catalysis B-Environmental*, 2005. **57**(4): p. 247-256.
44. Mélendrez, R., et al., 2000. - **157**(- 1-2): p. - 149.
45. Tichit, D. and B. Coq, *Cattech*, 2003. **7**(6): p. 206-217.
46. Kovanda, F., et al., *Applied Clay Science*, 2001. **18**(1-2): p. 71-80.
47. Shannon, I.J., et al., *Journal of the Chemical Society-Faraday Transactions*, 1996. **92**(21): p. 4331-4336.
48. Kannan, S., V. Rives, and H. Knozinger, *Journal of Solid State Chemistry*, 2004. **177**(1): p. 319-331.
49. Dow, W.P., Y.P. Wang, and T.J. Huang, *Applied Catalysis a-General*, 2000. **190**(1-2): p. 25-34.
50. Hadjiivanov K.I. , V.G.N., *Adv. Catal. ,* 2002. **47**: p. 307.
51. Hadjiivanov K.I. , D.L., *Microporous Mesoporous Mater.*, 1999. **27**: p. 49.
52. Hadjiivanov, K.I., Vayssilov, G.N., *Adv. Catal.*, 2002. **47**: p. 307.
53. Davydov, A.A., *Infrared Spectroscopy of Adsorbed Species on the Surface of Transition Metal Oxides*. 1990, Chichester: Wiley.
54. Fung S.C., S.J.H., *Journal of Catalysis*, 1987. **103**: p. 220-223.
55. Vadlamannati, L.S., et al., 2000. - **Volume 130, Part 1**: p. - 238.
56. Luebke, D.R., et al., 2002. - **35**(- 3): p. - 217.
57. Jugnet Y. , B.J.C., Barbosa L. A. M. M. ,and Sauteta P. , *Surface Science*, 2002.

- 505**: p. 153-162.
58. Bae, J.W., J.S. Lee, and K.H. Lee, Applied Catalysis a-General, 2008. **334**(1-2): p. 156-167.
59. Bae, J.W., et al., Applied Catalysis A: General, 2001. **217**(1-2): p. 79-89.
60. Choi, H.C., et al., 1996. **161**(2): p. 790-797.
61. Barrabés, N., et al. - **In Press, Corrected Proof**(-): p. -.
62. Riguetto, B.A., Damyanova, S., Gouliev, G., Marques, C.M.P., Petrov, L., and Bueno, J.M.C., J. Phys. Chem. B, 2004. **108**(17): p. 5349 - 5358.
63. Bensalem, A.M., J. C.; Tessier, D.; Bozon-Verduraz, J. Chem. Soc. Faraday Trans., 1996. **92**: p. 3233.
64. Daturi, M., et al., Surface and Interface Analysis, 2000. **30**(1): p. 273-277.
65. Jacobs, G., R.A. Keogh, and B.H. Davis, Journal of Catalysis, 2007. **245**(2): p. 326-337.
66. Holmgren, A., B. Andersson, and D. Duprez, Applied Catalysis B-Environmental, 1999. **22**(3): p. 215-230.
67. Beche, E., et al., Surface and Interface Analysis, 2008. **40**(3-4): p. 264-267.
68. Wrobel, R., et al., Surface Science, 2008. **602**(2): p. 436-442.
69. Fox, E.B., et al., Topics in Catalysis, 2008. **49**(1-2): p. 89-96.
70. Rama Rao, M.V., Shripathi, T, Journal of Electron Spectroscopy and Related Phenomena, 1997. **87**: p. 121-126.
71. Bera, P., et al., Chemistry of Materials, 2003. **15**(10): p. 2049-2060.
72. Allen, A., Berstein, R.B., Can J. , J.Chem, 1954. **32**: p. 1044.
73. Jugnet, Y., Bertolini, J.C., Barbosa, L.A.M.M., Sautet, P., Surface Science, 2002. **505**: p. 153-162.
74. de Rivas, B., et al., Catalysis Communications, 2008. **9**(10): p. 2018-2021.
75. Phillips, L.A. and G.B. Raupp, 1992. - **77**(- 3): p. - 311.
76. Chintawar, P.S. and H.L. Greene, Journal of Catalysis, 1997. **165**(1): p. 12-21.
77. Hazzazi, O.A., G.A. Attard, and P.B. Wells, Journal of Molecular Catalysis A: Chemical, 2004. **216**(2): p. 247-255.
78. Anderson, J.A., J. Mellor, and R.P.K. Wells, Journal of Catalysis. **In Press, Corrected Proof**.
79. Driessen, M.D., T.M. Miller, and V.H. Grassian, Journal of Molecular Catalysis A: Chemical, 1998. **131**(1-3): p. 149-156.
80. Föttinger, K., R. Schlögl, and G. Rupprechter, Chem. Commun., 2008(3): p. 320 - 322.

Experimental

2.1. Characterization Techniques

Several characterization techniques that have been showed in Chapter 3 such as: crystallographic analysis, specific surface area measurements, metallic dispersion, reducibility studies, spectroscopy (by FTIR and XPS) and morphology studies (TEM and SEM) have been performed. Furthermore, additional techniques have been applied in this chapter.

i) Thermo gravimetric analysis

The decomposition process and the weight loss of the precursor material as a function of the temperature were recorded by thermogravimetric analysis apparatus (Netzsch STA 409 PC/4/H Luxx) under O₂-N₂ atmosphere. The heating and flow rates were 10°C·min⁻¹ and 20 ml·min⁻¹, respectively.

ii) Spectroscopy

The experimental setup consisted of an in situ high-temperature diffuse reflectance IR cell (from Spectra-Tech) fitted with ZnSe windows. The DRIFTS cell was located in a Bruker Equinox 55 spectrometer, operating at a resolution of 4 cm⁻¹. The cell was connected to the feed gas cylinders through low-volume stainless-steel

lines. The gas flows were controlled by Aera mass flow controllers, which were regularly calibrated. A 4-way valve was used to allow fast switching between two reaction feeds, when appropriate.

The catalysts were analyzed by X-ray photoelectron spectroscopy (XPS) in a Kratos AXIS Ultra DLD equipped with a hemispherical electron analyzer and charge neutralizer. The measuring chamber pressure was kept below 10^{-8} mbar during data acquisition and the source was a monochromated Al K α radiation. All the spectra were signal-averaged of 30 sweeps for O 1s and C 1s and 200 sweeps for Pt 4f and Ce 3d with a step size of 0.1 eV and dwell time of 300 ms.

iii) Morphology study

High-Resolution Transmission Electron Microscopy (HRTEM) was carried out with a JEOL 2010F instrument equipped with a field emission gun. The point-to-point resolution was 0.19 nm and the resolution between lines was 0.14 nm. Samples were deposited on holey-carbon coated grids from alcohol suspensions. At least one hundred particles were used for particle size distribution calculation.

2.2. Set-up equipment

The catalysts were tested in the hydrodechlorination reaction of trichloroethylene (TCE) using a continuous fixed-bed glass reactor in the range of 100°C-300°C, at atmospheric pressure and stoichiometric amounts of hydrogen. The gas feed is obtained flowing an inert gas (He) and hydrogen through a saturator (at T=25°C) containing Trichloroethylene in liquid phase.



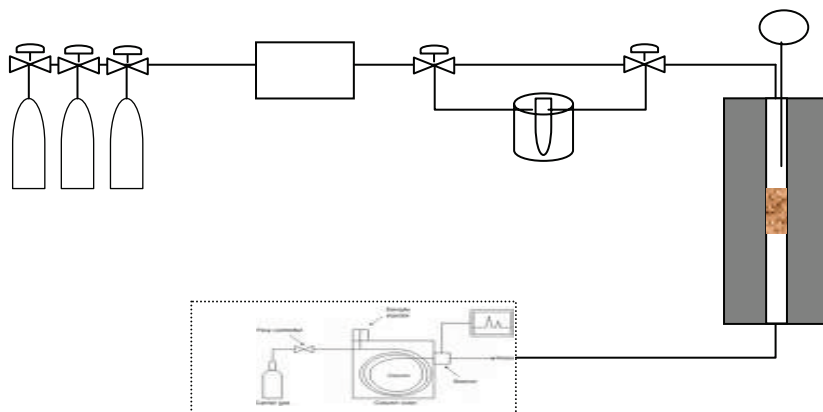


Figure 2.1. Experimental Set-ups: 1: Gas Bottles; 2: Mass flow controller; 3: Saturator; 4: Thermocouple; 5: Fixed-bed reactor with oven; 6: GC chromatograph.

The gas flows are adjusted by mass flow controller and introduced into the reactor, which is placed in an oven coupled with temperature control system. The outside reactor is connected by a six-ways valve to Gas Chromatograph (using HP-PoraPlot column). For all the experiments, 0.1g of catalyst was employed. The reaction conditions are shown in Table 2.1.

Table 2.1. Reaction Conditions

<i>Temperature (°C)</i>	100-300
<i>H₂ flow (ml/min)</i>	14
<i>He flow (ml/min)</i>	36
<i>TCE partial pressure (mbar)</i>	92
<i>Amount of catalyst (mg)</i>	100

UNIVERSITAT ROVIRA I VIRGILI
SELECTIVE HYDROGENATION CATALYSTS FOR ENVIRONMENTAL PROCESSES:
NITRATE AND CHLOROCOMPOUNDS REMOVAL
Noelia Barrabés Rabanal
DL: T-1539-2009/ISBN:978-84-692-4557-6

PdCu/Al₂O₃ catalysts

PdCu bimetallic catalysts supported on alumina prepared by different protocols have been studied, in order to establish the relationship between structure and activity/selectivity in the hydrodechlorination of TCE in gas phase. Surface properties related with the metals introduced are high influence by the protocol method preparation. An increase of ethylene selectivity is observed in all cases in comparison with monometallic Pd catalyst. The catalytic behaviour is strongly affected by the synthesis protocol method that shows a strong influence mainly related with the interaction between Pd and Cu.

3.1. Catalysts Synthesis

Four main procedures have been followed for the bimetallic catalyst preparation. In three syntheses, monometallic catalyst prepared is used as based. Sequential impregnation (SI), sequential reduction impregnation (SRI) and control surface reaction (CSR). In the Co-Impregnation (COI) is used an aqueous mixture of palladium and copper salts.

Firstly, monometallic Pd/Al₂O₃ was prepared by impregnation using an aqueous

solution of the precursor salt, $\text{Pd}(\text{NO}_3)_2 \cdot 2\text{H}_2\text{O}$. This step consists of a cationic exchange between the metallic complex and the alumina surface is an aqueous solution brought to $\text{pH} = 11$ by addition of ammonia. After evaporation of the aqueous phase, the catalyst was dried at 120°C , calcined in air at 450°C for 4h and reduced by flowing hydrogen at 300°C for 30 min.

The different catalyst preparation ways are shown in the following figure:

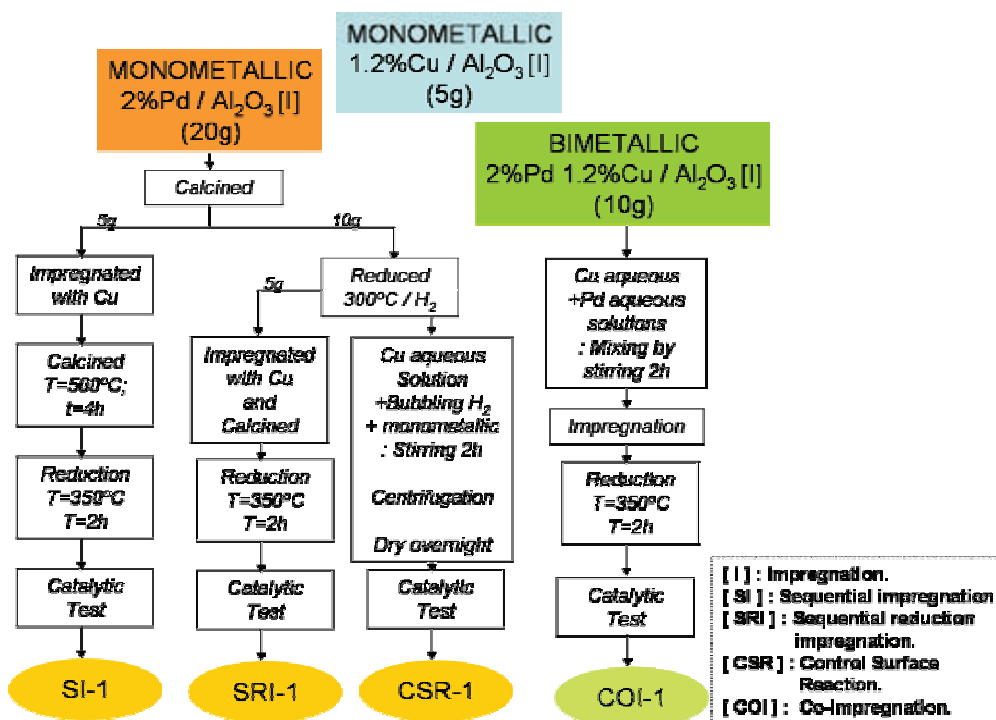


Figure 3.1. Catalysts synthesis procedures

3.2. Results and discussions

3.2.1. Characterization results

In order to study the reducibility of copper and palladium supported on alumina a TPR analysis was performed (Figure 3.2). The TPR of alumina and monometallic

Cu and Pd supported on alumina have been introduced as references. The TPR profile of the 1.2%Cu/Al₂O₃ catalyst exhibits peaks at 100°C and 300°C originating from the reduction step of the Cu²⁺ ion to metallic copper according to the literature[41]. The low temperature peak might be assigned to the reduction of several highly dispersed copper oxide species that include isolated copper anions, weak magnetic associates, and small two- and three-dimensional clusters. The high temperature peak might be attributed to the reduction of CuO oxide phase as well as the reduction of Cu⁺ ions to Cu⁰[41].

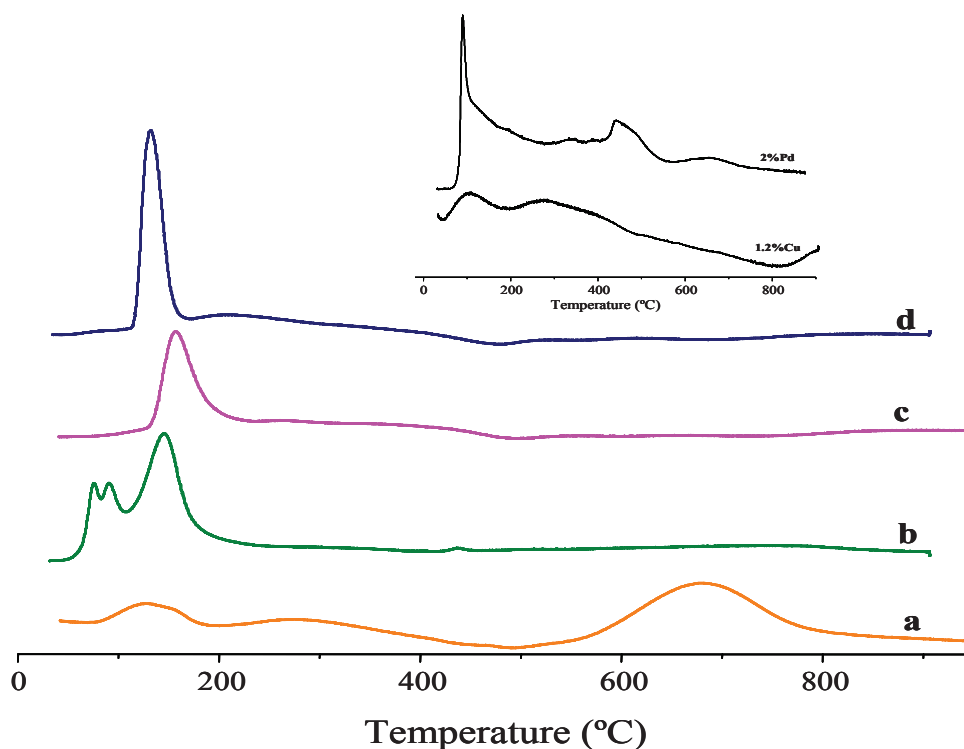


Figure 3.2. TPR profile of PdCu/Al₂O₃ catalysts: (a) CSR; (b) COI; (c) SRI; (d) SI

Figure 3.2 also shows as reference the reduction of monometallic Pd catalyst, showing the typical reduction of palladium at low temperature. The addition of copper (bimetallic catalysts) modifies the reduction profile. Previous works demonstrated the possibility of the formation of a Pd-Cu alloy to arise an interaction between copper and palladium oxides. In the TPR of SI(f) and SRI(e) catalysts a

new reduction peak appears around 150°C, that can be attributed to the reduction of Cu and Pd from the mixed oxide, Pd_xCu_yO [41]. For the COI preparation method an interaction between palladium and copper also occurs but the presence of some isolated palladium particles are observed in the TPR profile. The TPR shows a reduction peak around 170°C attributed to the Pd_xCu_yO mixed oxide and a peak at lower temperatures related with the reduction of isolated palladium particles. However when CSR protocol was used a new reduction peak was observed. The new reduction peak can be attributed to copper species and/or to the reduction of remaining species of the salts precursors. The results indicate that a good interaction between copper and palladium is observed when SRI and SI catalyst preparation protocols were used. However when COI and CSR protocols were employed, isolated palladium and copper particles, without the formation of bimetallic particles, were obtained.

Table 3.1 shows the results of nitrogen physisorption analysis. A slight decrease of BET area is observed after the incorporation of palladium that means a high dispersion of the noble metal (35%). When the copper is introduced, a decrease of the BET area is observed depending on the employed method. Whereas for CSR, SRI and SI, a slight decrease of BET surface area is observed, for COI catalysts the BET area decreases from 279 till 191 m²/g. This fact could be related with a poor dispersion of the metals in the catalysts.

Table 3.1. Physisorption results

<i>Catalyst</i>	<i>BET (m²/g)</i>
Al₂O₃	279
2%Pd/Al₂O₃	272
1.2%Cu/Al₂O₃	238
COI	191
CSR	258
SRI	245
SI	214

The adsorption of CO on Cu–Pd catalysts was examined using FT-IR spectroscopy, in order to study the state of the metals and their accessibility on the surface catalysts (Figure 3.3). CO adsorbed at room temperature on the different catalysts, leads to the appearance of three main bands between 1920 and 2150 cm^{-1} related with CO on palladium and copper particles (spectra a and b). The region from 1750 to 1900 cm^{-1} is generally assigned to CO adsorption on three-fold hollow Pd(111) sites [42]. These results are in agreement with the results obtained by other authors.

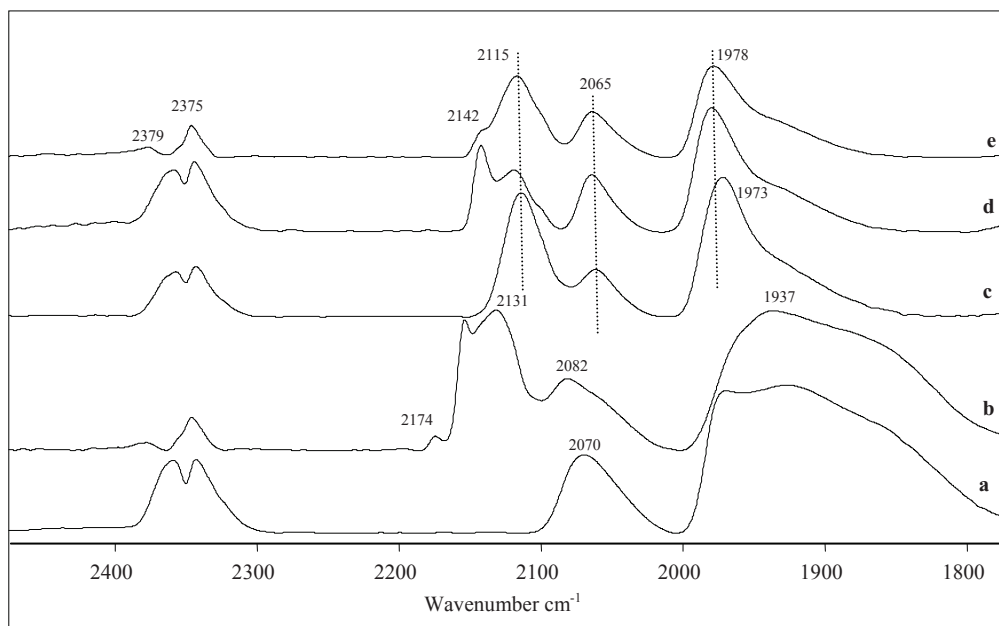


Figure 3.3. FTIR-CO of bimetallic catalysts: (a) 2%Pd/ Al_2O_3 ; (b) COI; (c) CSR; (d) SRI and (e) SI

The region from 1900-2050 cm^{-1} is often attributed to two-fold bridge CO adsorption. Finally, the bands between 2000- 2150 cm^{-1} are generally assigned to linearly bonded CO on Pd. These sites that bond CO linearly are mainly considered to be low coordinated (edges, corners). COI catalyst show a broad band at 1937 cm^{-1} related with a wide distribution of different Pd sites. This band also appears for the 2%Pd/ Al_2O_3 catalyst. It seems that no dilution of Pd ensemble by Cu atoms occurs, using this preparation protocol. Therefore separate Pd and Cu particles on the support are obtained, in agreement with TPR results.

The catalysts prepared by CSR, SRI and SI present four bands at 2142, 2115, 2065 and 1978 cm^{-1} . CO adsorption on metallic copper leads to a single CO vibration located between 2080 and 2120 cm^{-1} depending on the crystal plane and the nature of the support [43]. In this way the band around 2115 cm^{-1} corresponds to Cu^0 -CO species. The position at 2065 cm^{-1} is typical of terminal carbonyls of zero valent copper but also to carbonyls on zero valent Pd. Previous studies assigned this band to CO terminally bonded on Pd-Cu alloy[42]. The band at 1978 cm^{-1} suggests that Pd metal particles, where CO may adsorb linearly and bridging may also exist. CO adsorbed on oxidized Cu^+ is also observed, related with the band at 2142 cm^{-1} . This could be related with the reduction temperature inside the chamber (300°), not enough to reduce all the copper species.

Table 3.2. Vibrational frequencies of adsorbed CO on Pd and Cu surfaces

<i>Wavenumber [cm^{-1}]</i>	
1700 -1900	CO bridged over two and/or three Pd atoms
1981-2121	Cu^+ CO and Pd_2CO
1975-1990	CO in bridge configuration on Pd
2080 – 2120	CO adsorption on metallic Cu
2075 – 2091	CO bonded on metallic Pd
2110-2130	CO linearly bonded to Cu^0 and/or Cu^+
2122	Cu^0 – CO species
2135	CO adsorbed onto oxidized Cu^+
2163	Cu^{2+} CO species

The FTIR studies of the bimetallic catalyst showed that the Pd-Cu bimetallic catalysts prepared by redox reaction (SRI, SI and CSR) leads to a preferential deposit of the Cu on the surface of Pd. The Cu is deposited at the sites of lower coordination (edges and vertex)[44]. In the COI catalyst, a random distribution on the surface of the particles is observed.

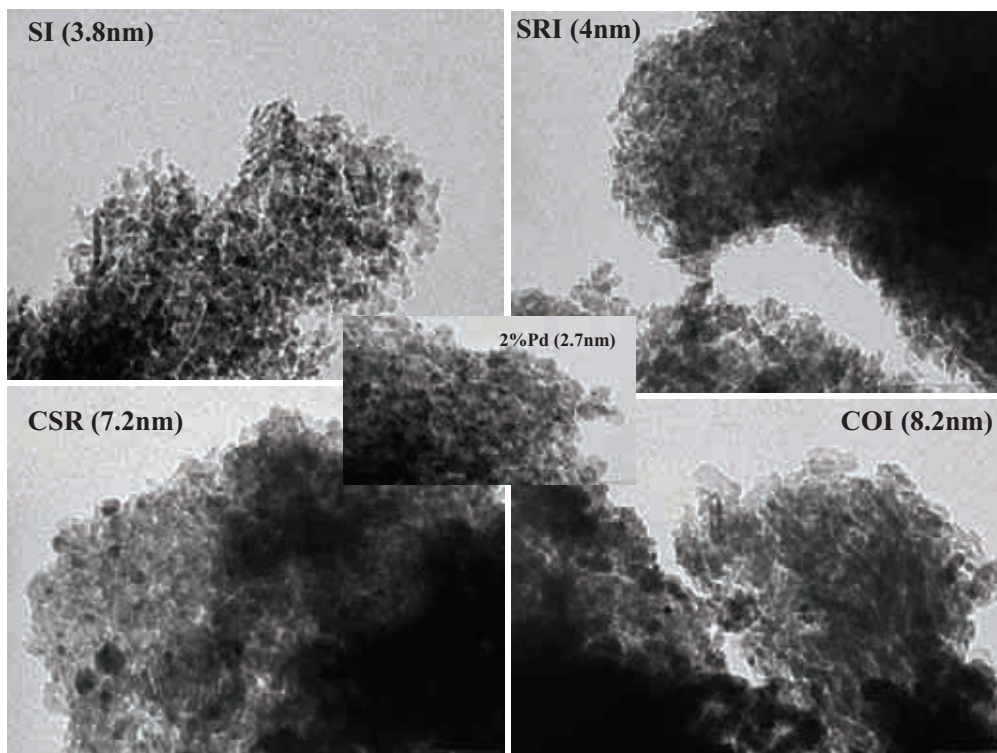


Figure 3.4. TEM from bimetallic catalysts

In order to obtain further information we studied the morphology of bimetallic Pd-Cu catalysts, TEM was taken and the representative photographs are shown in Fig.3.4. TEM images show that different particle sizes of palladium with each protocol method are obtained. Whereas SRI and SI catalysts present particles around 4nm, CSR and COI show particles of 7 and 8nm. These results are in agreement with TPR and FTIR results, where better distribution and higher interaction of Pd with Cu is observed.

4.2.1. Catalytic activity

The catalysts were tested in the hydrodechlorination reaction of TCE at 300°C using a stoichiometric molar ratio of TCE/H₂, in order to observe how the structural properties affect the catalytic behaviour. Whereas monometallic catalyst of 2%Pd/Al₂O₃ presents complete reduction of TCE to ethane, the use of bimetallic

catalyst increase the selectivity toward ethylene. Depending on the preparation protocol employed the activity and selectivity change (Fig. 3.5)

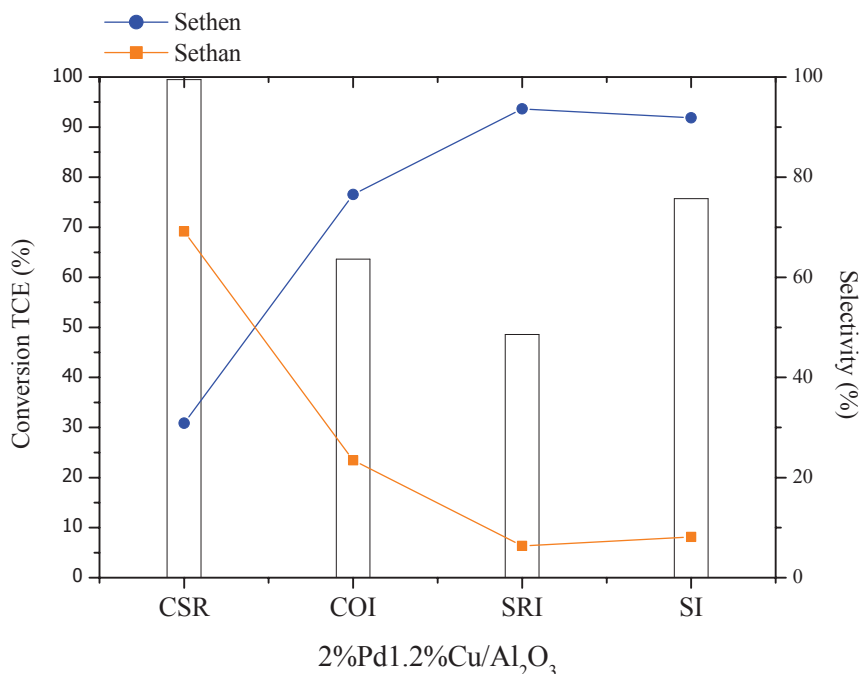


Figure 3.5. Catalytic activity of Pd-Cu/Al₂O₃ catalysts at 300°C and stoichiometric TCE/H₂ molar ratio

The catalyst prepared by CSR shows total conversion in the reduction of TCE with higher selectivity to ethane (70%). However the presence of ethylene is also observed (30%). This fact confirms previous results that show how the introduction of a second metal increases the selectivity to ethylene [2, 19]. When a different preparation protocol was performed (COI, SRI and SI catalysts) higher interaction between Pd-Cu could be expected. The catalytic behaviour of these catalysts showed in Figure 3.5 is quite different. A decrease in the conversion and an increase in the selectivity to ethylene, maintaining a higher conversion levels (50-70%), were observed. This could be explained taking into account the interaction between Pd and Cu, producing mostly bimetallic active sites, responsible for the selective hydrodechlorination of TCE to ethylene. Furthermore, COI catalysts present over

selectivity to ethylene (around 80%) than SRI and SI catalysts, where the selectivity to ethylene was always higher than 90%. From characterization results, it has been observed the presence of Pd-Cu bimetallic particles that could be responsible of the high selectivity to ethylene. However, the presence of some isolated Pd particles could be the responsible for the small amount of ethane that also is obtained.

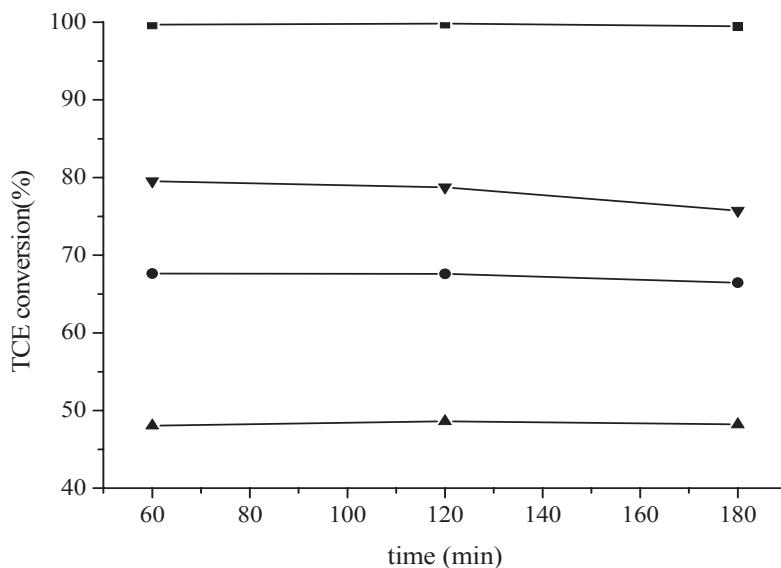


Figure 3.6. Catalytic activity of Pd-Cu/Al₂O₃ catalysts at 300°C and stoichiometric TCE/H₂ molar ratio vs time on stream (■ CSR; ▼ SI; ● COI; ▲ SRI)

Figure 3.6 shows the changes of TCE conversion versus time on stream for different bimetallic catalysts. Practically, no deactivation is observed after three hours of reaction. Only with the SI catalyst a slight decrease in the activity is observed after three hours. This fact is in agreement with previous works that explained how the use of bimetallic catalysts increases the stability against deactivation.

3.3. Conclusions

Whereas monometallic palladium catalyst deposited on alumina produce ethane as the unique product, this work shows that the incorporation of Cu increases the selectivity to ethylene.

The obtained results also show that the protocol for the formation of bimetallic Pd-Cu catalysts produces important changes in the catalytic behavior during the TCE hydrodechlorination reaction. Practically, a total selectivity to ethylene is obtained when SI and SRI preparation methods are employed. Better catalytic behavior in terms of activity is observed when CSR catalysts are used. However, it presents a poor selectivity toward ethylene. The changes in the catalytic behavior are related with the interaction of Pd-Cu, as well as, with the particle size and distribution on the surface. Higher level of interaction between the metals leads to higher selectivity toward ethylene, whereas isolated noble metal particles produces mainly ethane.

Pt,Pd-Cu/HT catalysts

Pt and Pd containing Cu-hydrotalcite-type precursors were applied as catalysts for selective hydrogenation of trichloroethylene to ethylene in gas phase. The catalytic materials were characterized by XRD, TGA, TPR, HRTEM and FTIR spectroscopy of CO adsorption. High activity and practically total selectivity to ethylene was obtained at 300°C. The Cu-hydrotalcite like materials (Cu-HT) were synthesized by co-precipitation. According to two different synthesis protocols the introduction of Pd or Pt, was performed. HRTEM measurements of the two differently prepared materials revealed fundamental differences at the microstructural level, detecting alloy formation on the samples prepared with a previous reduction step of the Cu-HT before Pd(Pt) introduction, whereas no alloy formation and the occurrence of larger Pt(Pd) particles was observed on the samples prepared without the previous reduction step of Cu-HT during the synthesis of Pd(Pt)-Cu-HT catalysts. Furthermore, whereas the former catalysts were stable during the reaction, the latter catalysts exhibited decreasing rate of ethylene formation with time on stream. This fact could be explained considering that during the reaction, the Cu particles are poisoning by Cl species produced during the reactions. It seems that a low regeneration capacity of these catalysts, due to a bad contact between noble metal and Cu, could be the responsible of this catalytic behavior. We propose that the reaction proceeds via cleavage of the C-Cl bond on Cu, which is then regenerated by spillover of hydrogen from the noble metal.

4.1. Catalysts Synthesis

Copper hydrotalcite like materials (Cu-HT) were prepared by a standard coprecipitation procedure combining two solutions. The first solution contained $\text{Mg}(\text{NO}_3)_2 \cdot 6\text{H}_2\text{O}$, $\text{Al}(\text{NO}_3)_3 \cdot 9\text{H}_2\text{O}$ and $\text{Cu}(\text{NO}_3)_2 \cdot 5\text{H}_2\text{O}$ in adequate amount, and the second NaOH as the precipitating agent. At room temperature, both solutions were slowly and simultaneously added to a beaker containing distilled water under vigorous stirring, at a pH-value around 9-10. The resulting suspension was then kept at 25°C with further stirring for 18h. The solid was filtered and washed several times with distilled water and dried at 100°C for 2 hours. The hydrotalcite was calcined at 450°C overnight obtaining a Cu/Mg/Al mixed oxide. Then, two different protocols were applied for the incorporation of the noble metal.

Table 4.1: Overview of the hydrotalcite materials used in this work

<i>Label</i>	<i>molar ratio (Cu+Mg)/Al</i>	<i>molar ratio Cu/Mg</i>
Mg₁Cu₂Al₁	≈3	≈2
Mg_{1.5}Cu_{1.5}Al₁	≈3	≈1
Mg₂Cu₁Al₁	≈3	≈0.5

In the first protocol (labeled as “-R”) the Cu/Mg/Al mixed oxides obtained after calcination, were reduced under hydrogen for 3 hours at 350°C. After reduction, the sample was introduced into an aqueous (or ethanol) solution containing the palladium or platinum nitrate salts under stirring at room temperature. In this step the palladium or platinum is reduced by a redox process with copper and is deposited on the surface of the catalyst. Then the solid was filtered and dried at 100°C, and again calcined for 2 h at 300°C. After that, a new reduction process was carried out in a hydrogen flow of 14 ml/min for 30 min at 300°C prior their use in hydrodechlorination reaction.

The second synthesis protocol (labeled as “-WR”), was performed omitting the reduction step before the noble metal introduction. The calcined material was impregnated with an aqueous solution of the noble metal salts. Then the solid was

dried at 100°C, calcined and reduced in the same way as in the first protocol. The obtained materials used in this study are compiled in Table 4.2.

Table 4.2: Overview of the noble metal promoted catalysts

<i>Label</i>	<i>Pd(Pt) loading wt%</i>	<i>Preparation procedure</i>
Pd(Pt)-Mg₁Cu₂Al₁-R	0.5	Protocol 1
Pd(Pt)-Mg_{1.5}Cu_{1.5}Al₁-R	0.5	Protocol 1
Pd(Pt)-Mg₂Cu₁Al₁-R	0.5	Protocol 1
Pd(Pt)-Mg_{1.5}Cu_{1.5}Al₁-WR	0.5	Protocol 2

4.2. Results and discussions

4.2.1. Characterization results

Thermogravimetric analyses of the uncalcined samples were carried out flowing nitrogen. For hydrotalcite-like materials, usually two or three weight losses due to 1) dehydration, 2) layer dehydroxylation, and 3) anion decomposition are observed [40]. Figure 4.1 shows the thermogravimetric analyses of Mg₁Cu₂Al₁ and Mg_{1.5}Cu_{1.5}Al₁ samples. Similar results are obtained for all the samples. Two main weight losses that are in agreement with previous works [38, 45, 46], are observed. The first weight loss occurs between 100°C-200°C and corresponds to the dehydration through removal of water in the interlayer space of the hydrotalcite as well as some water adsorption. The second weight loss between 220°C to 500°C is attributed to dehydroxylation of the brucite-like layers and decomposition of the anions located in the interlayer space. A decrease of the Cu²⁺ content in the brucite-like layers produces a slight increase of the dehydroxylation and decomposition temperature of the MgCuAl hydrotalcites. This behaviour was also observed by Kannan et al. [38] and was explained by the better stabilization of Mg²⁺ in the octahedral coordination of the HT lattice compared to copper.

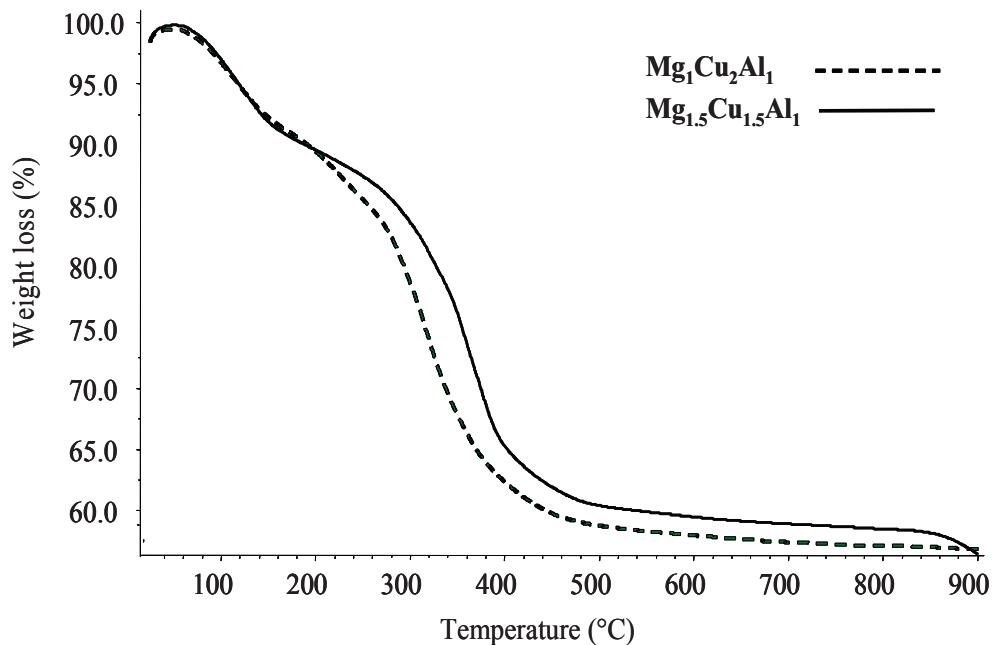


Figure 4.1. Thermogravimetric analysis of Cu-HT samples

Powder X-ray diffraction patterns of $Mg_1Cu_2Al_1$ and $Mg_{1.5}Cu_{1.5}Al_1$ before and after calcination are shown in Figure 4.2. The uncalcined hydrotalcite samples show the typical diffraction lines of the hydrotalcite-like phase without any additional peaks corresponding to other crystalline phases. The lower diffraction angles with 2θ values around 11° , 23° and 35° are ascribed to diffraction of (003), (006), and (009) planes, respectively. The broad and less intense diffraction lines at higher angles around $2\theta = 38^\circ$ ascribed to (015) plane and around $2\theta = 60^\circ$ for (110) and (113) planes, that are typical for hydrotalcite-like materials are also observed [38].

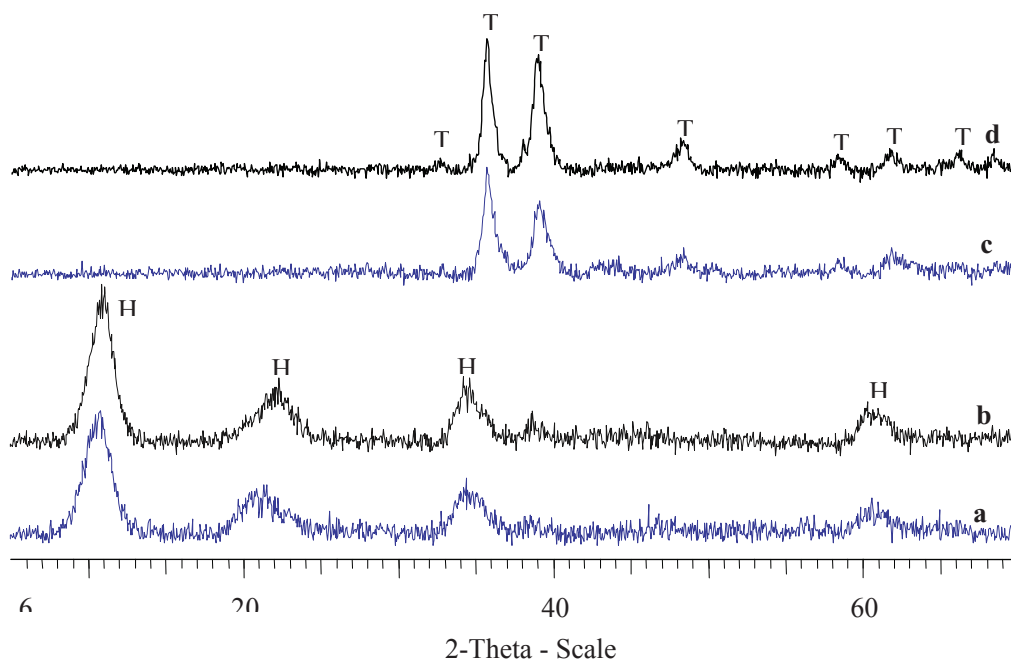


Figure 4.2: X-ray diffraction patterns of Cu-hydrotalcites: (a) $\text{Mg}_1\text{Cu}_2\text{Al}_1$ uncalcined; (b) $\text{Mg}_{1.5}\text{Cu}_{1.5}\text{Al}_1$ uncalcined; (c) $\text{Mg}_1\text{Cu}_2\text{Al}_1$ calcined; (d) $\text{Mg}_{1.5}\text{Cu}_{1.5}\text{Al}_1$ calcined (H=hydrotalcite, T=tenorite).

The X-ray diffraction patterns of both samples are nearly identical, which can be explained by the small difference in the octahedral ionic radii of Cu^{2+} (0.73 Å) and Mg^{2+} (0.72 Å) [47]. The broader diffraction lines obtained for both materials indicate a poor crystallinity. After calcination at 450°C the hydrotalcite phase disappears leading to formation of the tenorite phase (CuO , see Fig.4.2 c and d, indicated by “T”) in agreement with previous works [46, 48]. Similar powder diffraction patterns were obtained for materials with different CuMgAl molar composition. The noble metal containing materials exhibit the same XRD patterns. Diffraction patterns corresponding of the noble metals are not observed due to the small loading and good dispersion (observed by HRTEM, see later).

The results of the temperature-programmed reduction (TPR) of the calcined Cu-Mg-

Al mixed oxides (“Cu-HT”) and a corresponding Pt-containing sample (Pt-Mg_{1.5}Cu_{1.5}Al₁-R) are displayed in Fig.4.4. The Cu-HT samples show a broad peak around 300°C, which can be split into two components around 260°C and 320 °C, respectively. The first peak is attributed to the reduction of the highly dispersed copper oxide species, which include isolated copper cations and small two- and three-dimensional clusters [49]. The second peak around 320°C may be assigned to the reduction of large bulk-like CuO particles to Cu⁰, formed during the calcination process [40]. Reduction for all HT-samples is practically completed at a temperature below 400°C. With the gradual replacement of magnesium with copper cations, the first reduction peak decreases. This indicates a lower dispersion of the CuO phase that is created during the calcination and shows that smaller amounts of copper cations lead to a higher portion of easily reducible copper particles [46]. After peak deconvolution we estimated that about 70% of the total hydrogen consumption can be attributed to the feature at 320°C on Mg₁Cu₂Al₁, whereas this fraction decreases to 60% for the Mg_{1.5}Cu_{1.5}Al₁ sample. Thus, TPR measurements indicate a higher dispersion of CuO with increasing Mg content.

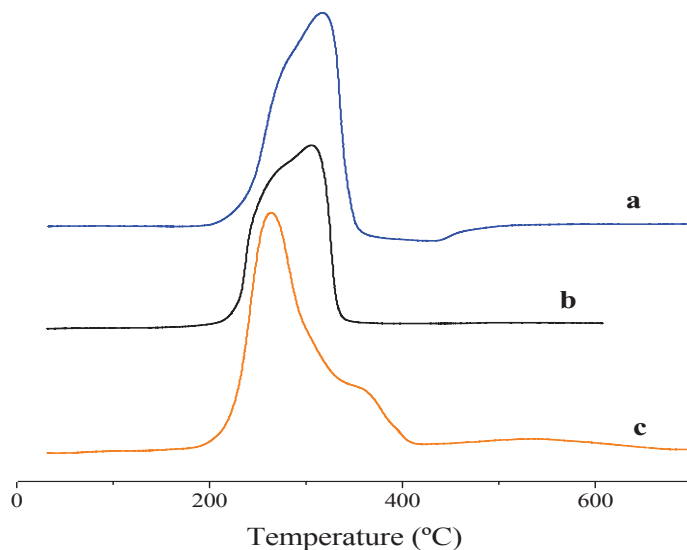


Figure 4.3: Temperature programmed reduction profiles of Cu-HT and Pt-Cu-HT catalysts: (a) Mg₁Cu₂Al₁; (b) Mg_{1.5}Cu_{1.5}Al₁ and (c) 0.5%Pt-Mg_{1.5}Cu_{1.5}Al₁-R

When the noble metal is introduced, the CuO reduction is facilitated, and the relative contribution of the low temperature reduction peak increases even more. Part of the CuO that is nearby Pt is reduced at lower temperatures, whereas the shoulder around 350°C is attributed to the reduction of bulk CuO isolated from Pt particles.

FT-IR spectra of CO adsorption were used to obtain information about the state of the noble metal particles and the copper species on the surface. Figure 4.4 shows a comparison of spectra after CO adsorption on $\text{Mg}_2\text{Cu}_1\text{Al}_1$ and $\text{Pd-Mg}_2\text{Cu}_1\text{Al}_1\text{-R}$ catalysts. In the presence of 5 mbar CO background pressure the main CO band appears at around 2114 cm^{-1} in all samples, with a small shoulder at higher frequencies at approximately 2144 cm^{-1} . After evacuation of the CO gas phase at room temperature the intensity of the band at 2114 cm^{-1} decreases strongly, whereas the high frequency band at 2144 cm^{-1} remains constant in intensity.

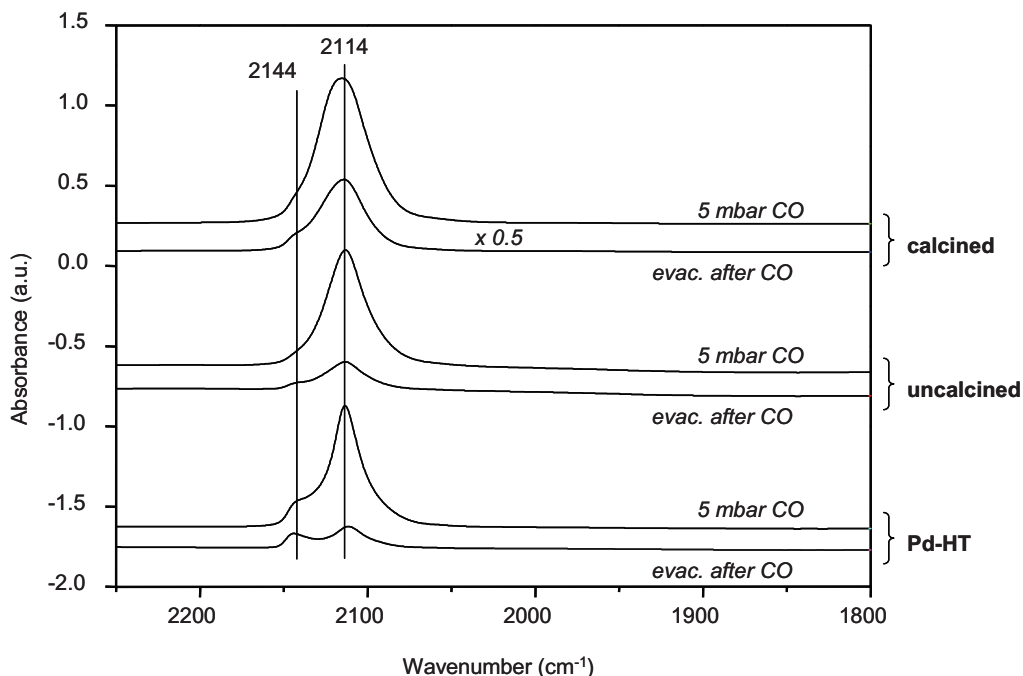


Figure 4.4: FTIR spectra of CO adsorption at 20°C in the presence of 5 mbar CO background pressure followed by evacuation at 20°C on calcined $\text{Mg}_2\text{Cu}_1\text{Al}_1$, uncalcined $\text{Mg}_2\text{Cu}_1\text{Al}_1$ and $\text{Pd-Mg}_2\text{Cu}_1\text{Al}_1\text{-R}$

For the $\text{Mg}_2\text{Cu}_1\text{Al}_1$ catalyst, the band at 2144 cm^{-1} is assigned to CO adsorbed on Cu^+ . This assignment is supported by the stability of this band at room temperature evacuation. When considering the frequency ranges reported in literature [50] the band at 2114 cm^{-1} could be attributed to CO on Cu^+ or on metallic Cu^0 .

Bands of CO adsorbed on copper in different oxidation states are not straightforward to identify and distinguish. Cu^{2+} is difficult to detect by CO adsorption, because it can easily get reduced by CO. Besides, CO- Cu^{2+} is a very weak interaction occurring typically at low temperatures and high pressures [51]. CO adsorption on Cu^+ leads to the most stable species. For CO adsorbed on Cu^+ the appearance of a high-frequency and a low-frequency band was reported at around 2160 and 2130 cm^{-1} [52], with the latter being less stable. But according to Davydov et al. [53] the high-frequency and a low-frequency band were observed at lower frequencies, around 2140 and 2115 cm^{-1} , which is very similar to our results. Discrimination of CO on Cu^0 and Cu^+ is possible via the different stability of the bands and via regarding the coverage-dependence of the band position. The frequency of νCO on Cu^+ is not or only weakly coverage-dependent in contrast to CO on Cu^0 [50]. The results show that the intensity of the band at 2114 cm^{-1} decreases after evacuation. Besides, the addition of Pd in the sample Pd- $\text{Mg}_2\text{Cu}_1\text{Al}_1$ -R also results in a decrease in the intensity of this band whereas the band at 2144 cm^{-1} remained constant (see Fig.4.4). By TPR we have observed that the addition of Pd shifts the reduction of copper to lower temperature. It is known that CO is adsorbed strongly on Cu^+ ions since the carbonyls formed are stabilized by π -back-donation that is not performed on Cu^0 due to the high electron density. The introduction of Pd increases the electron density of the metal phase weakening the CO-Metal bond. Based on this, the two bands at 2114 and 2144 cm^{-1} can most likely be assigned to Cu^0 -CO and Cu^+ -CO species, respectively.

On the other hand, bands of CO adsorbed linearly on Pd^0 or $\text{Pd}^{\delta+}$ could be overlapped by bands of CO on Cu^0 or Cu^+ due to the large excess of copper. Similar trend could be observed for 0.5% Pt on HT samples. However, no vibrational bands

in the range $2000\text{-}1800\text{ cm}^{-1}$ due to CO bonded to 2 or more adjacent Pd atoms were observed. This indicates that the noble metal is well dispersed, with absence of larger ensembles of Pd atoms.

Beside the CO stretching vibration bands, broad bands in the range of 3700 cm^{-1} - 2900 cm^{-1} due to residual water were observed as well as bands below 1670 cm^{-1} , which can be attributed to carbonate-type species.

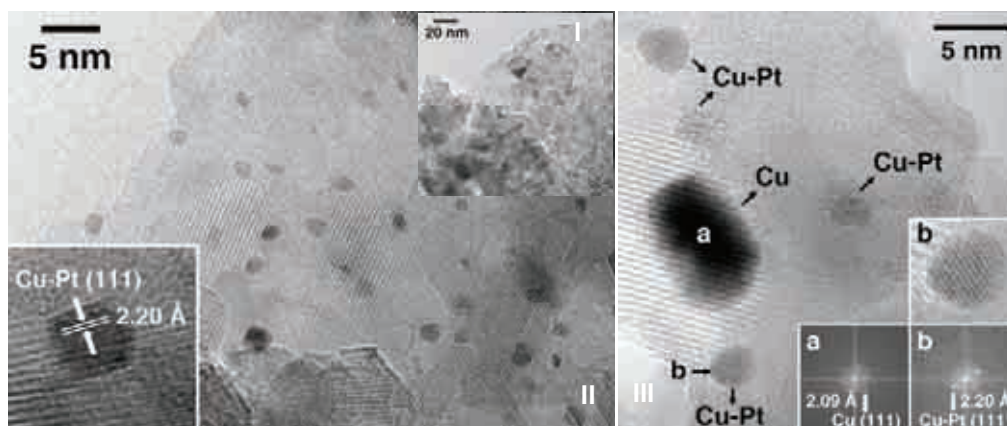


Figure 4.5: HRTEM image of $0.5\%\text{Pt-Mg}_{1.5}\text{Cu}_{1.5}\text{Al}_1\text{-R}$

The samples $0.5\%\text{Pt}$ and $0.5\%\text{Pd}$ on $\text{Mg}_{1.5}\text{Cu}_{1.5}\text{Al}_1\text{-R}$ samples were analyzed by HRTEM in order to study the distribution, size and state of the metallic particles. Figure 4.5(I) shows a bright field, low magnification image of the $0.5\%\text{Pt/Mg}_{1.5}\text{Cu}_{1.5}\text{Al}_1\text{-R}$ sample. It is mostly constituted by small, well-dispersed particles less than 2 nm in diameter. In order to get insight into their composition, numerous images were taken under high resolution mode (HRTEM). A representative HRTEM image is shown in Figure 4.5(II). A careful examination of this figure indicates that particles with diameters between 1 and 2 nm and exhibiting higher contrast are located at the borders of substrate crystallites, being the mean particle size of the particles centered at ca. 1.4 nm. An enlargement of one of these particles oriented along a crystallographic axis (see inset of Figure 4.6(II)) shows lattice fringes at 2.20 \AA . Taking into account that metallic copper exhibits (111)

spacings at 2.088 Å whereas the (111) planes of Pt metal are located at 2.265 Å, and that copper and platinum form solid solutions, the lattice fringes at 2.20 Å detected in this sample are indicative of solid solution formation between Cu and Pt. From the Vegard's law, $a_{\text{alloy}} = xa_{\text{Pt}} + (1-x)a_{\text{Cu}} + 0.01198x(1-x)$, a value of $x=0.6$ is deduced from $a_{\text{alloy}}=3.803$ Å (obtained from lattice fringes at 2.20 Å and assuming (111) crystallographic planes), thus meaning that the composition of Cu-Pt nanoparticles in these catalysts is approximately $\text{Cu}_{0.4}\text{Pt}_{0.6}$. Figure 4.5(III) shows another HRTEM image for this sample. Several Cu-Pt alloy particles are recognized. An analysis of particle labeled "b" in the image (see insets in direct mode and Fourier Transform images) reveals the presence of lattice fringes again at 2.20 Å, corresponding to (111) planes of the alloy. In addition to Cu-Pt alloy nanoparticles, the sample also contains other particles of about 8-10 nm in diameter which correspond to pure Cu. As an example, particle labeled "a" in Figure 4.5(III) corresponds to one of these Cu metal particles, identified by the presence of spots at 2.09 Å in the corresponding Fourier Transform image (see inset), which are ascribed to (111) crystallographic planes of metallic Cu. Therefore, this sample is mainly constituted by Cu-Pt alloy nanoparticles of 1-2 nm in size with approximate composition $\text{Cu}_{0.4}\text{Pt}_{0.6}$ and by larger Cu particles of 8-10 nm.

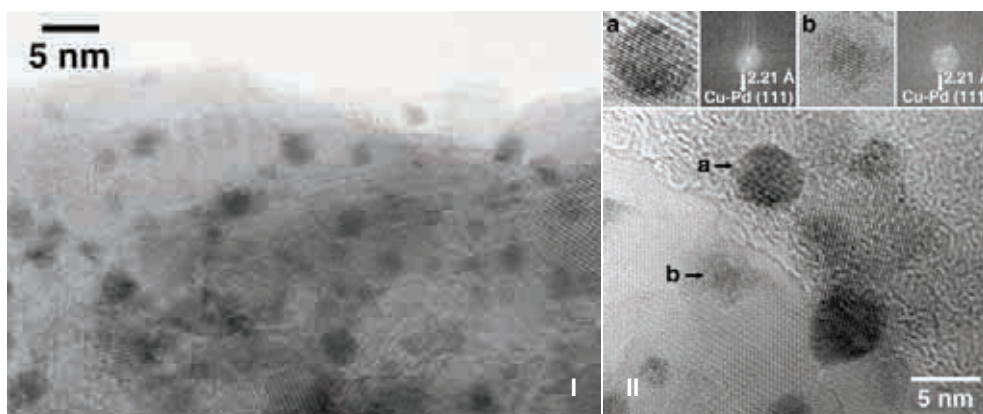


Figure 4.6: HRTEM image of 0.5%Pd-Mg_{1.5}Cu_{1.5}Al₁-R

Figure 4.6(I) shows a low-magnification image of 0.5%Pd-Mg_{1.5}Cu_{1.5}Al₁-R. Particles of about 1-5 nm are very well dispersed over the support, being the mean particle size of about 2.6 nm. The characterization of individual particles was accomplished by HRTEM analysis. Figure 4.6(II) corresponds to a representative HRTEM image. Particle labeled “a”, with a diameter of ca. 5 nm, exhibits lattice fringes at 2.21 Å (see the Fourier Transform image in the corresponding inset). Exactly the same lattice fringes at 2.21 Å are recognized in particle labeled “b” (see inset), which is much smaller, about 1.5 nm in diameter. Lattice-fringe images recorded through different parts of this sample yields similar values (2.21±0.01 Å). Assuming (111) planes, a lattice fringe of 2.21 Å implies a cell parameter of $a_{\text{alloy}}=3.824$ Å. From Vegard’s law for the Cu-Pd system, this cell parameter corresponds to an alloy composition of ca. Cu_{0.25}Pd_{0.75}.

Furthermore we performed a TEM study of the materials obtained according to the modified synthesis protocol, without reduction of the calcined Cu-HT before impregnation with the respective (Pt,Pd) noble metal. Following this protocol we expected to avoid alloy formation and to obtain worse noble metal dispersion. These samples (0.5%Pt-Mg_{1.5}Cu_{1.5}Al₁-WR and 0.5%Pd-Mg_{1.5}Cu_{1.5}Al₁-WR) were analyzed by HRTEM in order to confirm the hypothesis. The sample not reduced before Pt incorporation is different at the microstructural level from the sample discussed above, which was reduced before Pt impregnation. Figure 4.7(I) shows a general view of this sample in bright-field mode. Apparently, well-distributed particles of about 4-8 nm in diameter are present throughout the entire sample.

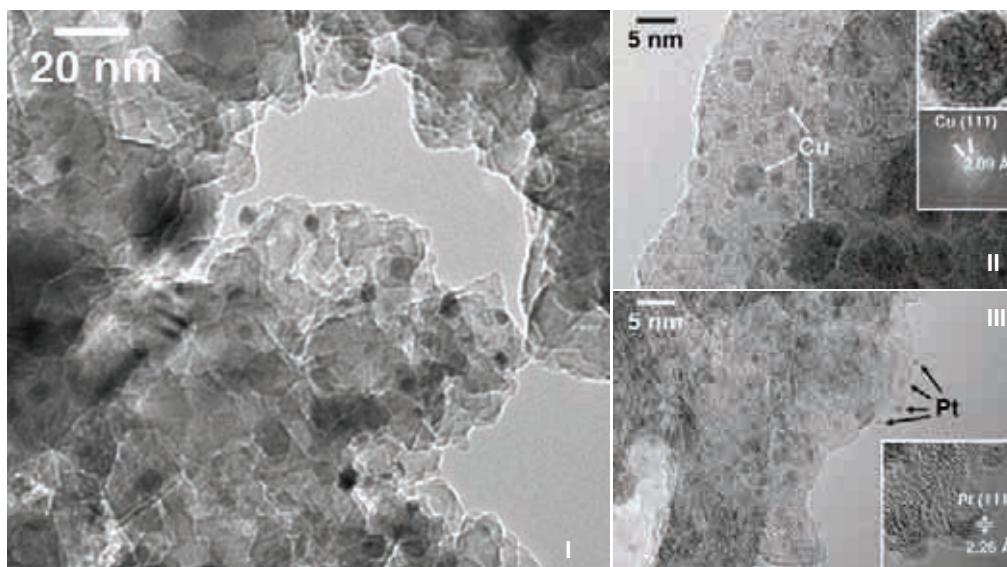


Figure 4.7: HRTEM image of 0.5%Pt-Mg_{1.5}Cu_{1.5}Al₁-WR

A close examination by HRTEM, however, reveals that the sample is in fact constituted by particles ranging from 0.8 to 10 nm in diameter. A representative example of this degree of particle dimensions is given in Figure 4.7(II). Lattice-fringe analysis of individual particles performed by HRTEM suggests that larger particles correspond to metallic Cu, whereas the smallest particles can be identified with Pt nanoparticles. Insets in Figure 4.7(II) show an enlargement of one of the big particles along with its Fourier Transform image. Spots at 2.09 Å are indicative of (111) crystallographic planes of metallic Cu. On the other hand, Figure 4.7(III) shows small Pt particles, which are marked by arrows. The lattice fringes at 2.26 Å shown in the inset of Figure 4.7(III) are ascribed to (111) planes of Pt metal. Although the presence of alloy particles in this sample cannot be completely ruled out, it appears from HRTEM analysis that the sample is mainly comprised by separate Cu and Pt entities.

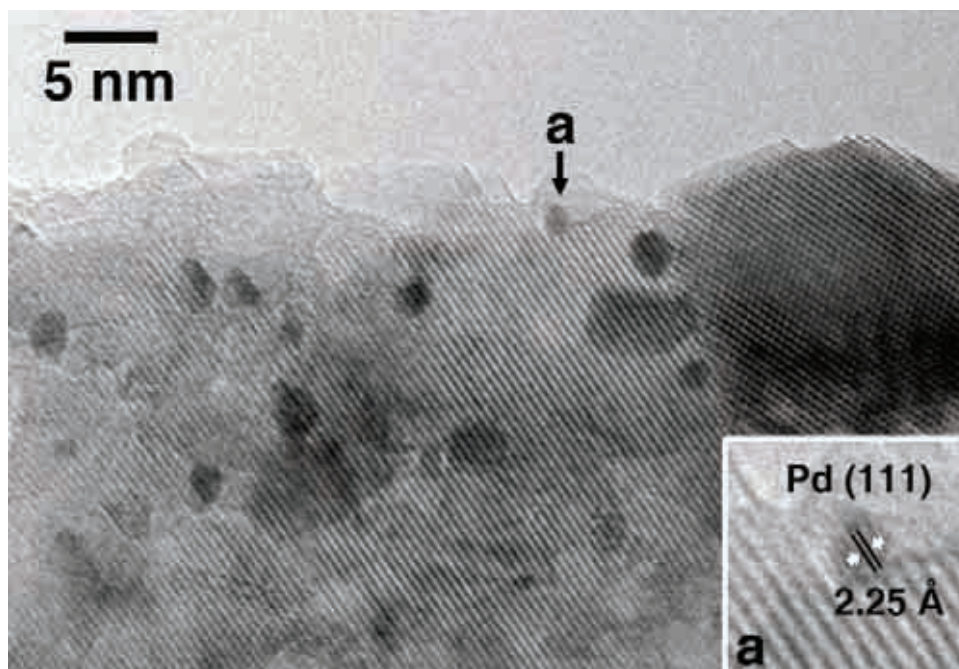


Figure 4.8: HRTEM image of 0.5%Pd-Mg_{1.5}Cu_{1.5}Al₁-WR

A general view of the 0.5%Pd-Mg_{1.5}Cu_{1.5}Al₁-WR sample is depicted in Figure 4.8. Particles ranging from 1 to 15 nm are distributed along the sample. In a similar way to that observed for the sample 0.5%Pt-Mg_{1.5}Cu_{1.5}Al₁-WR, which was similarly prepared (no reduction step prior to noble metal incorporation), this sample contains separate Cu and Pd particles. As an example, the inset in Figure 4.8 shows an enlargement of particle labeled “a”, which measures ca. 2 nm in diameter. Lattice fringes at 2.25 Å are ascribed to (111) planes of metallic Pd (nominal value 2.246 Å). No Cu-Pd alloy particles have been identified by HRTEM (but their presence cannot be completely excluded due to statistical limitation of the technique).

4.2.2. Catalytic activity

4.2.2.1 Influence of the composition

The catalysts prepared from hydrotalcites with different Mg/Cu ratios (Mg₁Cu₂Al₁,

Mg_{1.5}Cu_{1.5}Al₁ and Mg₂Cu₁Al₁) and impregnated with 0.5 wt% of Pd or Pt (-R samples) were tested in the hydrodechlorination of trichloroethylene (TCE) in a temperature range between 100°C-300°C. The results obtained at 300°C are summarized in Table 4.3. No clear trend is observed for the influence of the Mg/Cu ratio in the hydrotalcite precursor on activity and selectivity. 0.5wt% Pd-Mg₂Cu₁Al₁-R and 0.5wt% Pt-Mg₁Cu₂Al₁-R exhibited a slightly higher activity than the other samples.

Table 4.3: Influence of the catalyst composition on conversion and selectivity (reaction conditions: 300°C; molar ratio H₂:TCE = 2:1).

<i>Catalyst</i>	<i>Conversion (%)</i>	<i>Ethylene Selectivity (%)</i>
0.5%Pd-Mg₁Cu₂Al₁-R	22	97
0.5%Pd-Mg_{1.5}Cu_{1.5}Al₁-R	14	98
0.5%Pd-Mg₂Cu₁Al₁-R	29	96
0.5% Pt-Mg₁Cu₂Al₁-R	30	92
0.5% Pt-Mg_{1.5}Cu_{1.5}Al₁-R	25	93
0.5%Pt-Mg₂Cu₁Al₁-R	21	93

Note that the selectivity in Table 4.3 correspond to ethylene. Formation of ethane (mainly), 1,1-dichloroethylene, cis-1,2-dichloroethylene, trans-1,2-dichloroethylene, chloroethylene and chloroethane were also observed during the reaction but only in very small amounts (<10%). Without noble metal promotion a very fast deactivation was observed, most probably due to poisoning effect of Cu by chloride.

Consequently, stable catalytic performance can be achieved by noble metal addition. Hardly any influence was observed with respect to the nature of the noble metal (Table 4.3). Similar activities were found for Pt and Pd-promoted samples, with Pd containing materials exhibiting slightly higher ethylene concentrations compared to Pt-HT ones.

Lambert et al. [18] showed that pure copper samples show a very low activity at different temperatures for 1,2-dichloroethane hydrodechlorination towards ethylene. Chlorine atoms on the surface cannot be easily removed due to a lack of surface hydrogen. The role of the noble metal could, therefore, be to provide a sufficient supply of dissociated hydrogen for reduction of surface Cu-Cl_x species and formation of HCl, as it has been suggested by Fung and Sinfelt [54], and by Vadlamannati et al. [55] for 1,2-dichloroethane hydrodechlorination over Pt-Cu/C catalysts. Also the fact that the nature of the noble metal component does not influence the catalytic performance supports the idea that it is mainly needed for hydrogen activation regenerating the catalytic activity.

4.2.2.2 Effects of the reaction temperature

The hydrodechlorination reaction of TCE shows strong temperature dependence. The catalytic activity for 0.5 wt% Pd- $\text{Mg}_2\text{Cu}_1\text{Al}_1\text{-R}$ at different reaction temperatures is shown in Figure 4.9.

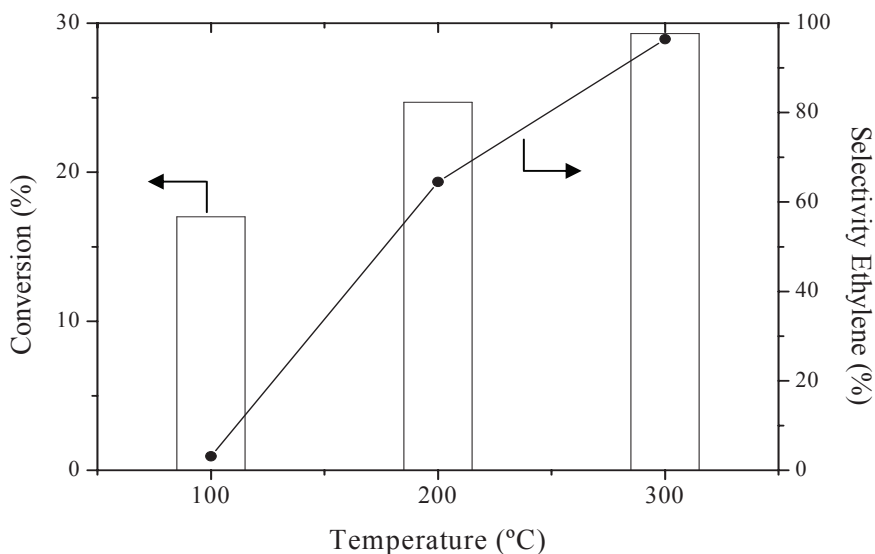


Figure 4.9: Conversion of TCE and selectivity to ethylene on 0.5%wt Pd- $\text{Mg}_2\text{Cu}_1\text{Al}_1\text{-R}$ at different reaction temperatures (molar ratio $\text{H}_2\text{:TCE} = 2\text{:}1$) [● Selectivity to ethylene, □ Conversion]

At a reaction temperature of 100°C the conversion of trichloroethylene was around 17% and the selectivity towards ethylene was very low (<5%). Upon increasing the reaction temperature to 300°C an slight increase of catalytic activity (around 30%) and a much stronger increase in ethylene selectivity was observed (>95%). This catalytic behaviour could be explained by several considerations. Because of at higher temperatures the residence time of trichloroethylene on the catalyst surface is much shorter, there is less time for complete hydrogenation of the double bond leading to production of more ethylene suppressing the reaction pathway towards ethane. Luebke et al. [56] showed that increasing the temperature in the hydrodechlorination of 1,2-dichloroethane catalyzed by Pt–Cu/C catalyst enhances the interaction between the metal and the reactant because of higher diffusion rates of the metal atoms at elevated temperatures, which result in increasing selectivity toward ethylene.

On the other hand, this effect could be related with the different reaction temperature for the activity of copper and the noble metal. Copper requires higher reaction temperatures for considerable activity. At lower temperature (100 °C) the reaction is performed on the surface of the noble metal, whereas at high temperatures (300°C) most of the reaction occurs on copper. Copper shows a high selectivity to ethylene whereas the noble metal shows a high selectivity to ethane. These facts can explain the strong increase of the selectivity toward ethylene at higher temperatures using this type of catalysts.

4.2.2.3 Influence of the preparation procedure

Two different catalyst preparation procedures had been applied (-R and -WR, see experimental section) with the aim to obtain catalysts possessing different noble metal dispersion and particle size as well as different degree of interaction with the Cu phase. This was investigated and confirmed by means of HRTEM measurements (see 4.2.1 section).

The materials prepared according to these two synthesis pathways were compared with respect to their catalytic properties. Figure 4.10 shows the catalytic activity and ethylene selectivity with time on stream obtained for 0.5wt% Pd-Mg₁Cu₂Al₁-R and 0.5 wt%Pt-Mg₁Cu₂Al₁-R catalysts, working at 300°C and understoichiometric hydrogen concentration (molar ratio H₂:TCE = 2:1). Both catalysts showed stable activity and selectivity for around 130 hours of time on stream. A slight higher activity and selectivity to ethane was observed for the Pd catalysts with respect to Pt ones. However, in both cases, the selectivity to ethylene was higher than 95% during time on stream.

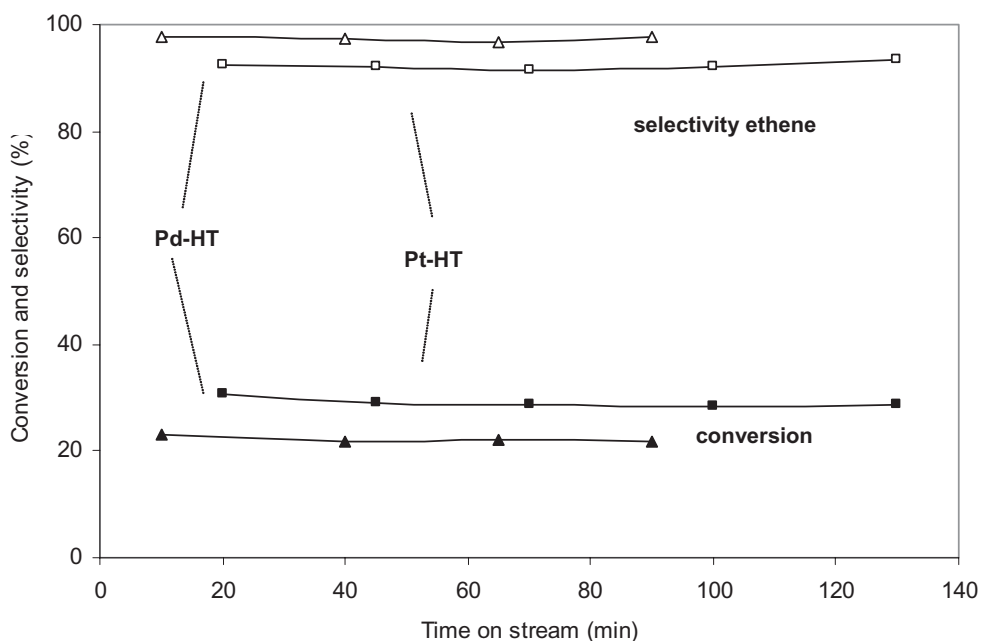


Figure 4.10: Conversion and selectivity to ethylene versus time on stream on Pd- and Pt-Mg₁Cu₂Al₁-R at 300°C and understoichiometric hydrogen concentration (molar ratio H₂:TCE = 2:1) [■ Pt-HT; ▲Pd-HT; ■ conversion of TCE, □ ethylene selectivity]

Table 4.4 shows a comparison of the catalytic properties obtained on 0.5%Pt-Mg_{1.5}Cu_{1.5}Al₁-R changing the H₂ : TCE molar ratio from understoichimometric amount of 2:1 up to stoichiometric amount of 3:1. Increasing the H₂ : TCE molar

ratio, increases the conversion from 24% up to practically total conversion (98%). However, the selectivity to ethylene remained practically constant (94%). This can be explained because at a higher hydrogen concentration, the chloride species linked to the copper surface are removed to a larger extent, leading to reactivation of copper active sites, without changing the catalytic behaviour.

Table 4.4: Effect of the H₂:TCE molar ratio (300°C; 0.5%Pt-Mg_{1.5}Cu_{1.5}Al₁-R)

<i>H₂ : TCE</i>	<i>Conversion (%)</i>	<i>Ethylene Selectivity (%)</i>
Understoichiometric 2:1	24	94
Stoichiometric 3:1	98	94

However, when the catalyst was prepared using the second synthesis protocol the performance at the same reaction conditions was different. The 0.5%Pd-Mg_{1.5}Cu_{1.5}Al₁-WR catalyst showed a total conversion of TCE, at 300°C and at a H₂ : TCE molar ratio 3:1, (see Figure 4.11). Constant activity is observed with time on stream, whereas the selectivity decreases. At the beginning of the reaction the main product was ethylene with selectivity around 90% and selectivity to ethane of around 10%. During time on stream the selectivity to ethylene decreases at the same time that the selectivity to ethane increases. After a time of stream of around 380 minutes the selectivity to ethylene was around 20% whereas the selectivity to ethane increased up to 80%.

The different catalytic behaviour obtained for the catalysts prepared by the two different protocols could be explained considering a different interaction between the noble metal (Pt or Pd) and Cu. From HRTEM measurements we have observed alloy formation between noble metal and Cu using the first protocol synthesis whereas using the second protocol the sample is mainly comprised by separate Cu and noble metal entities.

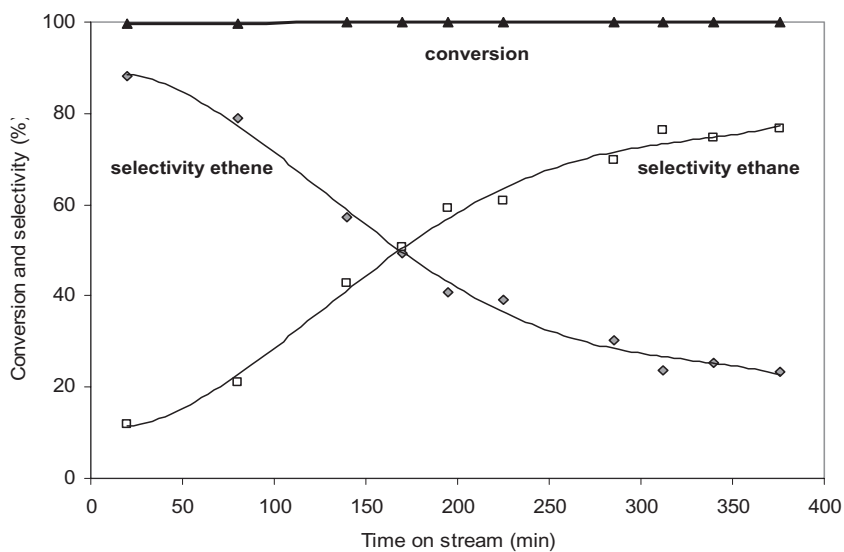


Figure 4.11: Catalytic activity and selectivity obtained on 0.5%Pd-Mg_{1.5}Cu_{1.5}Al₁-WR at 300°C under stoichiometric conditions (molar ratio H₂:TCE = 3:1) [□ TCE conversion; ○ ethane selectivity; △ ethylene selectivity]

4.2.2.4 Suggested reaction mechanism

Based on the results presented so far we propose a reaction mechanism that is displayed in Figure 4.12. The different catalytic behaviour observed for Pt- or Pd-Cu-hydrotalcite catalysts using the two different protocols could be related to a different reaction pathway. Due to the large amount and high dispersion of Cu in the hydrotalcite materials the TCE is adsorbed on the Cu phase, which is responsible for the cleavage of the C-Cl bond, producing a dechlorinated product. It is well known that copper is an extremely good metal for C-Cl bond cleavage, with dehalogenation occurring even at very low temperatures [57]. However, Cu shows a poor ability for hydrogen chemisorption to create H atoms that can react with the Cl species, on the surface of copper particles, cleaning the surface by formation of HCl. Consequently, the addition of a noble metal capable to hydrogen chemisorption is needed. Furthermore, noble metals are very efficient for the hydrodehalogenation of chlorocompounds to produce deep hydrogenation products [58]. According to our

results the following mechanism could be proposed.

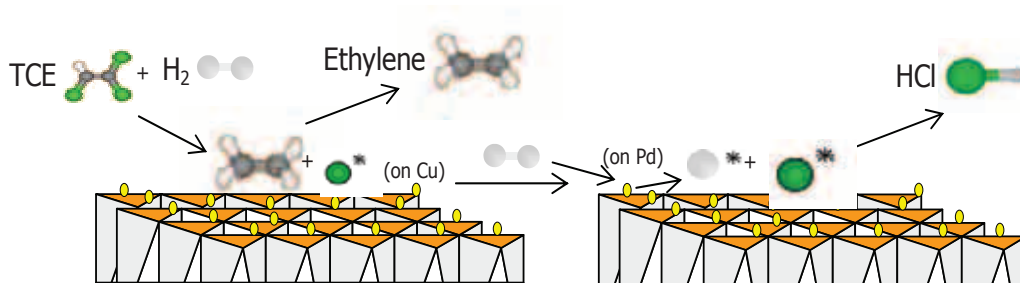


Figure 4.12: Scheme of the proposed reaction mechanism

For the catalysts prepared using the first protocol, showing alloy formation between noble metal and copper, copper is the responsible for the selective dehalogenation of TCE, whereas the noble metal-copper alloy is the responsible to provide hydrogen for the regeneration of the Cu-Cl_x surface by forming HCl species. Due to the presence of the alloy, the noble metal is not able to perform the full hydrogenation of the olefin obtaining a catalyst with a high selectivity to ethylene. For the catalysts using the second protocol, showing separate copper and noble metal phases, the selectivity toward ethylene is also high at short reaction time but decreases with time on stream. At the beginning of the reaction the copper surface is active resulting in ethylene formation as the main product. However, during the reaction copper surface is poisoned by chloride species and the main activity is taken over by the noble metal leading to ethane as the main product. Probably, the less effective regeneration of the Cu-Cl_x species on the surface of the catalysts due to the worse contact between noble metal and Cu for this type of catalysts could explain this catalytic behaviour.

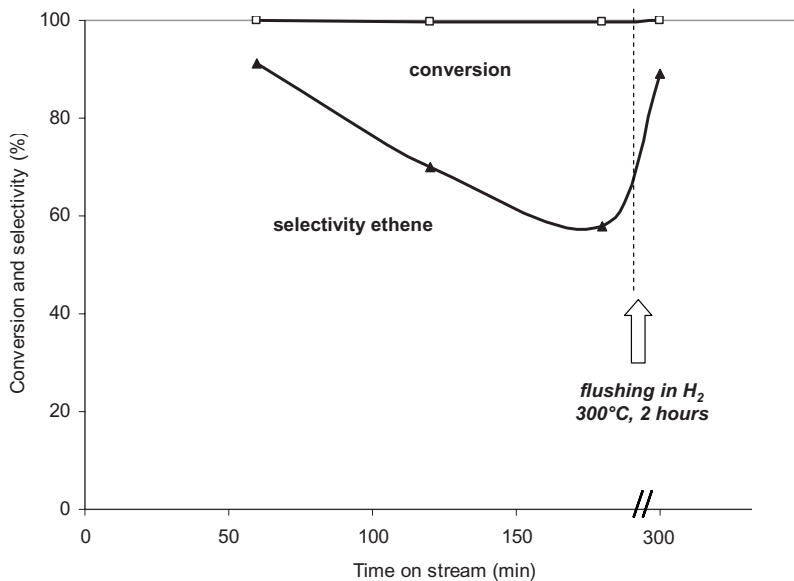


Figure 4.13: Conversion and selectivity to ethylene on 0.5%Pt-Mg_{1.5}Cu_{1.5}Al₁-WR at 300°C (molar ratio H₂:TCE = 3:1). After 3h time on stream flushing with H₂/He for 2 hours and then switching back to the reaction mixture [□ TCE conversion; △ ethylene selectivity]

To test this assumption we carried out the following experiment (see Fig. 4.13): the 0.5%Pt-Mg_{1.5}Cu_{1.5}Al₁-WR catalyst, after three hours on stream, was reactivated for two hours with hydrogen/helium mixture, and without the presence of TCE. During this process the removal of HCl species from the surface of the catalyst was observed. Then, the reaction was started again. Figure 4.13 shows that after this cleaning procedure the selectivity returns to the initial values, with ethylene as the main product, and then starts going down again.

4.3. Conclusions

Pt,Pd/Cu-hydrotalcite catalysts were prepared using different synthesis protocols. HRTEM measurements of the materials prepared by the two different protocols revealed fundamental differences at the microstructural level. PdCu-noble metal alloy formation was found on the samples prepared with a reduction step before Pd(Pt) introduction, whereas no alloy formation and the occurrence of larger Pt(Pd) particles was observed on the samples prepared without reduction step during synthesis. These catalytic materials showed high activity and selectivity to ethylene in the hydrodechlorination reaction of TCE. At higher reaction temperatures (300°C) and stoichiometric conditions of H₂/TCE, high conversion (>90%) and excellent selectivity towards ethylene (>90%) were obtained.

Hardly any influence of the Mg:Cu ratio both in activity and selectivity of the obtained catalysts was observed. However, a strong influence in the selectivity to ethylene during time on stream was observed changing the synthesis protocol of the Pt,Pd/Cu-hydrotalcite catalysts.

Changing the preparation procedure, performing a reduction step before introducing the noble metal (samples labeled as “-R”) or without this previous step (samples labeled as “-WR”), led to a different selectivity to ethylene. The interaction between copper with the noble metal forming an alloy or forming separate Cu and noble metal phases is the key to control the selectivity to ethylene.

A mechanism that involves adsorption of TCE on the Cu phase leading to dechlorination reaction giving ethylene is proposed. The main role of the noble metal forming the alloy is the regeneration of the Cu-Cl_x species by spillover of hydrogen. Catalysts where copper and the noble metal are in separate form, the dehalogenation reaction is carried out on the copper surface whereas on the surface of the noble metal a deep hydrogenation giving ethane is performed.

Since the role of the noble metal is mainly activation of hydrogen for regeneration of copper o to produce a deep hydrogenation of the chlorocompound, we did not observe a significant influence of the nature of the noble metal component.

UNIVERSITAT ROVIRA I VIRGILI
SELECTIVE HYDROGENATION CATALYSTS FOR ENVIRONMENTAL PROCESSES:
NITRATE AND CHLOROCOMPOUNDS REMOVAL
Noelia Barrabés Rabanal
DL: T-1539-2009/ISBN:978-84-692-4557-6

Pt/ceria catalysts

Two series of Pt/CeO₂ catalysts prepared by different synthesis protocol, co-combustion and impregnation, have been tested in hydrodechlorination of trichloroethylene in gas phase at mild reaction conditions (temperature between 100°C-300°C, and 1bar of pressure). The catalytic behaviour of Pt-Al₂O₃ catalysts was also studied for comparison. Several techniques (BET, XRD, FTIR, HRTEM, etc.) were performed for catalysts characterization. Using the combustion method, the platinum is introduced into the ceria matrix, whereas by the impregnation method, the platinum particles are deposited on the surface. In both cases a strong interaction between the support and the platinum particles is observed. Smaller platinum particles sizes are obtained using the impregnation method when compared with the combustion one. When the main product for Pt-Al₂O₃ catalysts was ethane, the use of CeO₂ as support increased the ethylene selectivity. Platinum catalysts obtained by combustion method showed the highest selectivity to ethylene. These results indicate that both, the presence of CeO₂ as support, as well as the interaction between ceria and platinum play an important role in the selectivity to ethylene. In order to study how the interaction of noble metal with the support affect the catalytic behaviour of Pt/CeO₂ catalysts in hydrodechlorination reactions. The surface species, as well as the reactivity and selectivity of the catalysts, were examined as a function of the catalyst pre-treatment conditions and noble metal precursor salts used in the preparation.

5.1. Catalysts Synthesis

Two procedures have been followed for Pt-CeO₂ preparation, impregnation **(I)** and solution co-combustion **(C)**. The synthesis of CeO₂ and impregnated catalysts was explained before in chapter 3. In these cases two different platinum salts were employed for sample preparation: a platinum chloride salt (H₂PtCl₆) that is indicated as **(WCl)** samples, and platinum acetylacetonate as a free chloride precursor **(NCl)**.

In the second method (co-combustion method **(C)**), different amounts of the platinum salt were introduced in the initial mixture containing cerium nitrate, Pluronic and ethanol. The homogeneous mixture is introduced into the muffle furnace preheated to 350°C, yielding a voluminous cerium oxide powder containing the platinum.

The catalysts were either pretreated under different gas atmospheres (atmospheric air, He, Ar, synthetic dry air) up to 300 °C and then reduced flowing pure hydrogen at 14 cm³ min⁻¹ for 15 min at the same temperature (this method is denoted as pretreatment throughout the text). On the other hand, the cerium oxide powder containing the Pt was reduced flowing pure hydrogen at 14 cm³ min⁻¹ from room temperature up to 300 °C at a heating rate of 10 °C/min and maintaining at 300 °C for 30min (the catalysts are denoted as reduced throughout the text).

5.2. Results and discussions

5.2.1. Characterization results

The characterization of Pt/CeO₂ obtained by impregnation was explained before in chapter 3. For the samples prepared by combustion (Fig. 5.1) broader peaks are observed between 200°C and 400°C that can be assigned to the combined reduction of Pt surface species, part of Pt introduced into the ceria lattice as well as the reduction of CeO₂ surface species. The broader peaks observed for these samples, in

comparison to the impregnation ones, are probably due to diffusion problems of the hydrogen into the Pt-CeO₂ system. Because the combustion involves rapid heating, large amounts of gases are generated during the process, leading to crystallite formation. The oxide formed at high temperature is quenched in this process. So in the combustion-derived Pt/CeO₂, Pt ions could either get separated into Pt metal or platinum oxide particles on the oxide support, or platinum ions could get incorporated into the CeO₂ matrix.

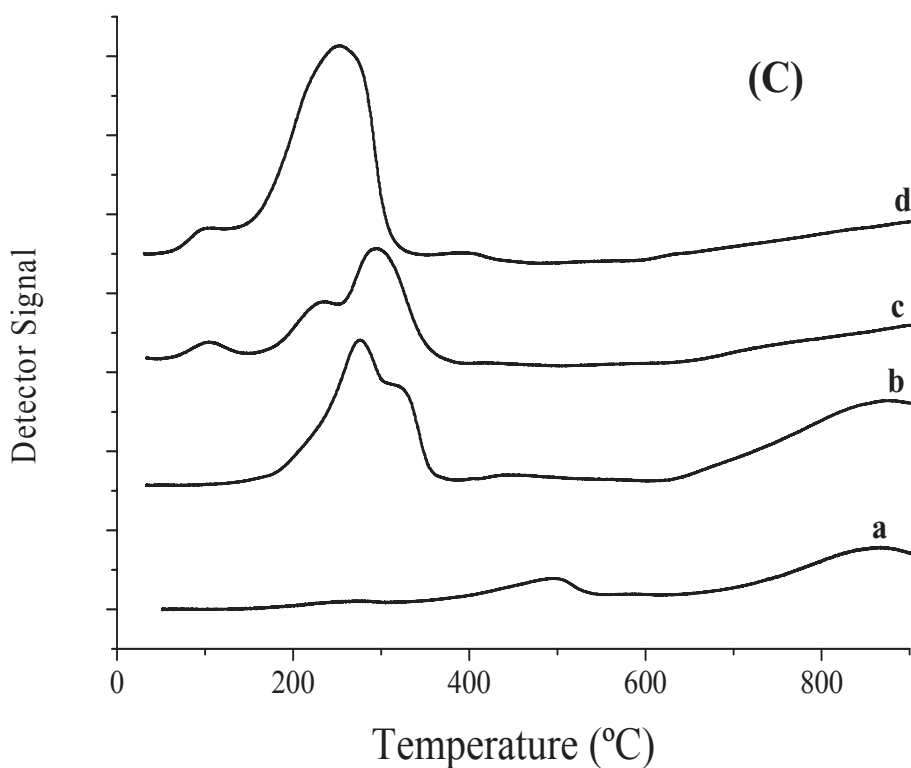


Figure 5.1: TPR profiles of Pt/CeO₂ catalysts prepared combustion (C): (a) 0%Pt; (b) 0.2%Pt; (c) 0.5%Pt and (d) 1%Pt

This behaviour was observed for 0.5 and 1% Pt/CeO₂ (C) samples, which exhibit small TPR peaks at 100°C attributed to the reduction of isolated platinum oxide to metallic platinum. This peak is not observed for the 0.2% Pt/CeO₂ (C) sample, probably due to the low amount of platinum in the sample. The main reduction peak for these combustion samples is observed between 180 and 350°C and can be

attributed to the reduction of the Pt-ceria and the ceria surface. The amount of surface ceria reduced to Ce^{3+} in this range of reduction temperature were 24.5%, 11% and 14.4% for 1%Pt/CeO₂ (C), 0.5%Pt/CeO₂ (C), and 0.2%Pt/CeO₂ (C) samples, respectively (see table 5.1).

Table 5.1: Pt metal dispersion and reduction degree of surface CeO₂ on Pt-ceria catalysts

<i>Catalyst</i>	<i>Calcination Temperature (°C)</i>	<i>Metal dispersion* (%)</i>	<i>TPR Reduction degree of CeO₂ (%)</i>
CeO₂	300	--	4
0.2Pt/CeO₂ (C)	300	10	14
0.5Pt/CeO₂ (C)	300	25	11
1Pt/CeO₂ (C)	300	50	24.5

*Obtained by H₂ chemisorption

The nanostructural modifications versus reduction temperature, in Pt/CeO₂ catalysts, were found to be dependent on the metallic salt precursors[29]. In particular, chlorine atoms remaining on the catalyst, after the impregnation of ceria with a chlorinated metal precursor, have been reported to prevent any interaction between metal and ceria compared with the strong interaction observed for the chloride-free material. To study this effect, different catalysts obtained by using Pt chloride salts (WCl) and non-chloride salt (NCl) were prepared using the combustion method. The TPR of these catalysts are shown in Figure 5.2. The NCl catalyst (Figure 5.2c) presents a broad peak between 50-300 °C. The low temperature peaks can be attributed to the reduction of oxidized platinum surface species and the very broad peak at ~200 °C could be attributed to the reduction of platinum species with interaction with the support. In contrast, the WCl catalyst shows three distinct features. Again a low temperature peak at 50 °C due to PtO_x reduction and two features at 250 and 320 °C representing the reduction of the surface of CeO₂. The higher temperature of the TPR profile for the chlorided sample indicates a different interaction between platinum and the support [58].

Previous works suggest that the product distribution in hydrodechlorination

reactions was mainly affected by the oxidation states of the various platinum precursors on alumina during the steady-state reaction. Therefore, the reducibility of platinum particle could also affect the catalytic activity and product distribution by influencing not only desorption properties of products but also the adsorption properties of reactants on the platinum sites [59, 60].

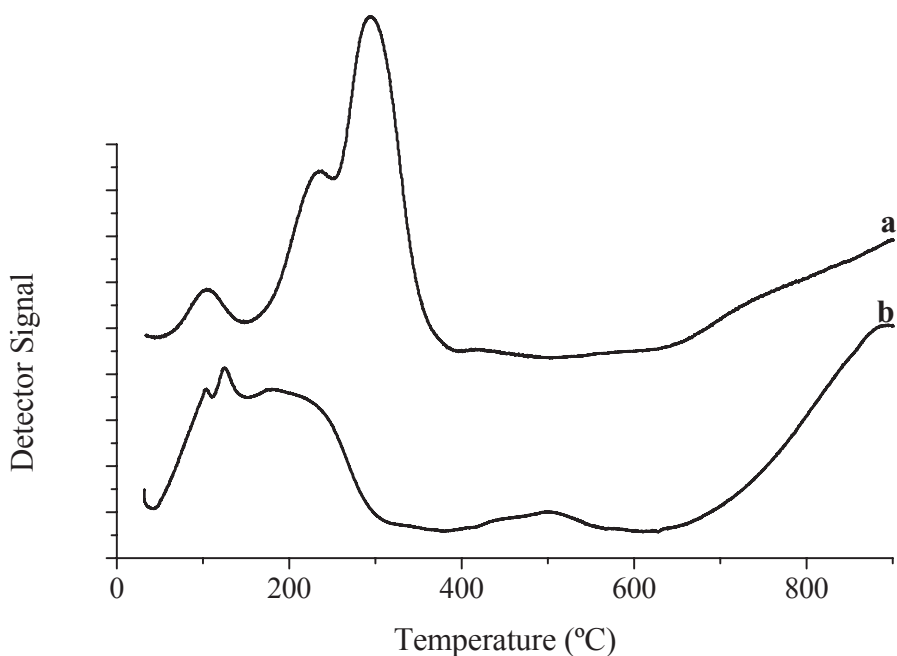


Figure 5.2. TPR 0.5%Pt/CeO₂ COC with different precursors: (a) 0.5%Pt/CeO₂ (C) with Cl; (b) 0.5%Pt/CeO₂ (C) without Cl;

XRD results show that CeO₂ obtained by combustion method as the samples of Pt/CeO₂ by both methods (C and I) have the typical fluorite-type oxide structure. No phases of Pt were detected. This could be explained by the low amount of noble metal in the samples and the high dispersion.

The platinum dispersion of these samples, obtained by hydrogen chemisorption, is shown in Table 5.1. (the metal dispersion for the impregnated samples are in chapter 3). The samples obtained by impregnation always showed the highest values of platinum dispersion when compare with the samples obtained by combustion

method. A 10% of metal dispersion was observed for the 0.2%Pt/CeO₂ (C) sample calcined at 300°C. When the amount of platinum increased the metal dispersion of the combustion samples also increased. The highest metal dispersion for the combustion samples was observed for the 1%Pt/CeO₂ (C) sample (around 50%). This fact could be explained by the presence of higher metal particles observed in these samples compared with the impregnated ones. These results are in agreement with the HTREM results. Furthermore, due to the preparation method, in which some part of the platinum particles could be encapsulated in the ceria matrix, could explain this behaviour.

The samples were analyzed by HRTEM. Figure 5.3 (I) shows a general view for the sample of 0.5%Pt/CeO₂ (C) after reduction process at low magnification. The sample is comprised by very well dispersed Pt nanoparticles over the CeO₂ support. The size of metal particles is very homogeneous and centred at 3.2 nm. The high dispersion of Pt nanoparticles in the sample merits to be highlighted since more than 90% of all nanoparticles exhibit diameters comprised between 2 and 4 nm. Two of these Pt nanoparticles are shown at higher magnification in Figure 5.3(II) (marked by arrows).

Although the particles are not structurally resolved, they show Moiré patterns due to interference with the lattice fringes of the CeO₂ support. Figure 5.3(III) shows a detailed image with atomic resolution of the contact area between a Pt nanoparticle and the CeO₂ support. The Fourier Transform (FT) image (inset) shows bright spots at 2.26 and 3.13 Å. The spots at 3.13 Å are ascribed to (111) planes of fcc CeO₂. The occurrence of these spots with less intense spots at 2.7 Å in the FT image at 54.7° indicates that the CeO₂ support crystallite is oriented along the [110] crystallographic direction. Spots at 2.26 Å correspond to (111) planes of metallic platinum. The Pt (111) and CeO₂ (111) spots are aligned along the same crystallographic direction, strongly suggesting the existence of an epitaxial relationship between them. The sample has been studied in detail over various locations and a large amount of particles exhibited epitaxial

relationship with the support, in samples prepared by the combustion synthesis method.

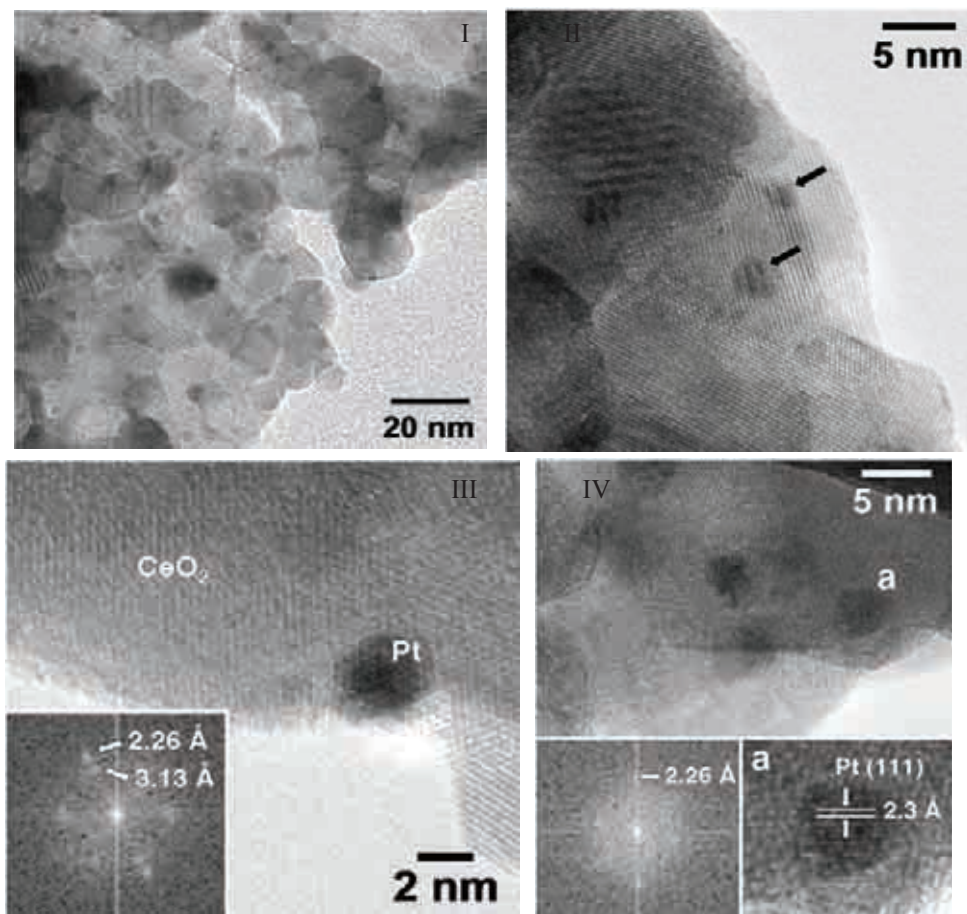


Figure 5.3. HRTEM of 0.5Pt/CeO₂ (C) catalyst

Figure 5.3(IV) shows other Pt nanoparticles. Particle labeled “a” exhibits lattice fringes at 2.3 Å (2.26 Å in the corresponding FT image), again corresponding to (111) planes of metallic Pt.

Particles in the sample prepared by impregnation (0.5%Pt/CeO₂ after reduction) are difficult to visualize by transmission electron microscopy due to their extremely small size. Figure 5.4(a) shows a typical HRTEM image for this sample, where Pt particles cannot be identified at all. Figure 5.4(b) corresponds to another area of the

same sample, where various particles of about 1.5 nm in diameter are marked by arrows. Whereas by combustion method epitaxi effect is observed, it has not been possible to perform a similar study over the sample prepared by impregnation, due to the small particle size.

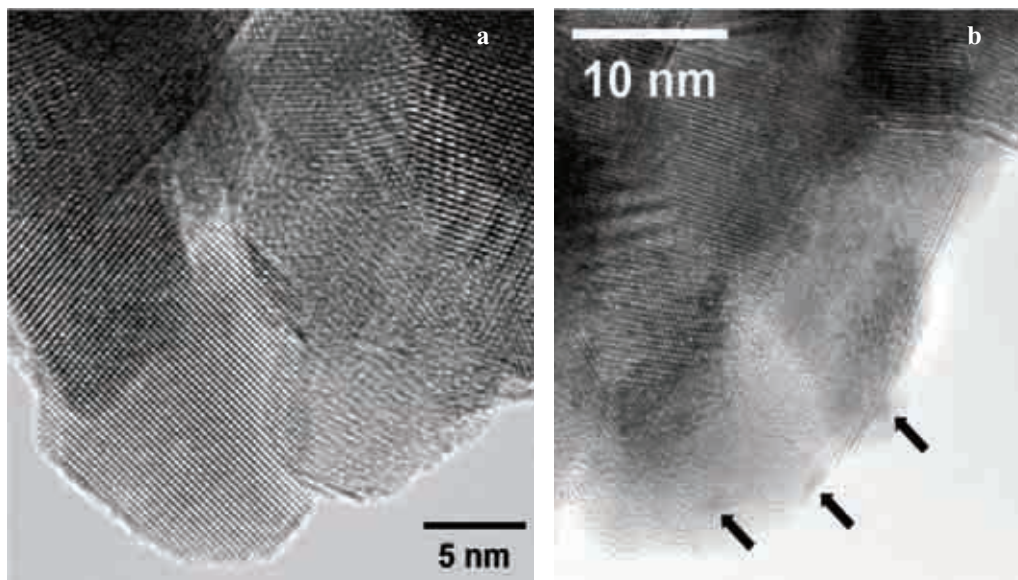


Figure 5.4. HRTEM of 0.5%Pt/CeO₂ (I) catalyst

A general view of the 0.5%Pt/CeO₂ (C-WCl) sample after reduction process at low magnification is show in Figure 5.5(b), where is comprised by very well dispersed Pt nanoparticles over the CeO₂ support. The size of nanoparticles is very homogeneous and centered at 3.2 nm (see histogram Figure 5.7). Figure 5.5(a) show low magnification images of 0.5%Pt/CeO₂ (C-WCl) sample after pretreatment. Pt nanoparticles continue to be well dispersed, although the mean particle size has increased slightly with respect to that the same sample after reduction, 3.9 vs. 3.2 nm. The pretreatment has resulted not only in an increase of the mean Pt particle diameter, but also in an increase of size heterogeneity. This is seen as a wide size distribution in the particle size histogram.

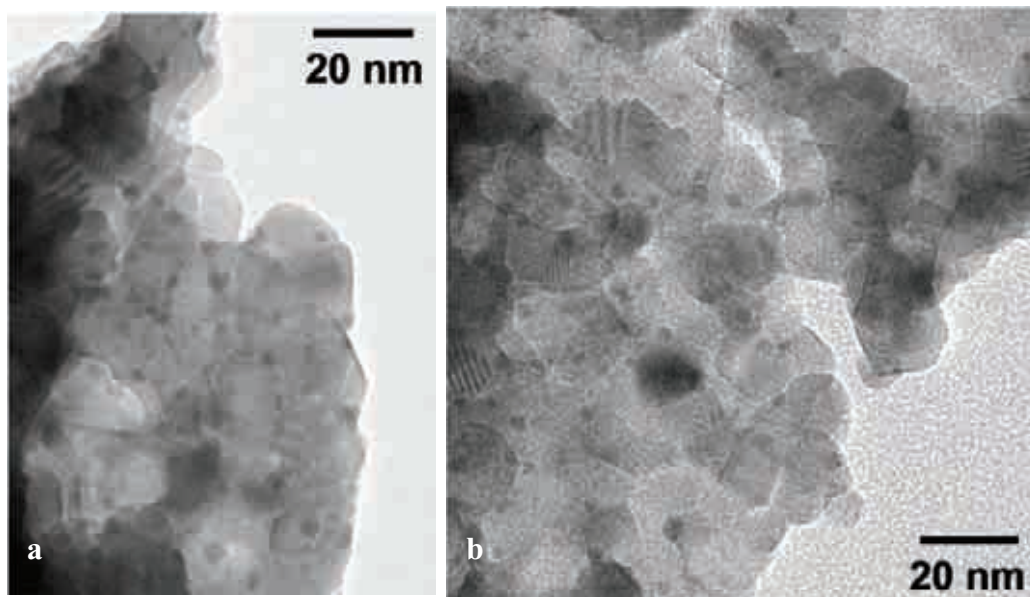


Figure 5.5. HRTEM of 0.5%Pt/CeO₂ (C): (a) after pretreatment and (b) after reduction

Figure 5.6 (B1) shows a detailed lattice fringe image of the sample. The enlargements correspond to particles labeled “a” and “b”. They differ in diameter, according to the increase of size heterogeneity as pointed above. Both particles show lattice fringes at 2.3 Å, which are ascribed to (111) planes of metallic Pt. The CeO₂ support crystallite of particle “b” shows fringes at 3.1 Å, which correspond to CeO₂ (111) planes. The image suggests that epitaxy between the particle and the support may be present after the pretreatment. Figure 5.6 (B2) corresponds to a profile view of another Pt particle showing (111) planes at 2.3 Å. The edges of Pt lattice fringes are well defined, meaning that there is no deposition of other phases onto the Pt metal crystallites.

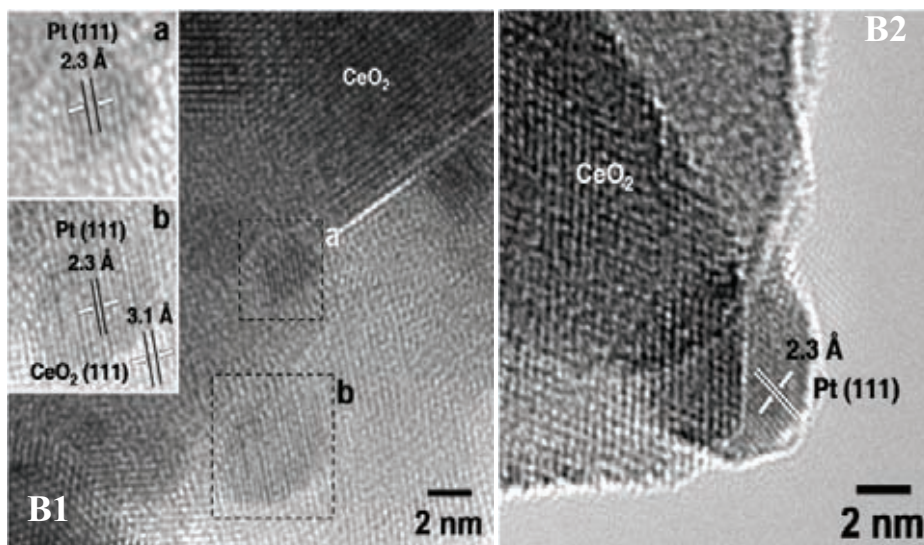


Figure 5.6. HRTEM of 0.5Pt/CeO₂ C after reduction [A1,A2]; 0.5%Pt/CeO₂ C after pretreatment [B1, B2]

The mean diameter of nanoparticles as determined by counting more than one hundred particles is around 1.7 nm; although it may be easily lower than that given the difficulties in identifying by TEM particles smaller than 1 nm. This is supported by the shape of the particle size distribution histogram, where there is a clear cut off at about 1nm. No structural information can be obtained by HRTEM on such small particles.

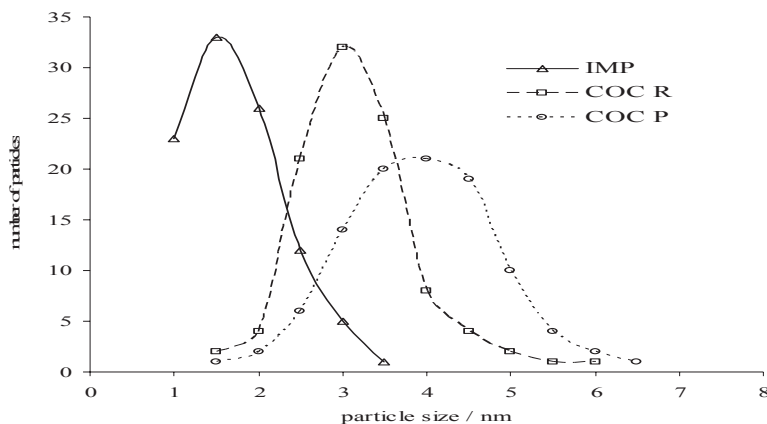


Figure 5.7. Particle size distribution determined by TEM (normalized to 100%)

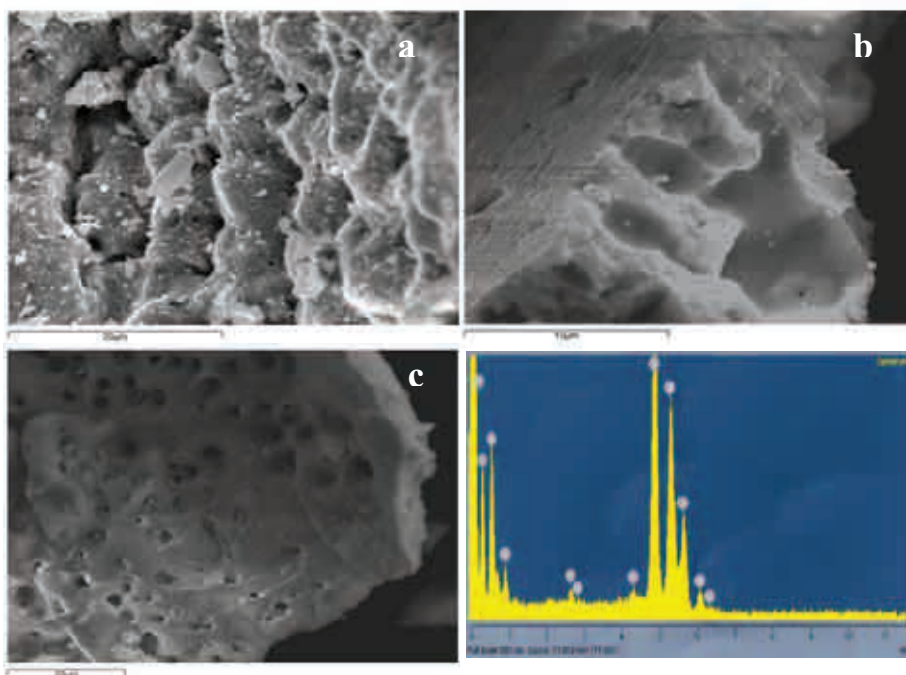


Figure 5.8. SEM photos from 0.5%Pt/CeO₂ catalysts: (a) C chloride precursor; (b) C free chloride precursor; (c) I chloride precursor and (d) spectra of C chloride precursor.

Figure 5.8 presents SEM pictures from the Pt/CeO₂ catalysts prepared with different precursors. No relevant information is obtained, it only shows aggregation pattern. Besides the XRD analysis in SEM equipment confirm the present of chloride species in the WCl samples.

The IR spectra obtained after room temperature CO exposure of impregnated (I) and co-combustion (C) Pt/CeO₂ catalysts (after prior H₂ reduction at 350°C) are shown in Figure 5.9. The results show that the CO is not adsorbed on CeO₂ (except for carbonates species; not shown [29]). For Pt containing catalysts, CO not well resolved bands were observed between 2120-2130 cm⁻¹ and 2080-2070 cm⁻¹. P. Panaglotopoulou et al. [27] proposed that Ce cations influence the adsorption state of CO by enhancing the back-bonding through the metal. The strong bands

observed at around 2068 and 2083 cm^{-1} are attributed to CO linearly bonded to surface-exposed metal Pt atoms [30]. The Pt-CO IR band at 2083 cm^{-1} is indicative of the presence of metal atoms in less dense close packing arrangements such as 100 faces, while the CO low-frequency band at 2068 cm^{-1} is related to the presence of Pt atoms in defect sites (steps and corners) [24, 30-32]. These results are in agreement with the observations made previously by TEM. Interestingly, no IR bands of Pt-dicarbonyl species (1984 cm^{-1}) and bridge CO species (1908 cm^{-1}) were detected [33]. This fact could be explained by a high dispersion of the Pt in the CeO_2 matrix.

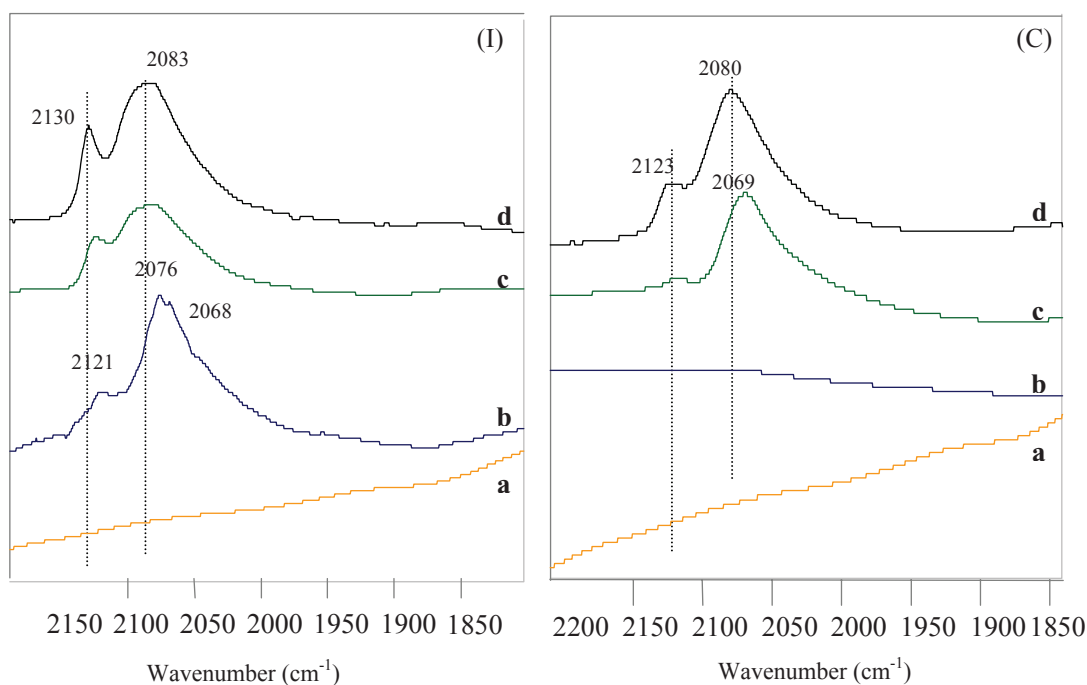


Figure 5.9. FTIR profiles of Pt/ combustion (C) catalysts. Profile of CO adsorption followed by short evacuation at room temperature [a: ceria; b:0.2%Pt; c:0.5%Pt; d:1%Pt]

The bands assignment in the region 2130-2110 cm^{-1} is a matter of controversy; the general assignment for the Pt- CeO_2 system is shown in Table 5.2.

Table 5.2. IR bands assignment on ceria and Pt/Ceria

<i>Wavenumber (cm⁻¹)</i>	<i>Surface Species*</i>
2085-2068	CO linearly adsorbed on reduced Pt ⁰ platinum sites. OC-Pt ⁰ without Ce ³⁺ interaction
2030 – 2062	OC-Pt ⁰ with Ce ³⁺ interaction
2120-2127	CO linearly adsorbed on Ce ³⁺ or on partially oxidized Pt
1820 – 1840	Bridge bonded CO on Pt ⁰ sites
1765	Pt ⁰ -CO-Ce ³⁺
1700-1690	Pt ₂ ⁰ -CO-Ce ²⁺
1641-1045	Surface formate and/or carbonate species (associated support)

The bands between 2120 and 2130 cm⁻¹ may have different origins, but it is mainly attributed to the presence of oxidized Pt in Pt/CeO₂. Pt is shown to be bonded to surface lattice oxygen and this kind of bond is not fully reducible even at high reduction temperature. Since the vibrational frequency of adsorbed CO is higher when the state of metal is more positive, the bands between 2120 and 2130 cm⁻¹ may be due to CO linearly adsorbed on Pt atoms interacting with oxygen; i.e., Pt atoms are in a more unsaturated coordination state (Pt[□]), probably created by a strong metal-support interaction (SMSI) [30]. On the other hand, these bands may also be attributed to the adsorption of CO on Ce³⁺, as well as to the presence of species like Cl. The presence of Ce³⁺ on the surface is related to a reduction of the CeO₂ promoted by the noble metal as has been detected by TPR. The presence of Cl species could arise from the precursor salt of platinum (H₂PtCl₆) [34]. In addition, using XRD Bera et al. [35] reported the formation of Ce_{1-x}Pt_xO_{2-δ} and the absence of platinum oxide phases in Pt/CeO₂ prepared by combustion. However, due to the low amount of Pt in the sample, surface PtO_x phase is difficult to detect by XRD. As a conclusion the IR results indicates a strong interaction between platinum and the support for the Pt-CeO₂ samples. However, for the 0.2%Pt/CeO₂ (C) catalyst, no CO adsorption was observed, probably due to the encapsulation of Pt in the CeO₂ matrix.

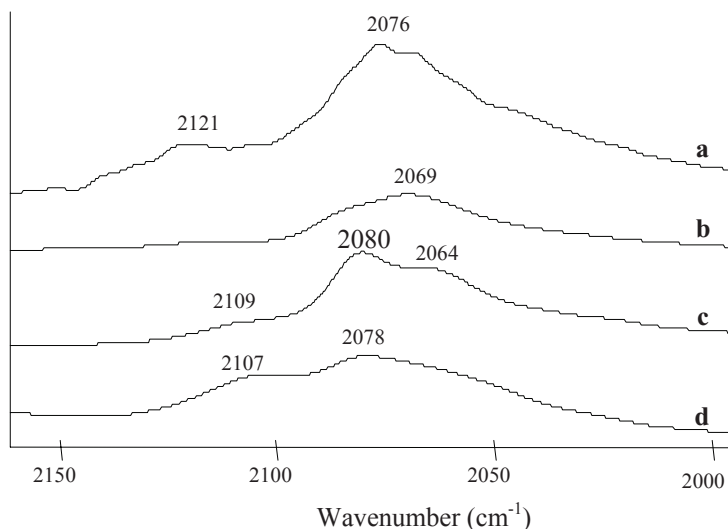


Figure 5.10. CO-FTIR of 0.2%Pt/CeO₂ (I) catalyst calcined at several temperatures: (a) 300°C; (b) 500°C; (c) 700°C; (d) 900°C.

Furthermore, when the calcination temperature was increased for the 0.2%Pt/CeO₂ (I) sample, some changes in the IR spectra were observed (see Figure 5.10). Increasing the calcination temperature from 300 to 500°C, and after reduction, the IR band located at 2121 cm⁻¹ disappears. This could be explained considering that at this calcination temperature the chloride species are removed from the surface as has been detected by EDS analysis. When the calcination temperature increased up to 700 and 900°C, a new band at around 2110 cm⁻¹ was detected. The intensity of this band increases with the increase of the calcination temperature. These facts indicate different CO-Pt interactions by modification of the calcination temperature.

The FTIR spectra obtained after room temperature CO exposure of 0.5%Pt/CeO₂ co-combustion (C) from chloride (WCl) and free-chloride precursor (NCl), after reduction and pretreatment process, are shown in Figure 5.11. It leads to identify the changes on the catalyst after the different treatments. In previous work was observed that CO does not adsorb on CeO₂ (except for carbonates species) [61].

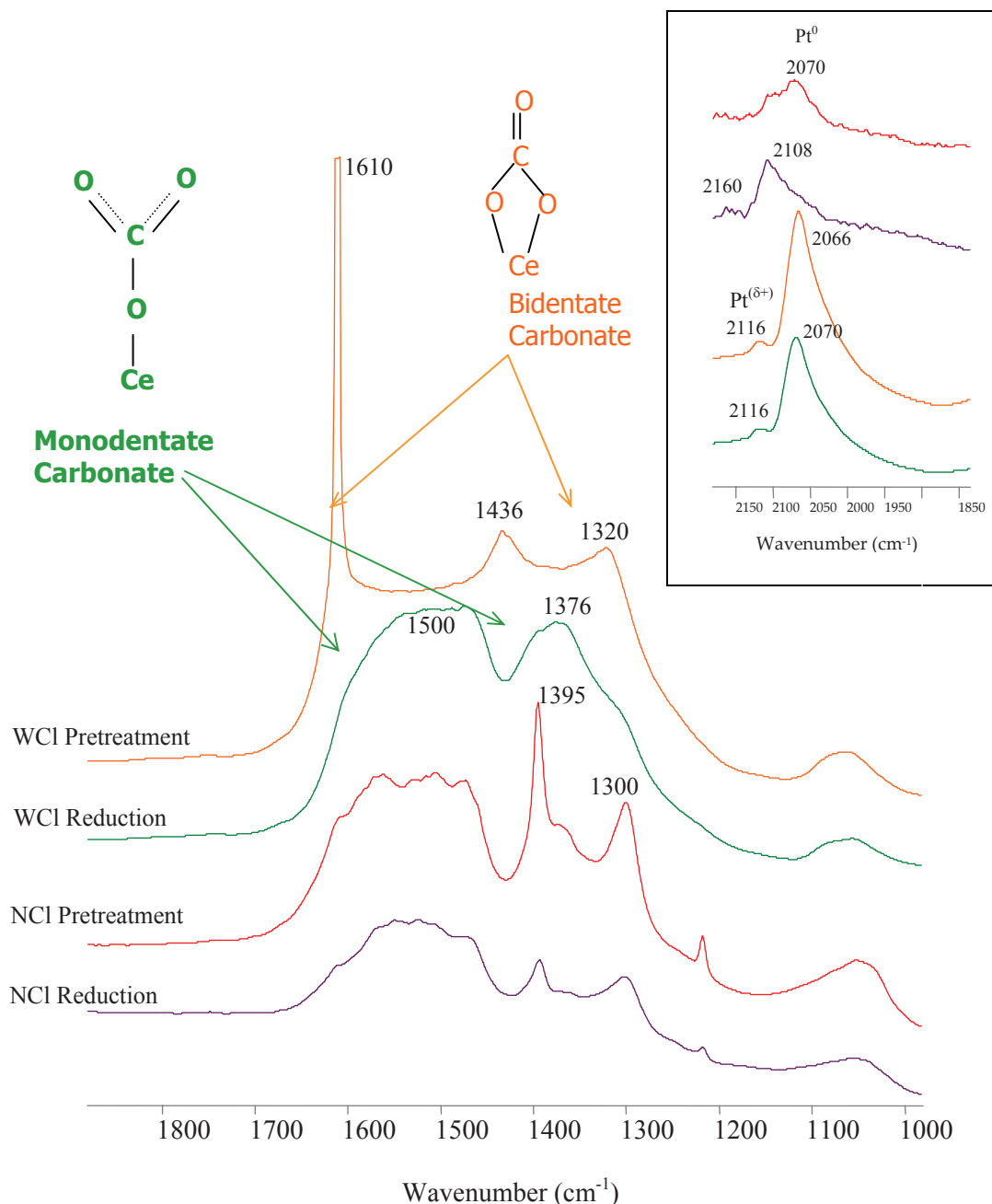


Figure 5.11. FTIR profiles of 0.5%Pt/ CeO₂ (C) catalysts. Profile of CO adsorption followed by short evacuation at room temperature.

The strong bands observed between 2060 and 2160 cm⁻¹ are attributed to CO

linearly bonded to surface-exposed metal Pt atoms [62]. The Pt-CO IR band at 2070 cm^{-1} is indicative of the presence of metal atoms [30, 62, 63]. The band at 2116 cm^{-1} is mainly attributed to the presence of oxidized Pt in Pt/CeO₂.

In the range of carbonates (1800-1000 cm^{-1}) a range of species are observed following CO adsorption. The broad bands around 1470 cm^{-1} observed are indicative of polydentate carbonate species [64]. Following reduction a monodentate carbonate at 1500 and 1376 cm^{-1} is observed whilst after the pre-treatment step bidentate carbonate at 1580 and 1320 cm^{-1} is found [65, 66]. As expected, significant modification of the cerium oxide surface occurs depending on the treatment applied, whereas the noble metal is not strongly affected. Recently, Shektman *et al.* [33] report that different atmospheric pressures pre-treatment and evacuation regimes had different effects on catalyst surface composition in agreement with the present results. In contrast, this effect was not observed when chloride free Pt precursors were used for catalyst preparation (Figure 5.11). This may indicate different surface chemistry and reactivity or the presence of different defective sites. From FTIR-CO results the main difference between applied reduction and pretreatment is in the ceria structure, whereas the most significant differences are found in the platinum by HRETM.

In order to obtain complementary information, as the distribution of the elements on the surface and the variation in the oxidation states of cerium and platinum, XPS analysis of the samples has been performed. Photoelectron spectra of the Pt 4f and Ce 3d core level region of 0.5%Pt/CeO₂ by combustion synthesis method (from chloride precursor) after reduction, and pre-treated under atmospheric air are shown in Figure 5.12. Table 5.3 summaries the binding energies for Pt 4f, Ce 3d, O 1s and Cl 2p core electrons.

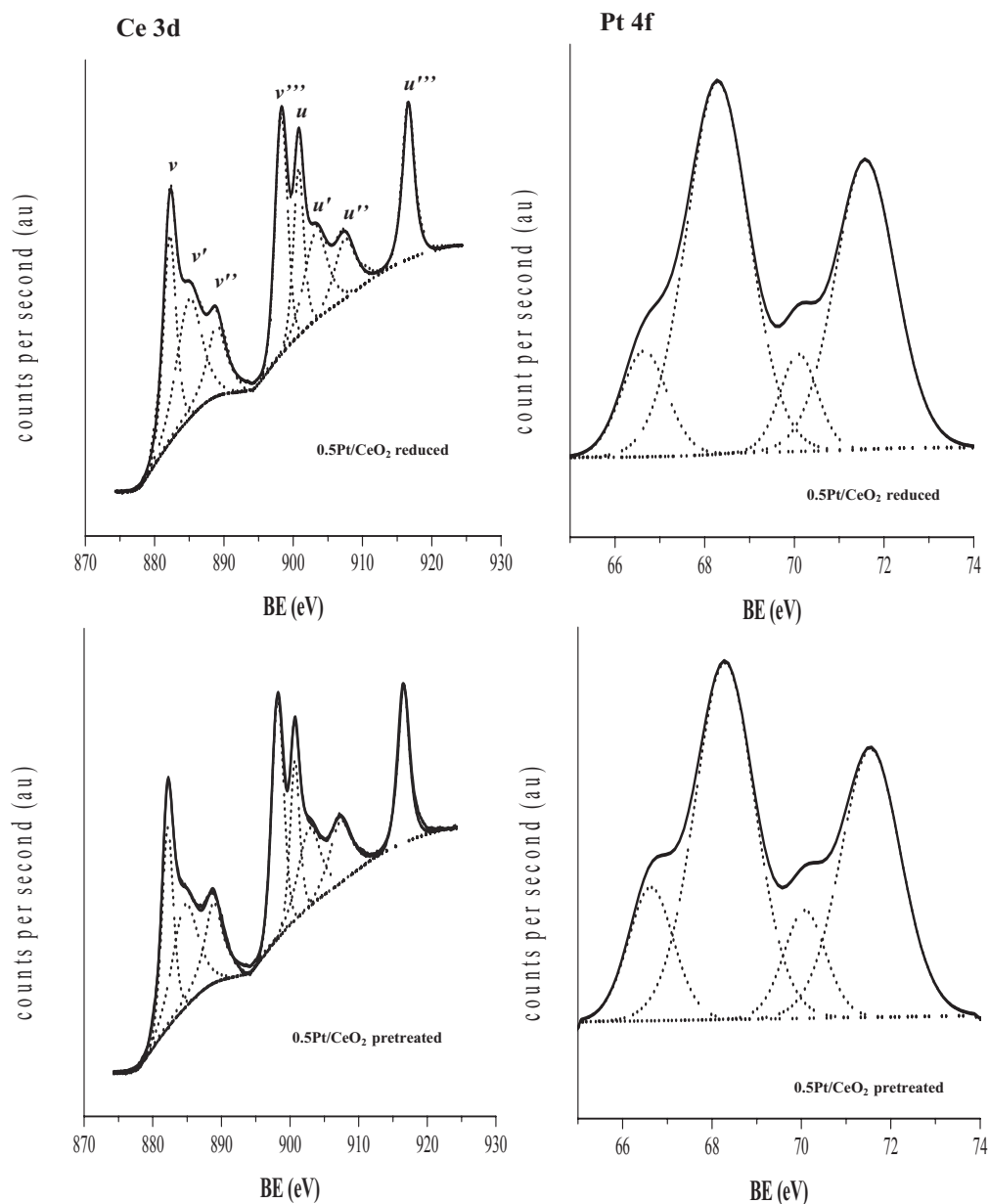


Figure 5.12. XPS of core level region of Pt(4f) and Ce(3d) for 0.5%Pt/CeO₂ prepared by combustion method, reduced and pre-treated.

The Ce 3d XPS spectra were analyzed; the curves are fitted with eight peaks corresponding to four pairs of spin-orbit doublets. The labelling of the peaks follows the convention. The satellite peak u''' associated to the Ce 3d_{3/2} is characteristic of

the presence of tetravalent Ce (Ce^{4+} ions) in Ce compounds[67]. The Ce $3d_{3/2,5/2}$ spectra are composed of two multiplets (v and u) corresponding to the spin-orbit split $3d_{5/2}$ and $3d_{3/2}$ core holes. Four peaks corresponding to the pairs of spin-orbit doublets can be identified in the Ce 3d spectrum from Ce(III) oxides, in agreement with other authors [67-69]. XPS investigation indicates that the Ce^{3+} and Ce^{4+} species can be differentiated with distinct line shapes corresponding to various final states: Ce(III) $v_0+v'+u_0+u'$ and Ce(IV) $= v+v''+v'''+u+u''+u'''$.

It is well known that rare earth oxides surfaces often hydroxylate relatively quickly in the presence of moisture. These surface hydroxyl species decomposed into oxides under X-rays irradiation leading to the formation of Ce_2O_3 and other sub-stoichiometric oxides between CeO_2 and Ce_2O_3 species [70]. The component of O 1s at 529eV increases with the reduction in comparison with pretreated sample (Table 5.3) suggesting a small increase in Ce_2O_3 , as expected. The same seems to happen for the Ce signals, therefore exists an increase in the vacancies increasing the content of Ce_2O_3 .

In the Pt metal $4f_{7/2}$ peaks are observed at around 71.3 and 72.9 eV consistent with Pt(0) and Pt(II) oxidation states. No evidence was found for Pt(IV) with the higher oxidation state found to be more prevalent at the surface than that of the low oxidation state. The results suggest that Pt is incorporated into the CeO_2 matrix, when COC method is employed, due to the higher percentage of oxidized platinum. If there is an ionic substitution of Pt^{2+} ions for Ce^{4+} sites in CeO_2 , the lattice parameter should decrease and an oxide ion vacancy should be created in order to maintain the charge neutrally due to lower valent ion substitution [71]. Higher Pt signal is observed in the reduced sample than in the pretreated (Table 5.3), which could be related with the different in particle size, smaller particle size lead to higher signal. However, the change in average particle size is small between the treatments and this is unlikely to be the cause. Another possibility is that the increase in Pt signal may be associated with migration of Cl from the metal to the support.

Table 5.3. Binding energies (eV) of core-levels and surface atomic ratios of the 0.5Pt/CeO₂ COC catalyst

	Ce 3d	O1s	Pt 4f _{7/2}	Cl 2p _{3/2}	O/ Ce	Pt/Ce	Cl/Ce	O ₈₈₅ / O ₈₉₈	O ₅₂₉ / O ₅₃₁	Pt ⁰ / Pt ²⁺
R	882.2	529.3	72.9	198.9	0.22	0.006	0.014	1.05	1.53	0.22
E	898.2									
D	884.7 888.9	531.7	71.3							
P	882.2	529.1	72.9	198.7	0.24	0.005	0.011	0.93	1.30	0.20
R	898.3									
E	885.0	531.3	71.3							
T.	888.9									

The Cl 2p_{3/2} reveals the presence of surface chloride species which has not been effectively removed following the catalyst synthesis and the binding energy is consistent with the formation of CeOCl showed by Kepinski et al. [34]. The higher percentage of Cl in the reduced sample in comparison of pretreated one may be due to the decomposition of CeOCl crystallites to cubic CeO₂ in oxidizing atmosphere whereas in the reduction process the phase CeOCl became more stable.

In order to study how the interaction of trichloroethylene molecule with the catalysts, the adsorption of TCE was studied by DRIFT. The spectra were recorded at several temperatures and with the different catalysts studied. IR gas-phase spectrum, given for comparison, shows bands centered at 3095cm⁻¹ (νCH), 1566cm⁻¹ ν(C=C), 1251cm⁻¹ δ(CH), 945cm⁻¹ (νCCl), 848cm⁻¹ (γCCl), 781cm⁻¹ (γCH) and 631cm⁻¹ (νCCl) (ν: stretching, δ: in plane bending, γ: out plane bending). These values, in Figure 5.14, are in good agreement with those found in the literature [72, 73]. Figure 5.15 displays the spectra corresponding to TCE adsorption on ceria. Most of the frequencies show a small shift from the gas phase values which indicate some interactions with the surface. This shift, associated with the adsorption

process, varied as a function of catalysts composition[74]. TCE can adsorb via the

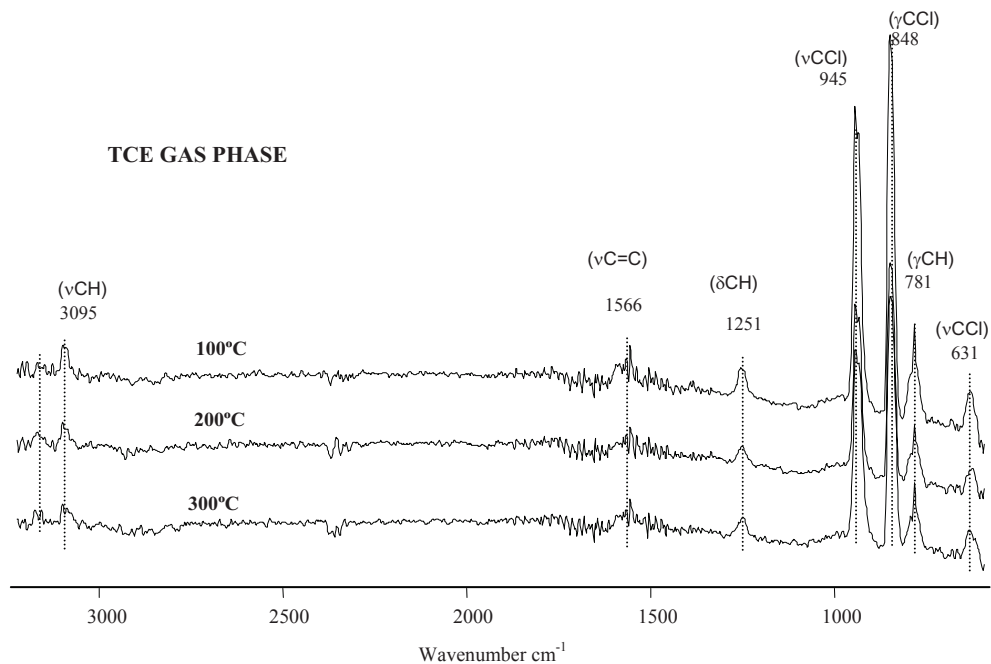


Figure 5.14. DRIFT of TCE gas phase

chlorine atoms keeping the C=C bond either parallel or perpendicular to the surface[73]. No significant changes in the C=C and C-Cl bonds have been observed in these modes, which suggest that both can be present on the surface at this temperature.

The evacuation not leads to the removal of the bands indicating that the adsorption is not only physical. The bands between 1630 and 1690cm^{-1} could be assigned to $\nu\text{C}=\text{O}$ vibrations of CHCl_2CHO as suggested Phillips and Raupp [75]. One important point is the decrease in the signal with an increase of the temperature. This could be attributed to TCE decomposition. This observations is strong in the bands associated with the C-Cl vibration, in this way could be related to the formation of chlorinated intermediates such as tetrachloroethylene[74]. The frequency at 1025cm^{-1} is related to the presence of a further dechlorination reaction product, mono-Cl species[73]. This peak decreases with an increase of the

temperature, which suggests the dissociation of this species. It is also observed with the band at 1255 cm^{-1} , also related with Cl species bond. . The adsorption of CH_3COOH rise to bands at 1418, 1478 and 1587 cm^{-1} [76], in this way the formation of carboxylate of the acetate type could be attributed to the bands at 1423, 1510 and 1588 cm^{-1} .

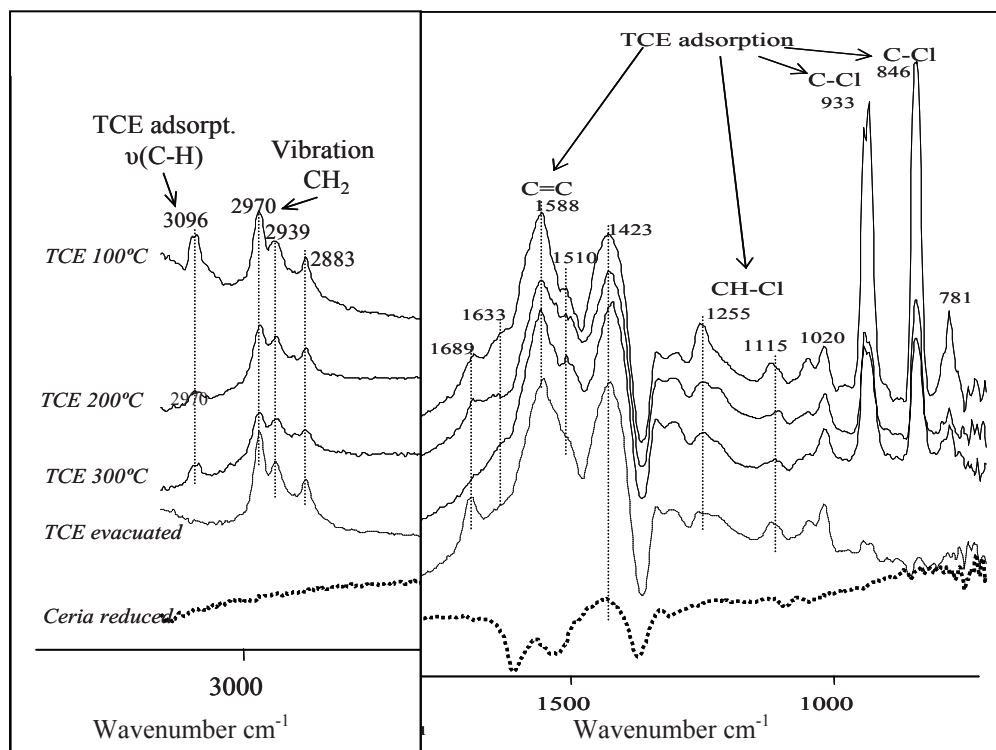


Figure 5.15. DRIFT of TCE adsorption on ceria reduced at 500°C

Figure 5.16 shows the spectra of TCE adsorption at 300°C on $0.5\%\text{Pt}/\text{CeO}_2$ catalysts with different precursor. Great variety of surface species occurs when TCE is adsorbed on Pt-ceria catalyst in comparison with ceria alone. In addition, different bands are observed depending on the precursor ($\text{WCl} - \text{NCl}$). Whereas with WCl sample two strong bands at 1422 and 1032 cm^{-1} related with $\nu(\text{CC})$ and $\delta(\text{CH})$ [73] of mono-chloro species are observed, with NCl ones the strong bands are at 1080 - 1170 cm^{-1} and 1276 cm^{-1} related with di-chloro species.

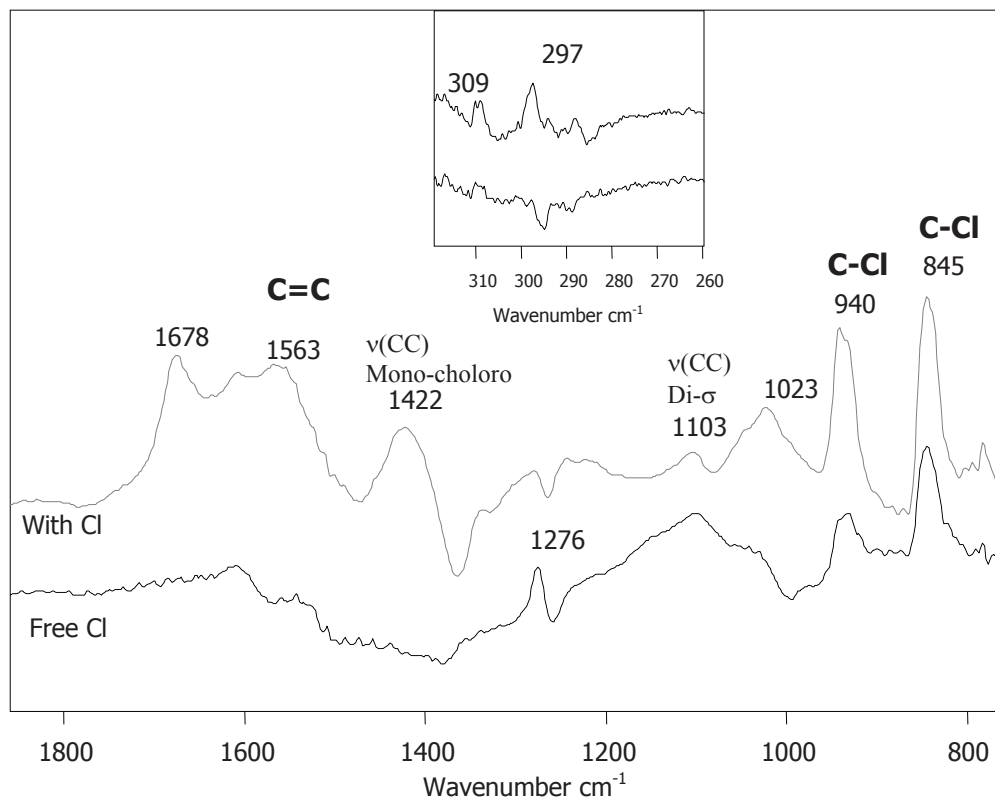


Figure 5.16. DRIFT of TCE adsorption on 0.5Pt/CeO₂ (WCl and NCl) at 300°C

This fact could be related with the platinum particle size; from characterization results were observed higher particle size in NCl samples than with WCl. In this way, less ceria surface is exposed in NCl leading to di-chloro species, whereas with WCl higher ceria surface is available to adsorb the TCE molecule and decompose to mono-chloride species. This fact could be related with that generally is accepted that alkene hydrogenation takes place on high energy sites, like kinks, steps, defect; mainly due to geometric effects. Therefore, bigger particle size leads to higher number of saturated sites, i.e., less high energy sites [77, 78].

The pretreatment leads to decomposition of CeClO to CeO₂ reducing the chloride present on the surface, assembling the NCl samples. Although, when free chloride precursor is employed bigger particle size and worst dispersion is obtained. In this way is necessary to prepare the catalyst using chloride precursor in order to obtain

small particle size well dispersed and then apply a pre-treatment to clean the surface of chloride species.

Table 5.4. Vibrational assignment of adsorbed TCE

Assignment [74, 76, 79]	Frequency (cm ⁻¹)	
	<i>Gas phase</i>	<i>CeO₂</i>
C-Cl stretch	635	
C-Cl stretch	781	
C-H bend	847	837
C-Cl stretch	941	930
CH-Cl bend	1254	1252
C=C stretch	1564	
C=C stretch	1593	1573
C-H stretch	3098	3082

5.2.2. Catalytic activity

The catalytic behaviour of Pt/CeO₂ catalysts, in the hydrodechlorination reaction of TCE, obtained by combustion (C) and impregnation methods (I), at a reaction temperature of 300°C and a molar ratio between TCE/H₂ = 1/3, is shown in Figure 5.17. In all cases the conversion increases for higher platinum loadings. However, the selectivity to ethylene decreased. The catalysts obtained via combustion and by impregnation show similar activities. But the selectivity towards ethylene is higher for the combustion derived catalysts. To study the effect of the support in the selectivity to ethylene, a 1%Pt/Al₂O₃ catalyst was tested at the same reaction conditions. Changing the WHSV, conversions of TCE from 10% up to 100% were obtained.

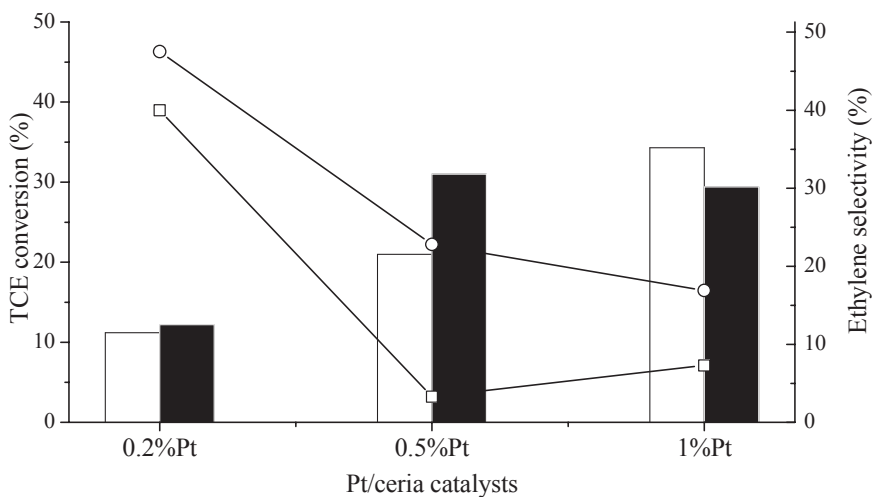


Figure 5.17. Catalytic results in the hydrodechlorination reaction of trichloroethylene at $T=300^{\circ}\text{C}$ at H_2/TCE stoichiometric molar ratio and 0.1g of catalyst (□: TCE conversion with (C); ■ : TCE conversion with (I); -□- : ethylene selectivity with (I); -○- ethylene selectivity with (C))

However, in all cases the selectivity to ethane was 100%. Consequently the product obtained using the 1%Pt/ Al_2O_3 catalyst is always the full hydrogenated compound. The difference between Pt- CeO_2 and Pt- Al_2O_3 catalysts could be attributed to a different metal-support interaction that has been observed by different characterisation techniques. Considering that the highest selectivity to ethylene was obtained for the 0.2%Pt- CeO_2 catalysts, a study of the influence of the reaction temperature was performed.

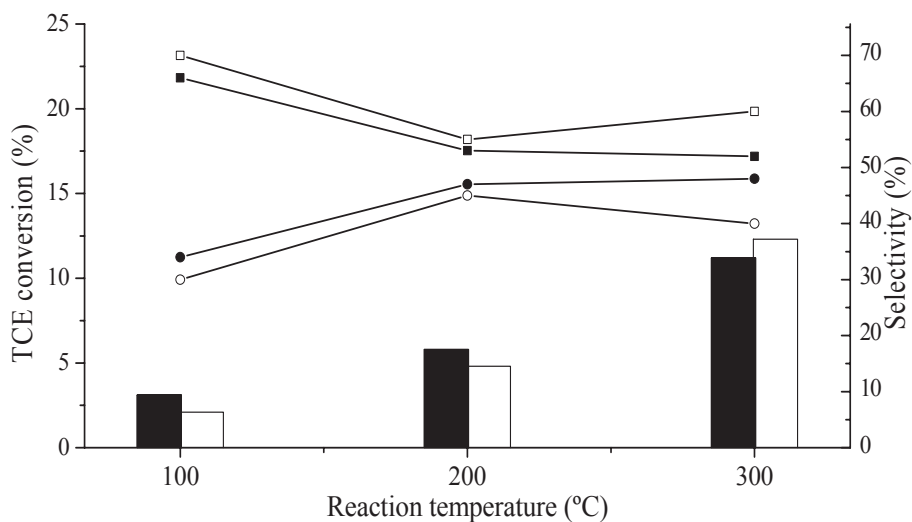


Figure 5.18. Catalytic results in the hydrodechlorination reaction of trichloroethylene with 0.2%Pt/CeO₂ by combustion (C) and impregnation (I) method (□: TCE conversion with (I); ■ : TCE conversion with (C); -○- : ethane selectivity; -●- ethylene selectivity)

Figure 6.18 shows the catalytic behaviour of the 0.2% Pt-CeO₂ catalysts obtained by combustion (C) and by impregnation (I) in the TCE hydrodechlorination reaction. As expected, the conversion increased when the reaction temperature increased from 100 up to 300°C. A TCE conversion of around 3% was obtained for combustion and impregnation catalysts when the reaction temperature was 100°C. When the reaction temperature was of 300°C the TCE conversion increased at around 12%, for both catalysts. A slight increase in the selectivity to ethylene was obtained for the combustion catalysts with respect to the impregnation ones, when the reaction temperature was between 100 and 200°C. The highest difference in the selectivity to ethylene was obtained working at higher reaction temperature (300°C). Selectivity to ethylene of around 50% was obtained for the 0.2%Pt-CeO₂ (C) catalyst, whereas a 40% of selectivity to ethylene was obtained for the 0.2%Pt-CeO₂ (I). Interestingly, the fact of increasing the reaction temperature produces an increase in the

conversion as well as in the selectivity to ethylene. This could be explained because at higher reaction temperature, the diffusion rate increases and the adsorption strength decreases, both leading to shorter residence time of TCE on the active sites of the catalysts.

Table 5.5. Catalytic activity of 0.2%Pt/CeO₂ (I) (T=300°C; H₂/TCE stoichiometric molar ratio; 0.1g catalyst)

<i>T calcination</i>	<i>Conversion</i>	<i>Selectivity ethane</i>	<i>Selectivity ethylene</i>
	<i>TCE</i>		
300°C	12%	60%	40%
500°C	37%	73%	27%
900°C	69%	84%	11%
900°C^a	15%	83%	15%

^a *The flow rate of reagents have been increased in 5 times.*

On the other hand, when the calcination temperature of the 0.2%Pt-CeO₂ (I) catalyst increased from 300°C up to 900°C, an increase in the TCE conversion was observed (see Table 5.5). However, a decrease in the selectivity of ethylene was also observed. This fact could indicate that the high calcination temperatures can produce a segregation of the Pt particles diminishing the interaction between Pt and CeO₂ as has been observed by TPR. Besides, the metal dispersion of the platinum decreased from 110% to 20% when the calcination temperature increased from 300°C up to 900°C. Consequently, the free metal platinum particles have a strong activity for hydrodechlorination but a low selectivity to the olefin obtaining (mainly) the full hydrogenated product in similar way that the results obtained for the Pt-Al₂O₃ catalyst.

Furthermore, the stability of some catalysts has been studied for a reaction time of around 24 hours as it is shown in Figure 5.19. After a slight conversion decrease during the first hour of reaction the activity of the catalysts remained practically constant. Besides, the selectivity to ethylene remained constant.

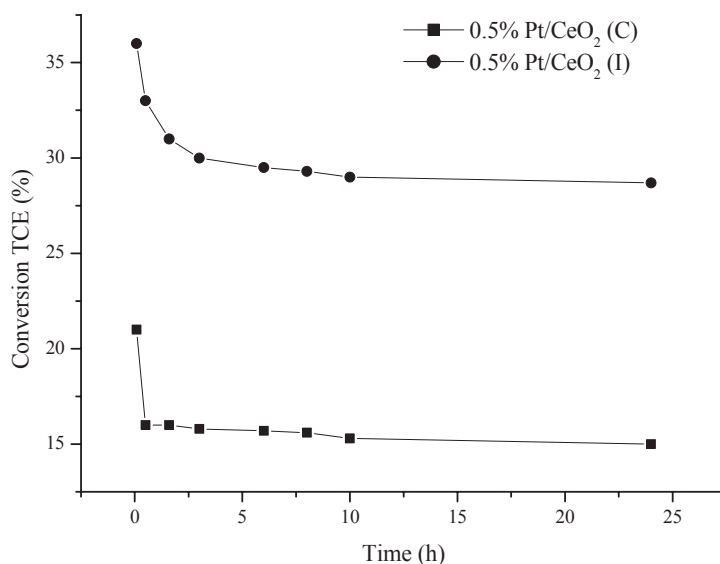


Figure 5.19. Study of catalyst deactivation during the hydrodechlorination reaction of trichloroethylene at $T=300^{\circ}\text{C}$ at H_2/TCE stoichiometric molar ratio and 0.1g of catalyst

From our results, the selectivity to ethylene using Pt-CeO₂ catalysts in the hydrodechlorination reaction of TCE is influenced by several parameters. Small platinum particles sizes (lower than 2 nm), that are obtained using the impregnation method, show a higher selectivity to full hydrogenated compounds (ethane). This could be explained considering that small metallic particles are often described as electron deficient species, less reactive towards electrophilic adsorbates like Cl, but presenting enhanced reactivity towards nucleophilic compounds [13]. Small particles, with low electron density of d-orbital, present higher selectivity to deep-dechlorinated compounds due to the strong adsorption strength of chlorinated compounds and the large amount of activated hydrogen [28]. Besides, the coverage

by Cl is higher at high conversion and on larger metal particles (small particles are chlorinated at a lower rate) [13]. These facts could explain the higher selectivity to ethylene observed using the combustion method where larger platinum particles between 2-4 nm are obtained.

On the other hand, it is well known that the modification of supported platinum catalysts by the addition of a second metal changes dramatically the catalytic performance for chlorocarbon dechlorination; the catalysts become highly selective toward olefins [4]. This has been observed in the hydrodechlorination reaction of 1,2-dichloroethane using Pt-Cu/C catalysts [36]. While Pt catalyzes the hydrodechlorination reaction of vicinal chlorocarbons to form saturated hydrocarbons, the modification of the noble metal with another metal shifts the reaction toward hydrogen assisted dechlorination to form the corresponding olefinic products [4]. From our results, the interaction between platinum and CeO₂ plays a similar role to the addition of a non noble metal. The presence of Ce³⁺ in the catalysts could interact with chlorine of the TCE obtaining the dechlorination product. Then, assisted by hydrogen, coming from platinum metal, the surface is regenerated. Contrarily, when the TCE is adsorbed on the metal particle (Pt), a deep hydrogenation is performed. Consequently, the metal-support interaction and the metal particle size govern both activity and selectivity in the hydrodechlorination reaction of TCE. However, the mechanism of this phenomenon requires further investigations.

In the TCE hydrodechlorination reaction, with the Pt-ceria catalysts, depending on the pretreatment conditions/atmosphere the selectivity towards ethylene changes both on combustion and impregnation catalysts, as it is shown at Table 5.6. The pretreatment was performed under atmospheric air, in order to detect the responsible component for these catalytic changes, where performed under inert gas and synthetic air.

Table 5.6. Catalytic activity different depending the treatment applied to the catalysts

<i>Catalysts</i>	<i>Treatment</i>	<i>Conversion TCE</i>	<i>Selectivity Ethylene</i>
0.2Pt/CeO₂	<i>Reduction</i>	11%	48%
	<i>Pre-treatment</i>	10%	58%
0.5%Pt/CeO₂	<i>Reduction</i>	21%	13%
	<i>Pre-treatment</i>	18%	85%
1%Pt/CeO₂	<i>Reduction</i>	34%	17%
	<i>Pre-treatment</i>	21%	50%

Table 5.6 shows the results obtained, when inert gas is used low selectivity toward is obtained whereas synthetic air is employed higher amount of ethylene is reached. However is still under the ethylene level obtained under atmospheric air, in this way, another component is CO₂, that could lead to the formation of carbonates and modify the oxygen vacancies on the surface like show the FTIR results.

Table 5.7. Catalytic activity different depend the gas pre-treatment applied to the catalysts (300°C, stoichiometric H₂/TCE)

<i>0.5%Pt/CeO₂ COC</i>	<i>Conversion TCE</i>	<i>Selectivity Ethylene</i>
Helium	8%	18%
Synthetic air	10%	49%

On the other hand, this effect was not observed when Cl-free Pt precursors were used for catalyst preparation (Fig.5.20). FTIR spectra of CO adsorption after the different pretreatment procedures show differences in nature of carbonate-type species, which are present before CO adsorption and additionally form upon CO addition. This could indicate different surface chemistry and reactivity or the presence of different defective sites.

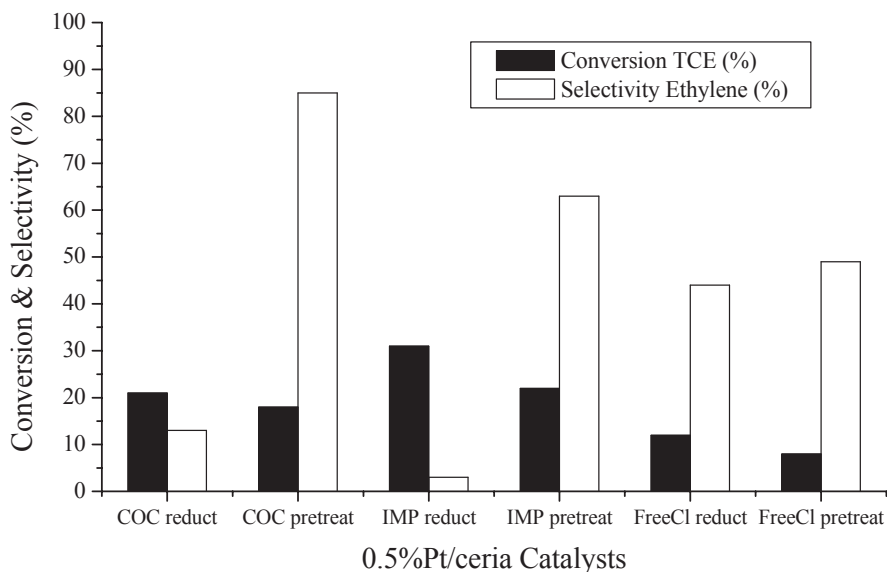


Figure 5.20. Activity and selectivity of 0.5%Pt/CeO₂ catalyst depending synthesis, precursor and treatment

Kepinski et al. [34] using PtCl₄ as precursor found that a CeOCl phase is formed during the reduction process whereas this CeOCl phase decomposes slowly in oxidizing atmosphere. This could be related with the formation of different reactive sites influencing the formation of different kinds of carbonates species [80]. It was shown that [33] some pretreatments produce surface carbonates which may block the active sites and cause changes in the catalytic behaviour. In addition, when a surface free of chloride species is obtained, more oxygen vacancies are obtained that performs the dechlorination step of TCE in the reaction. Then the noble metal recovers the vacancies blocked with chloride species with the hydrogen spillover producing HCl. In this way higher selectivity toward ethylene is obtained.

5.3. Conclusions

This work shows that, by modifying the synthesis protocol (combustion and impregnation), different platinum particle sizes and metal support interactions are obtained. Using the impregnation method smaller platinum particles is obtained when compared with the combustion ones. Furthermore, Pt-CeO₂ catalysts have shown high stability, activity and selectivity in the selective hydrodechlorination reaction of trichloroethylene to obtain ethylene. The catalytic behaviour depends on the used method for catalysts preparation. High interaction between platinum and the support is the key to obtain selective catalysts.

Surface changes are observed depending on the treatment applied to the catalyst. After pre-treatment of Pt/CeO₂ an increase in Pt particle size is observed by HRTEM, as well as, no deposition of CeO_x on platinum particles. IR spectroscopy shows different nature of carbonates formed upon CO adsorption denoting changes of the ceria surface sites. These differences are not observed when chloride-free Pt precursors are employed. In this way the surface changes are related with the presence of chloride species. Formation of a CeOCl phase from chloride precursor synthesis decomposes in oxidizing atmosphere (pre-treatment) leading to the formation of vacancies. This fact could facility a dechlorination step on the vacancies producing ethylene as product.

Although chloride precursors are necessary in the synthesis in order to obtain small particle size of platinum and well dispersed.

Further investigations are required in order to clarify the chloride influence in Pt-ceria catalysts in the hydrodechlorination of TCE.

UNIVERSITAT ROVIRA I VIRGILI
SELECTIVE HYDROGENATION CATALYSTS FOR ENVIRONMENTAL PROCESSES:
NITRATE AND CHLOROCOMPOUNDS REMOVAL
Noelia Barrabés Rabanal
DL: T-1539-2009/ISBN:978-84-692-4557-6

Chapter 5

Conclusions

Several monometallic and bimetallic heterogeneous catalysts has been designed, synthesised and characterized as well as studied their activities and selectivity in the treatment of harmful environmental compounds with exit.

- In the catalytic hydrogenation of nitrates, bimetallic catalysts supported on active carbon showed high activity in the nitrate removal as well as high selectivity toward nitrogen. The incorporation of metal nanoparticles presents an increase of the activity around 100 times more than common catalysts, with the minimization of the noble metal content. This fact decreases the economic cost of the catalysts and represents a viable application in industrial scale.
- The modification of acid-base properties of the support represents an alternative of the buffer use in the reaction media, in order to decrease the ammonia formation in the reduction of nitrates using ceria catalysts.
- In front of the high activity of the ceria catalysts, the used of structured catalysts, as monoliths, represent an advantage in front of the powder catalysts for industrial application.

- The reduction of trichloroethylene pollutant and the transformation to valuable olefin was performed using several monometallic and bimetallic catalysts. The use of ternary hydrotalcites show high activities and selectivities in this process. It denoted the importance of bimetallic alloy as active phase for the formation of ethylene as main product and high stability of the catalysts. From the catalytic and characterization data has been proposed the reaction mechanism for the hydrodechlorination of TCE reaction using bimetallic catalysts.
- The different synthesis protocols employed in Pt/ceria catalysts present the possibility of obtain the epitaxy phenomena, different particle size as well as different kind interaction between platinum and ceria. These facts, as well as, the pre-treatment applied to these catalysts determined the catalytic behaviour in the hydrodechlorination reaction.

Chapter 6

Curriculum Vitae

Academic Background

2004 –2009 PhD in Chemical Engineering

Thesis: “Selective hydrogenation catalysts for environmental processes: nitrate and chlorocompounds removal”

Supervisors: Dr. Francisco Medina and Dr. Anton Dafinov

Heterogeneous Catalysis Group, DEQ, Rovira i Virgili University, Tarragona (Spain)

12/01/2006 DEA (Advance Education Degree)

Topic: “Catalytic Reduction of nitrates using a three-phase continuous reactor”

Supervisors: Dr. Francisco Medina and Dr. Anton Dafinov

Heterogeneous Catalysis Group, DEQ, Rovira i Virgili University, Tarragona (Spain)

1997 - 2004 B. Sc. in Chemical Engineering

Final Project: Design of N-Butanol process plant ; supervisor Dr. Chillida from BASF

ETSEQ, Rovira i Virgili University, Tarragona (Spain)

Research Stage

03/08/08 –28/09/08 Centacat, Queen’s University Belfast (UK)

Topic: “Synthesis of ceria-zirconia materials in order to improve redox properties”

Supervisors: Prof. Robbie Burch and Prof. Chris Hardacre

01/10/07 –31/01/08 Institut für Materialchemie, TU-Wien (Austria)

Topic: “Catalytic hydrodechlorination reaction of chloride olefins”

Supervisors: Prof. Günther Rupprechter and Dr. Karin Föttinger

01/06/07 –31/06/07 CICbiomagune, San Sebastian (Spain)

Topic: “AFM studies on Pt-ceria and hydrotalcites materials”

Supervisor: Dr. Jose L. Toca

01/09/06 –20/12/06 Institut für Materialchemie, TU-Wien (Austria)

Topic: Catalytic hydrodechlorination reaction of chloride olefins

Supervisors: Prof. Günther Rupprechter and Dr. Karin Föttinger

Courses

02-04/07/2007 Summer School

Topic: Catalysis: A strategy for sustainable development.

Place: University of Basque Country, SECAT07, Bilbao (Spain)

06-09/06/2006 Summer School

Topic: Introduction on catalysts and adsorbents characterization

Place: CSIC/ University of Extremadura / Inst. Rocasolano, Jarandilla (Spain)

30/06/2005-01/07/2005 Summer School

Topic: Zeolitics and Mesostructure Materials

Place: University Rey Juan Carlos, SECAT05, Madrid (Spain)

14/04/2004-14/05/2004 DOW course

Topic: Security and Sustainability in Chemical Industry

Place: Rovira I Virgili University and Dow Chemical

2004 Course

Topic: Basic course in prevention of working risks.

Place: Rovira i Virgili University

2002 - 2003 DOW courses

Topic: Quality in Chemical Industry

Topic: Chemical Industry and Environmental

Place: Rovira i Virgili University and Dow Chemical

2002 Course

Topic: Tracom : Team working

Place: Rovira i Virgili University

Skills

COMPUTING

Excellent knowledge of Word, Powerpoint, Excel, Internet Explorer

Programming in Fortran, Matlab and Gams

Drawing: Autocad

Simulators: Hysys Plant and Aspen Plus

Working knowledge of SAP R3, EES, Origin, Endnote

Analytical Software: Grams, Opus (Spectra IR), Eva (XRD)

EQUIPMENTS

Working knowledge of Gas and Liquid Chromatography, TPR/D/O (Temp. program. Reduct. Desorpt. Oxidation) Scanning and Transmission Electronic Microscope,

Physisorption and Chemisorption, FTIR (fourier transformed infrared spectroscopy)

DRIFT. Basic knowledge AFM (atomic force microscope)

Languages

Spanish: mother tongue

Catalan: mother tongue

English: fluently

German: basic

Awards

2007 Best Oral Communication SECAT 07

Topic: Nitrates Elimination with Pt/CeO₂ catalysts: selectivity optimization by support modifications. SECAT 07 (Spanish Catalysis Society Meeting)

2006 Environmental Award of Catalonia Government, Research and development

Topic: Catalytic reduction of nitrates from drinking waters.

2005/06 Best Enterprising Idea

Topic: Recuperation of hydrous contaminated resources with nitrates with catalytic hydrogenation technology.

Place: Consell Social, University Rovira i Virgili

Participation in financed projects

- "Preparació de catalitzadors, disseny de reactors, assessorament, assistència tècnica i direcció en el projecte de construcció d una planta d eliminació de nitrates al municipi de El Morell": Dr. Francesc Medina, Dr. Jesús E. Sueiras Romero, 2008-2009. Empresa finançadora : Aplicacions de la Catàlisi, S.L.
- "Escalat a planta pilot de la tecnologia d eliminació de nitrats/nitrits": Dr. Francesc Medina, 2005-2007. Empresa finançadora : Ingenieros Asesores y Profesionales, S.L.
- "PCB s and PCT s removal from flows by selective catalytic hydrodechlorination": Jesús E. Sueiras Romero, Q9999/2007/309-118, (RESI)Waste minimization, (AREC)Agència de Residus de Catalunya, 2007
- "Recovery of hydrous contaminates resources with nitrates and nitrites by catalytic hydrogenation technology: Scale to pilot plant" Francesc Medina, PET2006_0816 Ministerio de Educación y Ciencia (PETRI), Spanish government 2006
- "Environmental catalysis: Pd-bimetallic catalysts for the reduction of pollutants as nitrates and halogenated organic compounds in aqueous solutions" Francesc Medina, HU2006-0026 Ministerio de Educación y Ciencia (Acciones integradas), Spanish and Austrian government 2006
- "New catalysts synthesis protocols with controlled basic properties for green chemistry: Application in reactions of aldolic condensation using continuous and discontinuous reactor" Francesc Medina, 1CTQ2006-08196 Ministerio de Educación y Ciencia (Proyecto de I+D), Spanish government 2006
- "Nanocatalysts in advanced oxidation process: application to industrial effluents treatment", Francesc Medina, A/5188/06 Ministerio de Asuntos Exteriores y Cooperación (PCI), Spanish government 2006
- "Catalytic Materials", Jesús E. Sueiras Romero, 2005SGR-00547, GRQ Investments for the quality research group promoting, DGRE General management research 2005

Contract R+D with companies

- "Preparació de catalitzadors, disseny de reactors, assessorament, assistència tècnica i direcció en el projecte de construcció d una planta d eliminació de nitrates al municipi de El Morell": Dr. Francesc Medina, Dr. Jesús E. Sueiras Romero, 2008-2009. Empresa finançadora : Aplicacions de la Catàlisi, S.L.

- "Escalat a planta pilot de la tecnologia d eliminació de nitrats/nitrits": Dr. Francesc Medina, 2005-2007. Empresa finançadora : Ingenieros Asesores y Profesionales, S.L.

Publications

- [1] N.Barrabés, K.Föttinger, A.Dafinov, F.Medina, J.E. Sueiras, G. Rupprechter. *"Atmosphere pre-treatment effect on Pt/CeO₂ catalyst in the selective hydrodechlorination of trichloroethylene"*; Journal of Physical Chemistry C (to be submitted)
- [2] R.G. Pavelko, A.A. Vasiliev, E. Llobet, X. Vilanova, N. Barrabés, F. Medina, V.G. Sevastyanov; *"Comparative study of nanocrystalline SnO₂ materials for gas sensor application: thermal stability and catalytic activity"*; Journal of Sensors and Actuators B: Chemical. (in press)
- [3] N.Barrabés, D.Cornado, K.Föttinger, A.Dafinov, F.Medina, J.E. Sueiras, G. Rupprechter. *"Selective hydrodechlorination of trichloroethylene on noble metal-promoted Cu hydrotalcite-derived catalysts"*; Journal of Catalysis (submitted)
- [4] N.Barrabés, K.Föttinger, A.Dafinov, F.Medina, J.E. Sueiras, G. Rupprechter. *"Study of Pt-CeO₂ interaction and the effect in the selective hydrodechlorination of trichloroethylene"*; Applied Catalysis B: Environmental, 2008 (in press)
- [5] N.Barrabés, A.Dafinov, F.Medina, J.E. Sueiras. *"Study the effect of acid-base properties of the support on the catalytic reduction of nitrates, using Pt/CeO₂ catalysts"*; Catalysis Today 2009 (from SICAT congress)
- [6] R.J. Chimentao, N.Barrabés, F. Medina, J.E. Sueiras. *"Synthesis, characterization and catalytic activity of metal nanoparticles in the selective oxidation of olefins in gas phase"*; Journal of experimental nanoscience. Vol.1 No4 (2006) 399-418
- [7] N.Barrabés, J. Just, A. Dafinov, F. Medina, J.E.Sueiras, Y. Cesteros, P. Salagre *"Catalytic reduction of nitrate on Pt-Cu and Pd-Cu /AC using a continuous reactor. Effect of copper nanoparticles"*; Applied Catalysis B: Environmental, 62 (2005) 77-85.

Contributions in congress

5th International Congress on Environmental Catalysis, Belfast (UK), 2008

- N.Barrabés, A.Dafinov, K.Föttinger, G. Rupprechter, F.Medina, J.E. Sueiras; Study of the effect of different pretreatments on Pt/CeO₂ catalysts for the hydrodechlorination of trichloroethylene (TCE) - (POSTER)
- K.Föttinger, N.Barrabés, D. Cornado, A. Haghofer, F.Medina, G. Rupprechter; Noble metals supported on Cu-hydrotalcites for selective reduction of chlorinated contaminants (POSTER)

14th International Congress in Catalysis; Seoul (Korea), 2008

- N.Barrabés, A.Dafinov, K.Föttinger, G.Rupprechter, F.Medina, J.E. Sueiras; Pt/CeO₂ catalysts by different synthesis for the selective hydrodechlorination of trichloroethylene into ethylene - (POSTER)
- N.Barrabés, A.Dafinov, F.Medina, J.E. Sueiras; Study the effect of acid-base properties of the support on the catalytic reduction of nitrates using Pt/CeO₂ catalysts - (POSTER)

Sicat 08 meeting of Iberoamerican catalysis society; Málaga (Spain), 2008

- N.Barrabés, A.Dafinov, F.Medina, J.E. Sueiras; Catalytic reduction of nitrates using Pt/CeO₂ catalysts in a continuous reactor (ORAL)
- N.Barrabés, A.Dafinov, K. Föttinger, G. Rupprechter F.Medina, J.E. Sueiras; Study of Pt-CeO₂ interaction and the effect in the selectivity hydrodechlorination of trichloroethylene - (POSTER)

Europacat 07 meeting of European catalysis society, Turku (Finland), 2007

- N.Barrabés, A.Dafinov, K.Föttinger, H.Vinek, F.Medina, J.E. Sueiras; Bimetallic catalysts for selective hydrodechlorination of tetrachloroethyle - (POSTER)

Secat 07 meeting of Spanish catalysis society; Bilbao (Spain), 2007

N.Barrabés, A.Dafinov, F.Medina, J.E. Sueiras; Nitrates elimination with Pt/CeO₂ catalysts: selectivity optimization by support modifications - (ORAL)

1st International Congress on Green Process Engineering; Toulouse (France) 2007

N.Barrabés, A.Dafinov, F.Medina, J.E. Sueiras; Catalytic Reduction of NO₃⁻ over monometallic Pt/CeO₂ catalysts using a continuous reactor. Tuning the acid-base properties to improve the selectivity - (POSTER)

Low temperature oxidation of aqueous ammonium solutions over Fe₂O₃ / WO₃ / CeO₂ catalysts - (POSTER)

Nanospain Workshop; Pamplona (Spain), 2006

N.Barrabés, A.Dafinov, F.Medina, J.E. Sueiras; Copper-platinum nanoparticles supported on active carbon as catalyst for desnitrification of drinking waters - (POSTER)

Secat 05 meeting of Spanish catalysis society; Madrid (Spain), 2005

N.Barrabés, A.Dafinov, F.Medina, J.E. Sueiras; Catalytic reduction of nitrate on Pt-Cu and Pd-Cu /AC using a continuous reactor. Effect of copper nanoparticles - (ORAL)

Working Experience

1/10/2004- Heterogeneous catalysis group / AMIC / URV

- Research work as PhD student in synthesis, characterization and testing catalysts for environmental processes
- Teacher assistant in several lectures like: Chemical Engineering Laboratory, Industrial Chemistry and Kinetics. In addition I was laboratory supervisor in research laboratory lecture in the last four years.

1/03/2003- 1/09/2004 Heterogeneous catalysis group / AMIC

Research support in environmental catalytic processes and nanotechnology synthesis

Place: Tarragona, Spain

1/07/2002- 22/11/2002 Bayer Polymers, Engineering Department KU

Chemical Engineering Training

Build and programming a preventive maintenance plan for process plants with SAPR3. Study of pneumatic transport lines.

Place: Tarragona, Spain

1999- 2002 Half time works during studies

Waiter, shop assistant

Place: Tarragona, Spain

Interest

Studies in Music (till Harmony). Medium degree of piano (Terrassa municipal conservatorium)

Football player in a team for 5 years

I am interested in music, sports, cinema and travelling.